

LOCKHEED MISSILES & SPACE COMPANY
HUNTSVILLE RESEARCH & ENGINEERING CENTER
HUNTSVILLE RESEARCH PARK
4800 BRADFORD DRIVE, HUNTSVILLE, ALABAMA

CR-128891
C. 2

CASE FILE COPY

HEAT TRANSFER TESTS OF THE
NASA-MSC SPACE SHUTTLE
CONFIGURATION AT THE
LANGLEY RESEARCH CENTER
MACH 8 VARIABLE DENSITY
FACILITY - FINAL REPORT

February 1971

Contract NAS9-10506
(Item 7)


by

L. E. Connor
V. W. Sparks
A. G. Bhadsavle

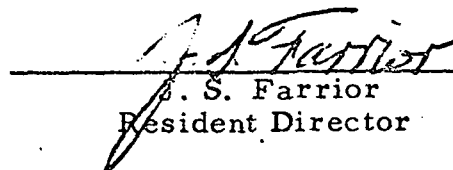
APPROVED:



Juan K. Lovin, Supervisor
Thermal Environment Section



George D. Reny, Manager
Aeromechanics Dept.



J. S. Farrior
Resident Director

FOREWORD

Results are presented of aerothermodynamic wind tunnel tests performed by Lockheed's Huntsville Research & Engineering Center. This constitutes the Final Report for Contract NAS9-10506. The tests were performed in the Mach 8 Variable Density Facility at the Langley Research Center, Hampton, Virginia. The NASA-Manned Spacecraft Center technical monitor for this contract is Mr. W. D. Goodrich, Mail Code ES57.

CONTENTS

Section	Page
FOREWORD	ii
NOMENCLATURE	x
1 INTRODUCTION AND SUMMARY	1
2 DISCUSSION	2
2.1 Models	2
2.2 Test Procedure and Run Schedule	3
2.3 Data Reduction	3
2.4 Test Results	8
2.5 Recommendations	8
REFERENCES	10

ILLUSTRATIONS

Figure	Page
1 NASA-Manned Spacecraft Center Space Shuttle Heat Transfer Models	11
2 NASA-Manned Spacecraft Center Space Shuttle Launch Configuration	12
3 Thermal Diffusion Time vs Depth of Penetration for Stycast Used in NASA-MSC Heat Transfer Models	13
4 Lower Surface Local to Stagnation Point Heat Transfer Coefficients (Run No. 435)	14
5 Upper Surface Local to Stagnation Point Heat Transfer Coefficients (Run No. 436)	15

Figure		Page
6	Lower Surface Local to Stagnation Heat Transfer Coefficients (Run No. 437)	16
7	Upper Surface Local to Stagnation Point Heat Transfer Coefficients (Run No. 438)	17
8	Upper Surface Local to Stagnation Point Heat Transfer Coefficients (Run No. 439)	18
9	Lower Surface Local to Stagnation Point Heat Transfer Coefficients (Run No. 440)	19
10	Upper Surface Local to Stagnation Point Heat Transfer Coefficient (Run No. 441)	20
11	Lower Surface Local to Stagnation Point Heat Transfer Coefficients (Run No. 442)	21
12	Upper Surface Local to Stagnation Point Heat Transfer Coefficients (Run No. 443)	22
13	Upper Surface Local to Stagnation Point Heat Transfer Coefficients (Run No. 444)	23
14	Lower Surface Local to Stagnation Point Heat Transfer Coefficients (Run No. 445)	24
15	Lower Surface Local to Stagnation Point Heat Transfer Coefficients (Run No. 446)	25
16	Upper Surface Local to Stagnation Point Heat Transfer Coefficients (Run No. 447)	26
17	Upper Surface Local to Stagnation Point Heat Transfer Coefficients (Run No. 448)	27
18	Lower Surface Local to Stagnation Point Heat Transfer Coefficients (Run No. 449)	28
19	Lower Surface Local to Stagnation Point Heat Transfer Coefficients (Run No. 450)	29
20	Upper Surface Local to Stagnation Point Heat Transfer Coefficients (Run No. 451)	30
21	Lower Surface Local to Stagnation Point Heat Transfer Coefficients (Run No. 452)	31

Figure		Page
22	Lower Surface Local to Stagnation Point Heat Transfer Coefficients (Run No. 453)	32
23	Lower Surface Local to Stagnation Point Heat Transfer Coefficients (Run No. 454)	33
24	Lower Surface Local to Stagnation Point Heat Transfer Coefficients (Run No. 455)	34
25	Lower Surface Local to Stagnation Point Heat Transfer Coefficients (Run No. 456)	35
26	Upper Surface Local to Stagnation Point Heat Transfer Coefficients (Run No. 460)	36
27	Upper Surface Local to Stagnation Point Heat Transfer Coefficients (Run No. 461)	37
28	Upper Surface Local to Stagnation Point Heat Transfer Coefficients (Run No. 462)	38
29	Lower Surface Local to Stagnation Point Heat Transfer Coefficients (Run No. 463)	39
30	Lower Surface Local to Stagnation Point Heat Transfer Coefficients (Run No. 464)	40
31	Side Panel Local to Stagnation Point Heat Transfer Coefficients (Run No. 435)	41
32	Side Panel Local to Stagnation Point Heat Transfer Coefficients (Run No. 436)	42
33	Side Panel Local to Stagnation Point Heat Transfer Coefficients (Run No. 437)	43
34	Side Panel Local to Stagnation Point Heat Transfer Coefficients (Run No. 438)	44
35	Side Panel Local to Stagnation Point Heat Transfer Coefficients (Run No. 439)	45
36	Side Panel Local to Stagnation Point Heat Transfer Coefficients (Run No. 440)	46
37	Side Panel Local to Stagnation Point Heat Transfer Coefficients (Run No. 441)	47

Figure		Page
38	Side Panel Local to Stagnation Point Heat Transfer Coefficients (Run No. 442)	48
39	Side Panel Local to Stagnation Point Heat Transfer Coefficients (Run No. 443)	49
40	Side Panel Local to Stagnation Point Heat Transfer Coefficients (Run No. 444)	50
41	Side Panel Local to Stagnation Point Heat Transfer Coefficients (Run No. 445)	51
42	Side Panel Local to Stagnation Point Heat Transfer Coefficients (Run No. 446)	52
43	Side Panel Local to Stagnation Point Heat Transfer Coefficients (Run No. 447)	53
44	Side Panel Local to Stagnation Point Heat Transfer Coefficients (Run No. 448)	54
45	Side Panel Local to Stagnation Point Heat Transfer Coefficients (Run No. 449)	55
46	Side Panel Local to Stagnation Point Heat Transfer Coefficients (Run No. 450)	56
47	Side Panel Local to Stagnation Point Heat Transfer Coefficients (Run No. 451)	57
48	Side Panel Local to Stagnation Point Heat Transfer Coefficients (Run No. 452)	58
49	Side Panel Local to Stagnation Point Heat Transfer Coefficients (Run No. 453)	59
50	Side Panel Local to Stagnation Point Heat Transfer Coefficients (Run No. 454)	60
51	Side Panel Local to Stagnation Point Heat Transfer Coefficients (Run No. 455)	61
52	Side Panel Local to Stagnation Point Heat Transfer Coefficients (Run No. 456)	62
53	Side Panel Local to Stagnation Point Heat Transfer Coefficients (Run No. 460)	63

Figure		Page
54	Side Panel Local to Stagnation Point Heat Transfer Coefficients (Run No. 461)	64
55	Side Panel Local to Stagnation Point Heat Transfer Coefficients (Run No. 462)	65
56	Side Panel Local to Stagnation Point Heat Transfer Coefficients (Run No. 463)	66
57	Side Panel Local to Stagnation Point Heat Transfer Coefficients (Run No. 464)	67
58	NASA-MSC Orbiter/Launch Configuration Wing Chordwise Heat Transfer Distribution at 50% Span, Alpha = 0°, yaw = 0°	68
59	NASA-MSC Orbiter/Launch Configuration Wing Chordwise Heat Transfer Distribution at 50% Span, Alpha = 0°, yaw = 6°	69
60	NASA-MSC Booster/Launch Configuration Wing Chordwise Heat Transfer Distribution at 50% Span, Alpha = 0°, yaw = 0°	70
61	NASA-MSC Booster/Launch Configuration Wing Chordwise Heat Transfer Distribution at 50% Span, Alpha = 0°, yaw = 6°	71
62	NASA-MSC Booster/Launch Configuration Wing Chordwise Heat Transfer Distribution at 50% Span, Alpha = 10°, yaw = 0°	72
63	NASA-MSC Orbiter Configuration Bottom Wing Chordwise Heat Transfer Distribution at 25% Span	73
64	NASA-MSC Orbiter Configuration Bottom Wing Chordwise Heat Transfer Distribution at 50% Span	74
65	NASA-MSC Orbiter Configuration Wing Top Chordwise Heat Transfer Distribution at 25% Span, Alpha = 0°, yaw = 6°	75
66	NASA-MSC Orbiter Configuration Wing Top Chordwise Heat Transfer Distribution at 50% Span, Alpha = 0°, yaw = 6°	76

Figure		Page
67	NASA-MSC Orbiter/Launch Configuration Wing Chordwise Heat Transfer Distribution at 50% Span, Alpha = $+10^{\circ}$, yaw = 0°	77
68	NASA-MSC Booster Configuration Wing Bottom Chordwise Heat Transfer Distribution at 50% Span, Alpha = 0° , yaw = 6°	78
69	Schlieren Photographs of Run 430; Pitch = 0° , Yaw = 0°	79
70	Schlieren Photographs of Run 431; Pitch = 0° , Yaw = 0°	80
71	Schlieren Photographs of Run 434; Pitch = -10° , Yaw = 0°	81
72	Schlieren Photographs of Run 441; Pitch = 0° , Yaw = 0° , $R_N/FT = 6.026 \times 10^5$	82
73	Schlieren Photographs of Run 444; Pitch = $+10^{\circ}$, Yaw = 0° , $R_N/FT = 5.84 \times 10^5$	83
74	Schlieren Photographs of Run 445; Pitch = $+10^{\circ}$, Yaw = 0° , $R_N/FT = 6.43 \times 10^5$	84
75	Schlieren Photographs of Run 446; Pitch = -10° , Yaw = 0° , $R_N/FT = 6.43 \times 10^5$	85
76	Schlieren Photographs of Run 447; Pitch = 0° , Yaw = $+6^{\circ}$, $R_N/FT = 6.3 \times 10^5$	86
77	Schlieren Photographs of Run 448; Pitch = 0° , Yaw = $+6^{\circ}$, $R_N/FT = 5.95 \times 10^5$	87
78	Schlieren Photographs of Run 449; Pitch = 0° , Yaw = $+6^{\circ}$, $R_N/FT = 5.79 \times 10^5$	88
79	Schlieren Photographs of Run 450; Pitch = 0° , Yaw = -6° , $R_N/FT = 6.26 \times 10^5$	89
80	Schlieren Photographs of Run 454; Pitch = $+20^{\circ}$, Yaw = 0° , $R_N/FT = 2.04 \times 10^6$	90
81	Schlieren Photographs of Run 456; Pitch = $+30^{\circ}$, Yaw = 0° , $R_N/FT = 6.38 \times 10^5$	91

Figure		Page
82	Schlieren Photographs of Run 462; Pitch = -5° , Yaw = 0° , $R_N/FT = 3.72 \times 10^6$	92
83	Schlieren Photographs of Run 464; Pitch = -20° , Yaw = 0° , $R_N/FT = 1.97 \times 10^6$	93

NOMENCLATURE

Symbols

a	thermal diffusivity, $K/\rho C$
C	specific heat
g_c	universal gravitational constant
h	heat transfer coefficient
H	enthalpy
K	thermal conductivity
l	depth
P	pressure
R_n	nose radius, 0.005 ft
t	time
T	temperature
X/L	nondimensional wetted length along bottom centerline
R_N	freestream Reynolds number

Greek

α	angle of attack
μ	viscosity
ρ	density

Subscripts

AW	adabatic wall conditions
i	initial
pc	phase change melt temperature
o	total conditions
s	stagnation point
w	wall conditions
∞	free stream

Section 1

INTRODUCTION AND SUMMARY

This report presents results of the experimental investigations performed on the NASA-Manned Spacecraft Center Space Shuttle orbiter and booster configurations at the Mach 8 Variable Density Facility at Langley Research Center, Hampton, Virginia, from 13-16 October 1970. The test program reported here was a series of aerothermodynamic wind tunnel tests that were run over a range of angles of attack, yaw angles, and Reynolds numbers. This report documents the tests performed and presents results obtained.

Objectives of the test program were to obtain heat transfer data over the NASA-Manned Spacecraft Center Space Shuttle orbiter, booster, and launch configurations for a range of angles of attack from -20 to +30 degrees, yaw angles of 0 and +6 degrees, and Reynolds numbers of 0.6, 2.0, and 3.7×10^6 . The phase-change coating technique was used to obtain heat transfer data. Information received from these tests will be instrumental in performing thermal protection systems studies and vehicle aerodynamic design.

Review of the data shows that the principal objectives of the test were attained. Side, bottom, and top view data were obtained which consisted of isotherm melt contours. Schlierens of most test attitudes and conditions were also taken and are presented.

Section 2

DISCUSSION

Heat transfer tests were performed on the NASA-Manned Spacecraft Center Space Shuttle orbiter, booster and launch configurations in the Mach 8 Variable Density Facility at Langley Research Center. The tests were conducted at a nominal Mach number of 8, with the freestream unit Reynolds number varying from 0.6×10^6 to 3.7×10^6 . Heat transfer data were obtained by coating 0.005-scale plastic models of the NASA-MSC configurations with a material that melts at a known temperature and recording the phase-change patterns by motion picture photography. The data were reduced by measuring the time required for the surface to reach a known temperature, as indicated by the phase-change, and calculating the corresponding heat transfer rates by the semi-infinite slab transient heat conduction equation. This technique has been developed (Ref. 1) and used at the NASA-Langley Research Center (Refs. 2 and 3).

2.1 MODELS

The NASA-Manned Spacecraft Center heat transfer models were fabricated in the laboratory facilities at Lockheed's Huntsville Research & Engineering Center, Huntsville, Alabama. Three pair of identical boosters and orbiters were fabricated with one booster and one orbiter mated for a launch configuration. These models, which are shown in Figs. 1 and 2, were fabricated from a material known commercially as Stycast, a 600°F castable plastic. Hemisphere models were also cast with each MSC model to provide a means for determining the $\sqrt{\rho CK}$ for the material. All MSC test models (except the orbiter/launch configuration) were instrumented with two chromel-alumel thermocouples imbedded to a depth of one-eighth inch below the surface at midpoint bottom and top centerline. These thermocouples were used to monitor the model temperature before each run.

2.2 TEST PROCEDURE AND RUN SCHEDULE

Before each run, the Stycast models were cleaned and coated with a phase-change material known commercially as "Tempilaq." This material consists of wax crystals having calibrated melting points which are suspended in an inert, volatile, nonflammable fluid. Tempilaq, with a melt temperature of 150°F, was used on all runs. The coating was sprayed on the model. It dried in approximately one minute, leaving a dull, opaque film.

After the models were dry, the test configuration was attached to the tunnel injection mechanism at the desired test attitude. Motion picture cameras, positioned at the top and side of the test section, were set in motion when the model was injected into the airstream. The duration of each test was limited to approximately fifteen (15) seconds. Recorded data consisted of 35 mm double-frame black and white film which showed the phase-change patterns. Upon the completion of each test, the model was washed and cooled with acetone to prepare for the next test. Table 1 shows the complete run schedule with the Reynolds numbers calculated from wind tunnel conditions.

Schlieren photographs, which were made during most of the runs, are presented.

2.3 DATA REDUCTION

Surface heating rate distributions on the models were determined by measuring the time required for the surface to reach a known temperature, indicated by the observed phase change, and utilizing the solution of the transient one-dimensional heat conduction equation:

$$\frac{\partial T}{\partial t} = \frac{K}{\rho C} \frac{\partial^2 T}{\partial l^2} \quad (1)$$

Table 1
RUN CONDITIONS

Run No.	Configuration*	P _o (psig)	T _o (°F)	T _i (°F)	Pitch (deg)	Yaw (deg)	Roll (deg)	R _N (10 ⁶)	h _o (Btu/ft ² -sec°F)
429	L	110	875	79	0	0	15	—	—
430	L	110	785	80	0	0	90	—	—
431	O	—	790	83	0	0	90	—	—
432	B	—	810	80	0	0	0	—	—
433	B	—	800	80	+10	0	0	—	—
434	L	—	810	85	-10	0	0	—	—
435	L	—	855	85	+10	0	180	0.614	0.0356
436	B	—	850	84	-10	0	0	0.618	0.0356
437	O	—	860	83	+10	0	0	0.610	0.0356
438	L	—	850	81	-10	0	0	0.618	0.0356
439	B	—	835	81	0	0	0	0.630	0.0355
440	O	—	855	84	0	0	180	0.614	0.0356
441	L	—	870	82	0	0	0	0.603	0.0357
442	L	—	840	80	0	0	180	0.626	0.0356
443	B	—	900	86	+10	0	0	0.581	0.0358
444	L	110	895	86	+10	0	0	0.584	0.0358
445	L	115	850	80	+10	0	180	0.643	0.0363
446	O	115	850	86	-10	0	180	0.643	0.0363
447	L	110	835	83	0	+6	0	0.630	0.0355
448	O	110	880	79	0	+6	0	0.595	0.0358
449	B	110	875	80	0	+6	0	0.599	0.0357
450	L	110	840	82	0	-6	0	0.626	0.0356
451	O	110	840	84	0	-6	0	0.626	0.0356
452	B	110	840	84	0	-6	0	0.626	0.0356
453	O	110	825	84	+20	0	0	0.638	0.0355
454	O	410	875	82	+20	0	0	2.04	0.0659
455	O	430	865	84	+30	0	0	2.16	0.0674
456	O	110	825	80	+30	0	0	0.638	0.0355
457	S	110	810	82	0	0	0	0.651	0.0354
458	S	110	825	82	0	0	0	0.638	0.0355
459	S	110	815	82	0	0	0	0.647	0.0355
460	L	805	925	83	0	0	15	3.70	0.0922
461	L	800	910	83	+5	0	0	3.74	0.0917
462	L	820	935	81	-5	0	0	3.73	0.0931
463	O	110	825	83	-20	0	0	0.638	0.0355
464	O	420	920	80	-20	0	0	1.98	0.0671

* L Launch
B Booster
O Orbiter
S Sphere

To solve this equation a set of boundary conditions which most nearly describes the actual tunnel test was used. In this case the boundary conditions are:

$$T(l, 0) = T_i$$

$$T(\infty, t) = T_i$$

$$\frac{\partial T(0, t)}{\partial l} = \frac{h}{K} [T_{AW} - T(0, t)] \quad (2)$$

Coating temperature and model surface temperature were initially assumed to be identical. The solution of the above equation yields the test time required for the surface temperature to reach T_{pc} , the coating melt temperature. Other assumptions are:

1. Depth of heat penetration into the model is small compared with the Stycast thickness so that the model acts like a semi-infinite slab.
2. The model is initially isothermal.
3. The surface is subjected to an instantaneous step in aerodynamic heating at time zero and the heat transfer coefficient does not vary with time.
4. The product of model thermal conductivity, density, and specific heat does not vary with temperature.

The solution of the transient one-dimensional heat conduction equation with stated boundary conditions is:

$$\bar{T} = \frac{T_{pc} - T_i}{T_{AW} - T_i} = 1 - e^{\beta^2} \operatorname{erfc} \beta \quad (3)$$

where

$$\beta = \frac{h \sqrt{t}}{\sqrt{\rho CK}} \quad (4)$$

To minimize errors due to nonuniform heating rates encountered while the model passes through the tunnel boundary layer and errors in determining the test time, the time required for the phase change to occur should be large compared with the time from initial exposure of the model until steady flow is established. However, the time required for the phase change to occur must be short compared with the thermal diffusion time of the model wall. The thermal diffusion time is given approximately by the expression (Ref. 1):

$$t \approx \frac{0.2l^2}{\alpha} \quad (5)$$

This expression was obtained by assuming a cubic distribution of temperature with depth in a slab subjected to an instantaneous applied constant heat transfer rate at one surface and solving for the time for which a significant change in temperature occurs at a depth l . For the NASA-MSC models made from Stycast, the assumption that the model acts as a semi-infinite slab is valid for all test times encountered only for the fuselages. The wings and fins were very thin. To illustrate data validity, a plot of thermal diffusion time versus depth of penetration is given in Fig. 3. This plot shows thicknesses and corresponding melt times for which the data are valid or invalid. For a given depth, the data are invalid if the melt time is to the right of the curve. The case then would require a finite-slab solution with two heat inputs. Depending upon the depth and magnitude of heat inputs, large errors can be encountered if the data are reduced by a semi-infinite slab solution.

The model thermal property, $\sqrt{\rho CK}$, is required to reduce the heating data by the semi-infinite slab heat conduction solution. The density, specific heat, and thermal conductivity of one of two representative samples of Stycast have been measured by NASA-Langley for Lockheed under a different contract. It was assumed that density and specific heat did not vary from batch to batch. The variation in thermal conductivity was determined by

comparing the heat transfer rate through a slab cast from each batch with that measured on a sample whose thermal conductivity had been measured. These tests were performed by using a NASA-Langley apparatus which incorporates a heat meter to measure the heat transfer rate through a 0.5-in. thick specimen when the two faces are exposed to a known temperature differential. The thermal conductivity tests of the model material gave a value for $\sqrt{\rho CK}$ of 0.0622 Btu/ft²sec ^{$\frac{1}{2}$} -°R.

To provide another means for obtaining the value of $\sqrt{\rho CK}$, three hemispherical models were fabricated and tested as indicated in Table 1. Stagnation point heat transfer coefficients for the three spheres were calculated for their respective run conditions, by the method as outlined in Ref. 2. A similarity boundary layer solution was used with a Newtonian pressure distribution to obtain the heat transfer coefficients at scribe marks located on the hemispheres. By using these values of h , the value of $\sqrt{\rho CK}$ was found by using Eq. (4) and the times at which the phase change occurred at the scribe marks. This procedure was followed to check the measured value of $\sqrt{\rho CK}$. The average value of $\sqrt{\rho CK}$ so determined was 0.060 Btu/ft²sec ^{$\frac{1}{2}$} -°R. This value was used to reduce all data for the NASA-MSC models. The method has also been used in previous test programs as discussed in Refs. 3 and 4. Consistently, a value of approximately 0.062 was obtained through several batches of models.

To limit the number of errors made in producing and interpolating curves for the heat transfer coefficients, a digital computer program had been written previously to reduce phase change data. The run conditions are read in; the correct \bar{T} and β are calculated with h being output directly as a function of time required to melt.

The Fay and Riddell method for calculating the stagnation point heat transfer coefficient to a sphere was programmed and values calculated for each run. The equations on the following page were used:

$$h_s = \frac{0.94(\rho_w \mu_w)^{0.1} (\rho_o \mu_o)^{0.4} \sqrt{B} (H_o - H_w)}{(T_o - T_w)} \quad (6)$$

where

H_o = total enthalpy

H_w = wall enthalpy

$$B = \frac{1}{R_n} \left(2 g_c \left(\frac{P_o - P_\infty}{\rho_o} \right) \right)^{\frac{1}{2}}.$$

The values of h/h_s were calculated and output for each case as a function of time required to melt.

2.4 TEST RESULTS

A Telereadax machine at NASA-MSFC was used to draw melt contours for all runs, except Runs 429 through 434. Data for these runs were invalid because of camera failure. Repeat runs were made. In these runs, each melt contour represents an isotherm or constant heat transfer coefficient.

The data are presented as ratios of local heat transfer coefficient based on the stagnation conditions for that run and calculated with a nose radius of 0.005 feet.

Figures 4 through 30 present the upper and/or lower surface contours for Runs 435 through 464. Figures 31 through 57 present the side panel surface contours for Runs 435 through 464.

Wing chordwise heat transfer distributions for several spanwise locations are presented in Figs. 58 through 68. Those runs whose test conditions varied such that meaningful comparisons could be made are presented.

Lockheed-Huntsville's experience with phase change testing, indicate that there is a breakdown in the assumptions of the data reduction procedure used on certain portions of the wings. Certain portions of the wings cannot

be treated as a semi-infinite slab. A finite slab data reduction procedure must be used to calculate the heat transfer coefficients. This would require a new data reduction technique development and was considered beyond the task assignments of this contract. All data presented was reduced with the semi-infinite slab solution.

Figures 69 through 83 present schlieren photographs taken during the test series.

2.5 RECOMMENDATIONS

One test program ordinarily does not provide all data needed for a complete analysis of a space vehicle configuration. Data are obtained, surveyed, and analyzed; and additional test programs are usually required, which are designed to obtain very specific information.

Much data were obtained on this NASA-MSC test program, as results indicate; however, there are regions on the model surface where heat transfer data are lacking or cannot be reduced by the semi-infinite slab solution. The phase-change technique has limitations and models and test procedures must be designed around these limitations. Models used in the test program performed extremely well and remain in excellent condition so that they could be used in other tests. Based on the results of this test program the following items are recommended for consideration:

- Conduct heat transfer tests on the NASA-MSC configuration with lower melt temperatures and increased tunnel conditions.
- Conduct shock impingement heat transfer tests on the NASA-MSC launch configuration, utilizing the mated model configuration and a separate orbiter and booster. Staging maneuvers could be simulated with a correct sting arrangement.
- Investigate data reduction errors due to model thickness effects. Develop a data reduction program that will solve the finite slab solution with heat inputs to both surfaces. Such a program could be expanded to account for surface gradients.
- Conduct oil flow tests with silicone oils and zinc oxide. Such information would provide insight to shock impingement, flow separation, and streamline divergence.

Complete detailed recommendations will be forthcoming in a Lockheed-Huntsville document.

REFERENCES

1. Jones, R. A., and J. L. Hunt, "Use of Fusible Temperature Indicators for Obtaining Quantitative Aerodynamic Heat Transfer Data," NASA TR-R-230, 1966.
2. Connor, L. E., "Heat Transfer Tests of the Lockheed Space Shuttle Orbit Configuration Conducted at the Langley Research Center Mach 8 Variable Density Tunnel," LMSC/HREC D149470, Lockheed Missiles & Space Company, Huntsville, Ala., December 1969.
3. Connor, L. E., V. W. Sparks, and A. G. Bhadsavle, "Heat Transfer Tests of the NASA-MSFC Space Shuttle Booster at the Langley Research Center Hypersonic Continuous Flow Facility," LMSC/HREC D162722, Lockheed Missiles & Space Company, Huntsville, Ala., December 1970.
4. Reshotko, E. and C. B. Cohen, "Heat Transfer at the Forward Stagnation Point of Blunt Bodies," NACA TN-3513, 1955.

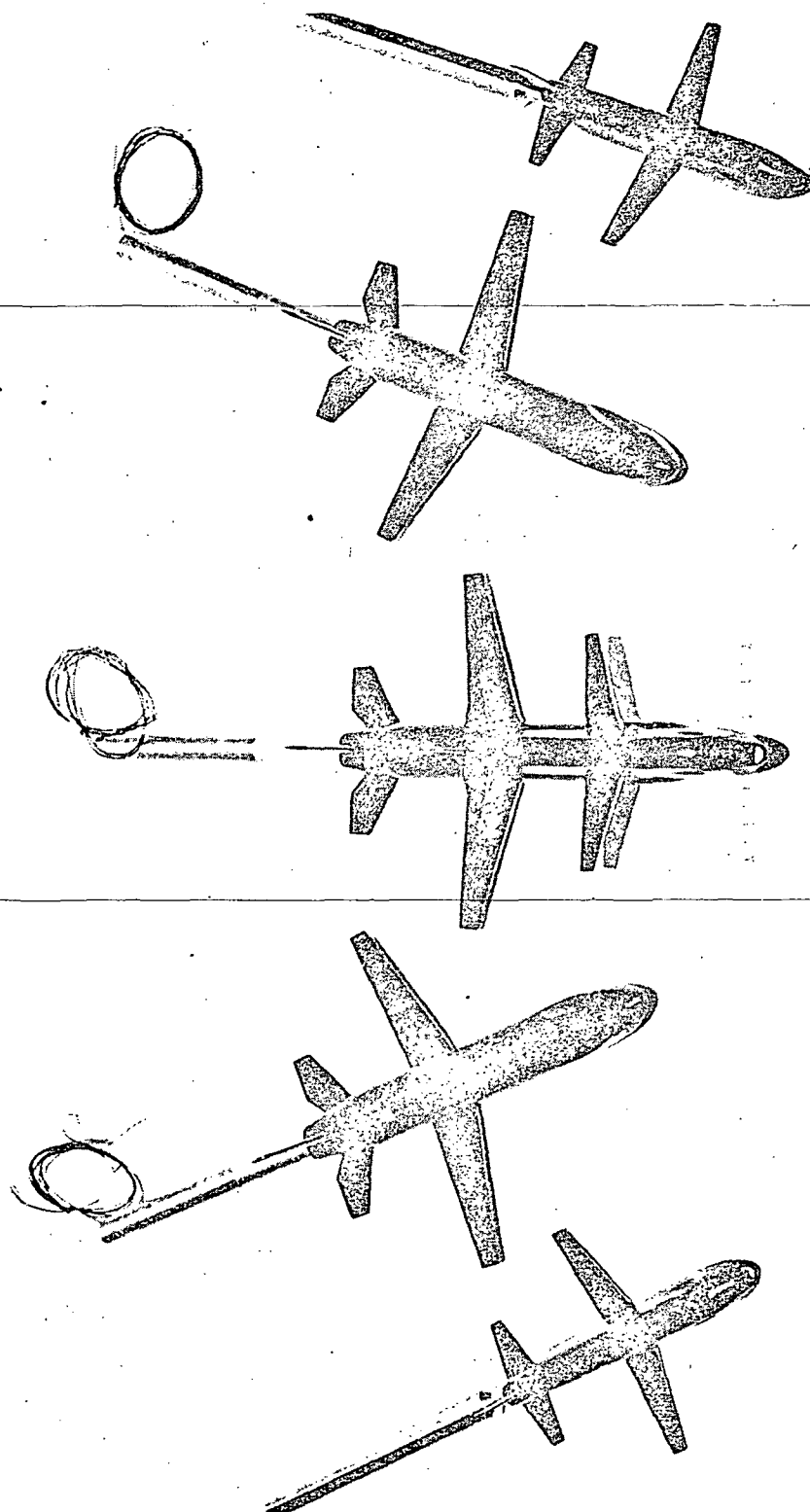


Fig. 1 - NASA-Manned Spacecraft Center Space Shuttle Heat Transfer Models

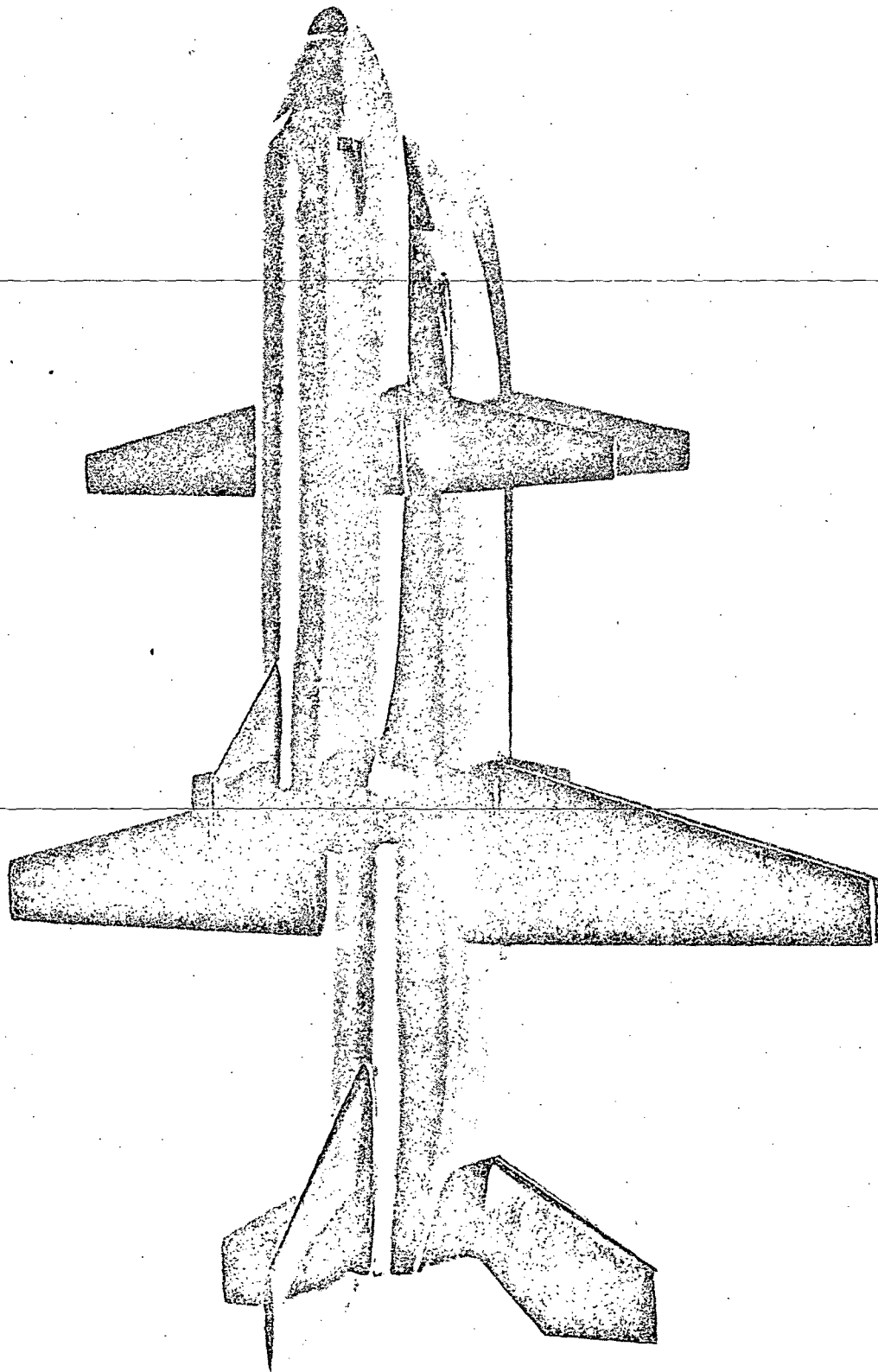


Fig. 2 - NASA-Manned Spacecraft Center Space Shuttle Launch Configuration

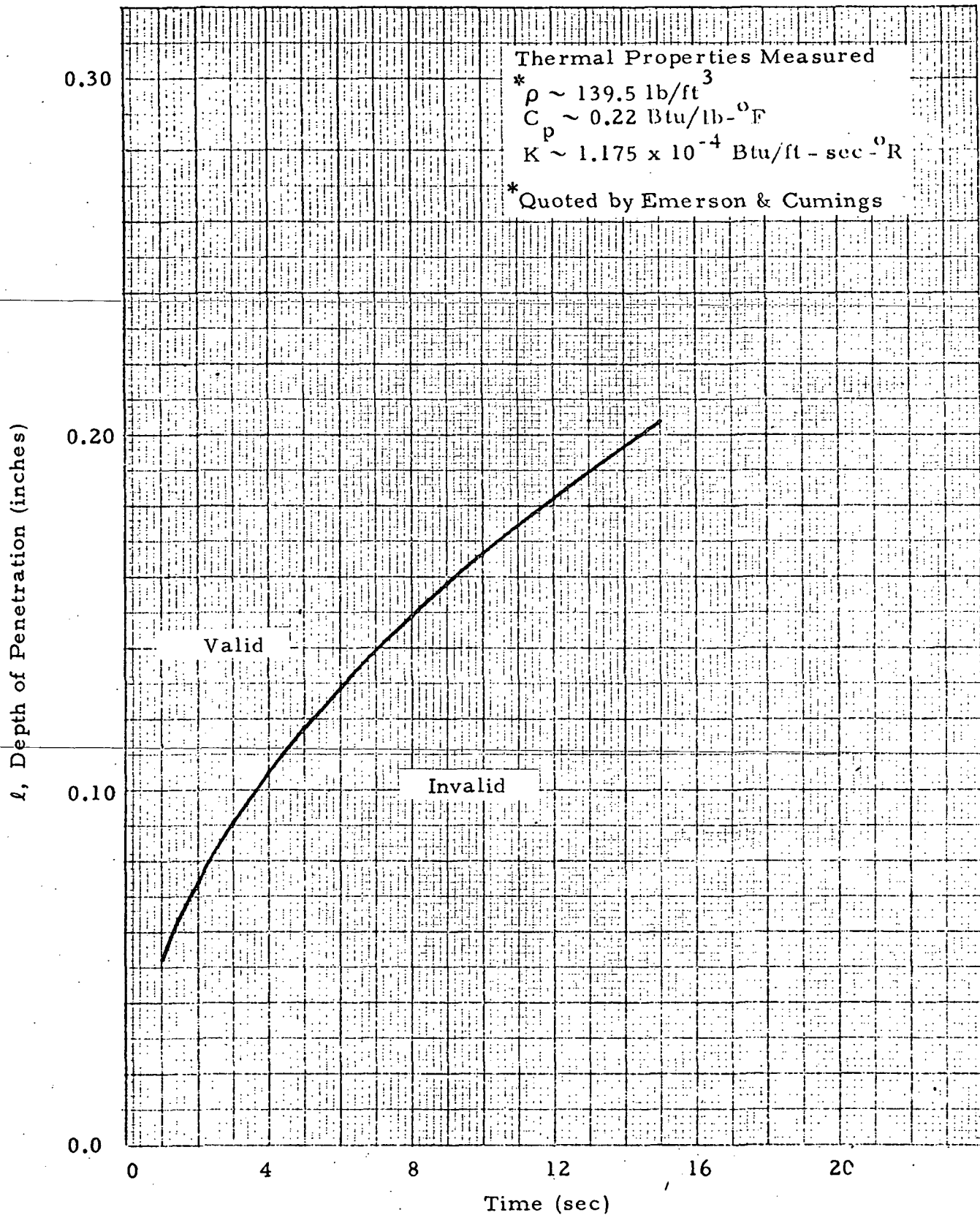
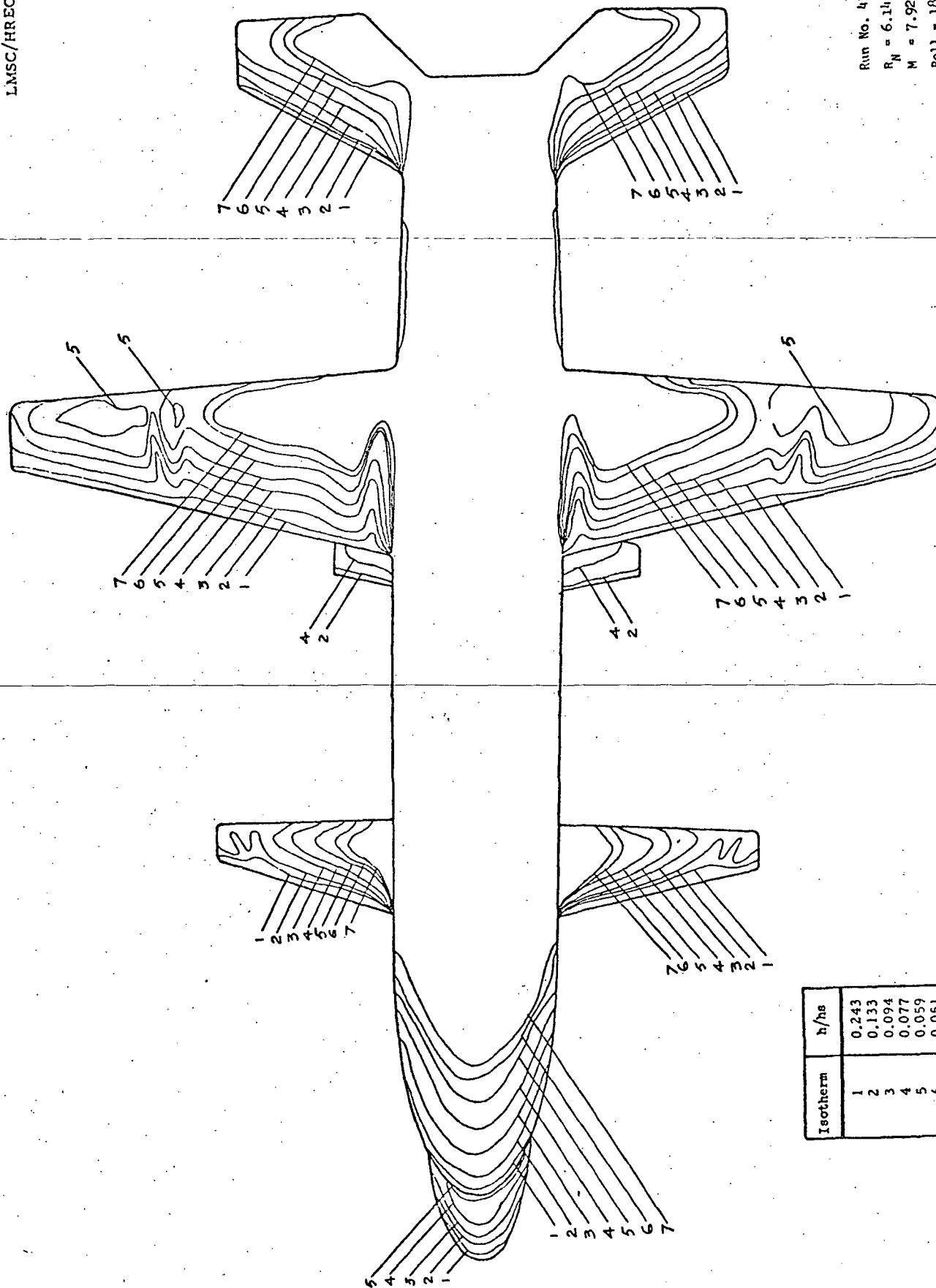
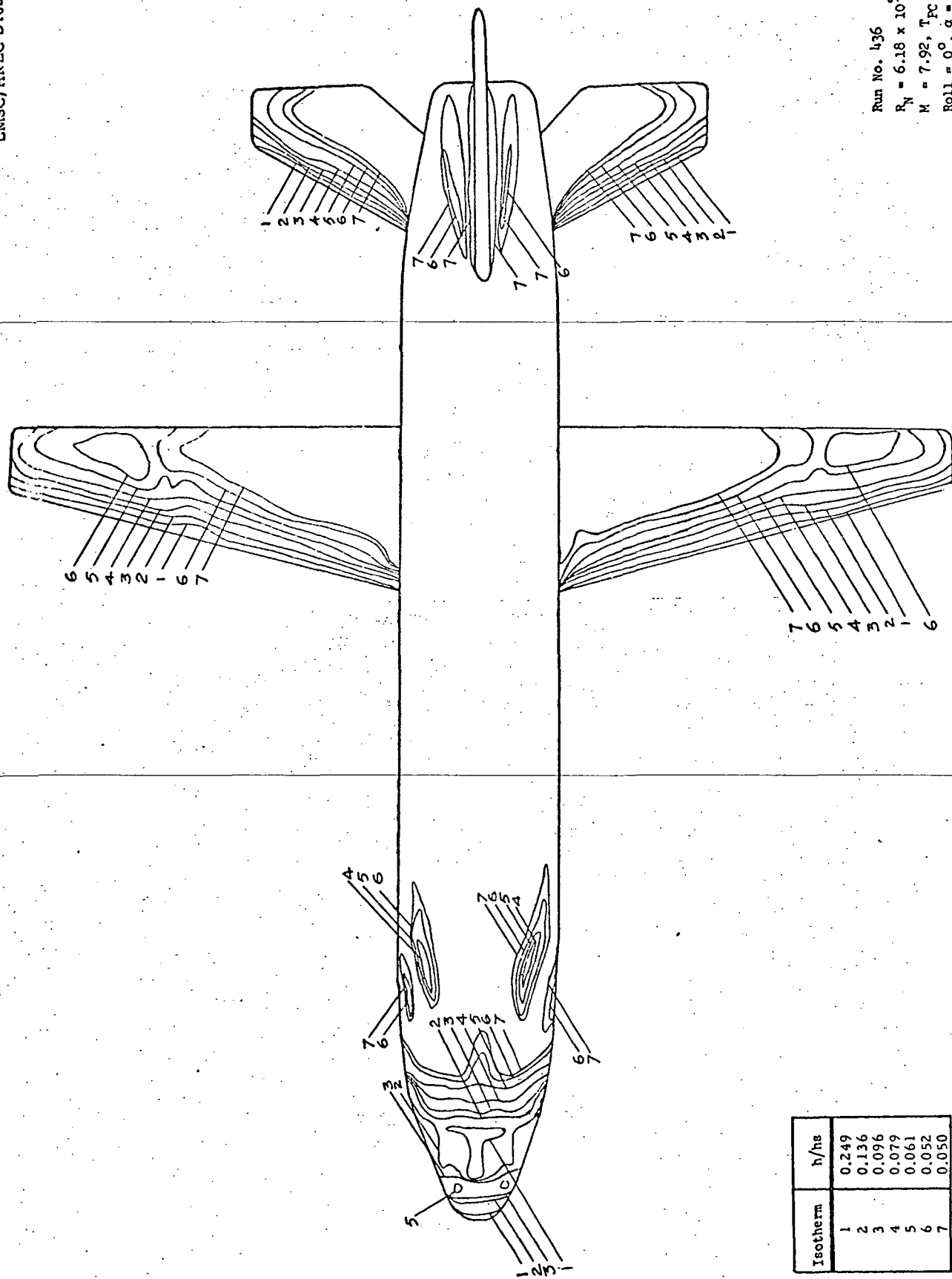


Fig. 3 - Thermal Diffusion Time vs Depth of Penetration for Stycast Used in NASA-MSC Heat Transfer Models



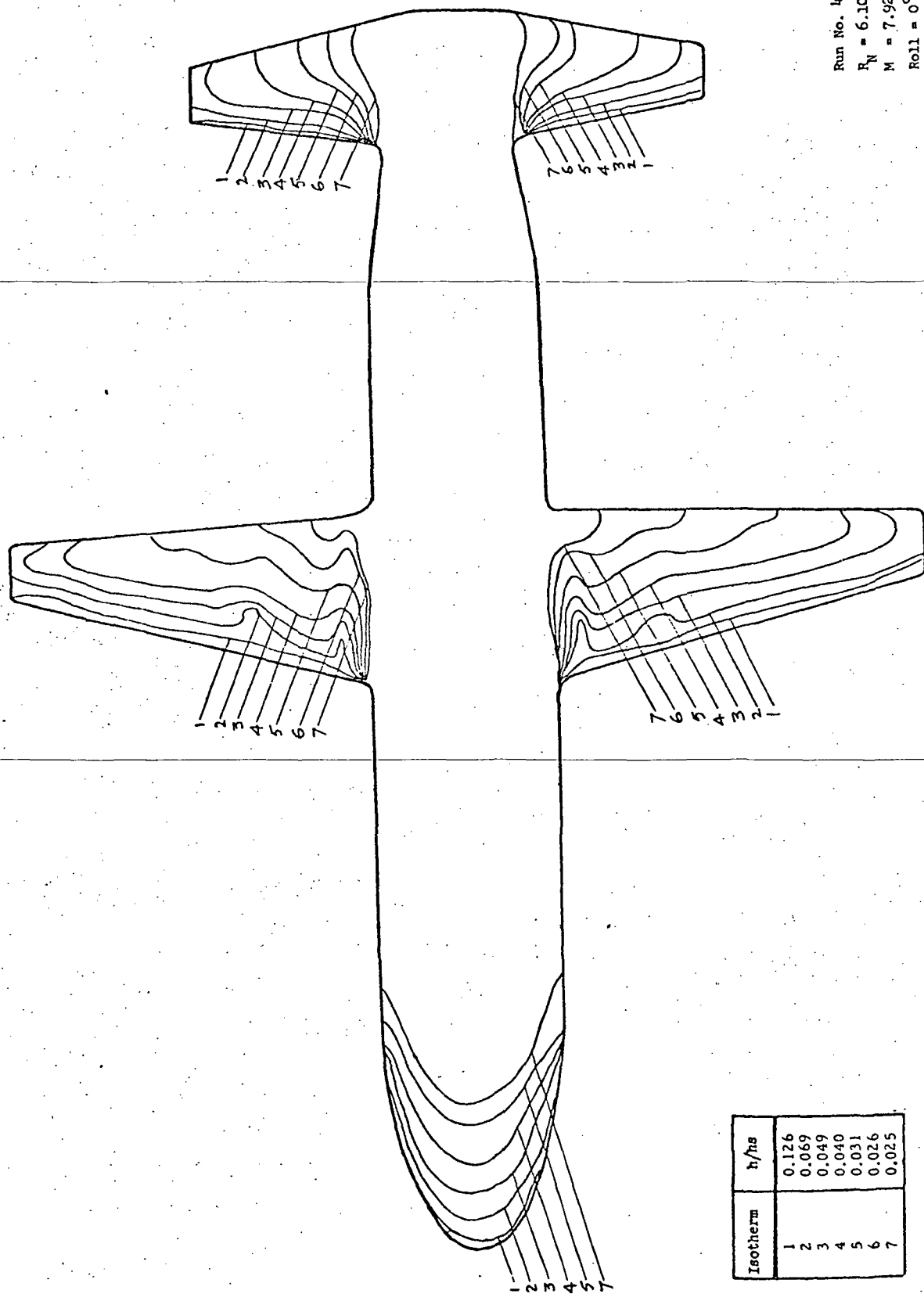
Run No. 435
 $R_N = 6.14 \times 10^5$ 1/Ft
 $M = 7.92$, $T_{TC} = 150^\circ F$
 $Roll = 180^\circ$, $\alpha = 10^\circ$
 Launch Config., Bottom View

Fig. 4 - Lower Surface Local to Stagnation Point Heat Transfer Coefficients



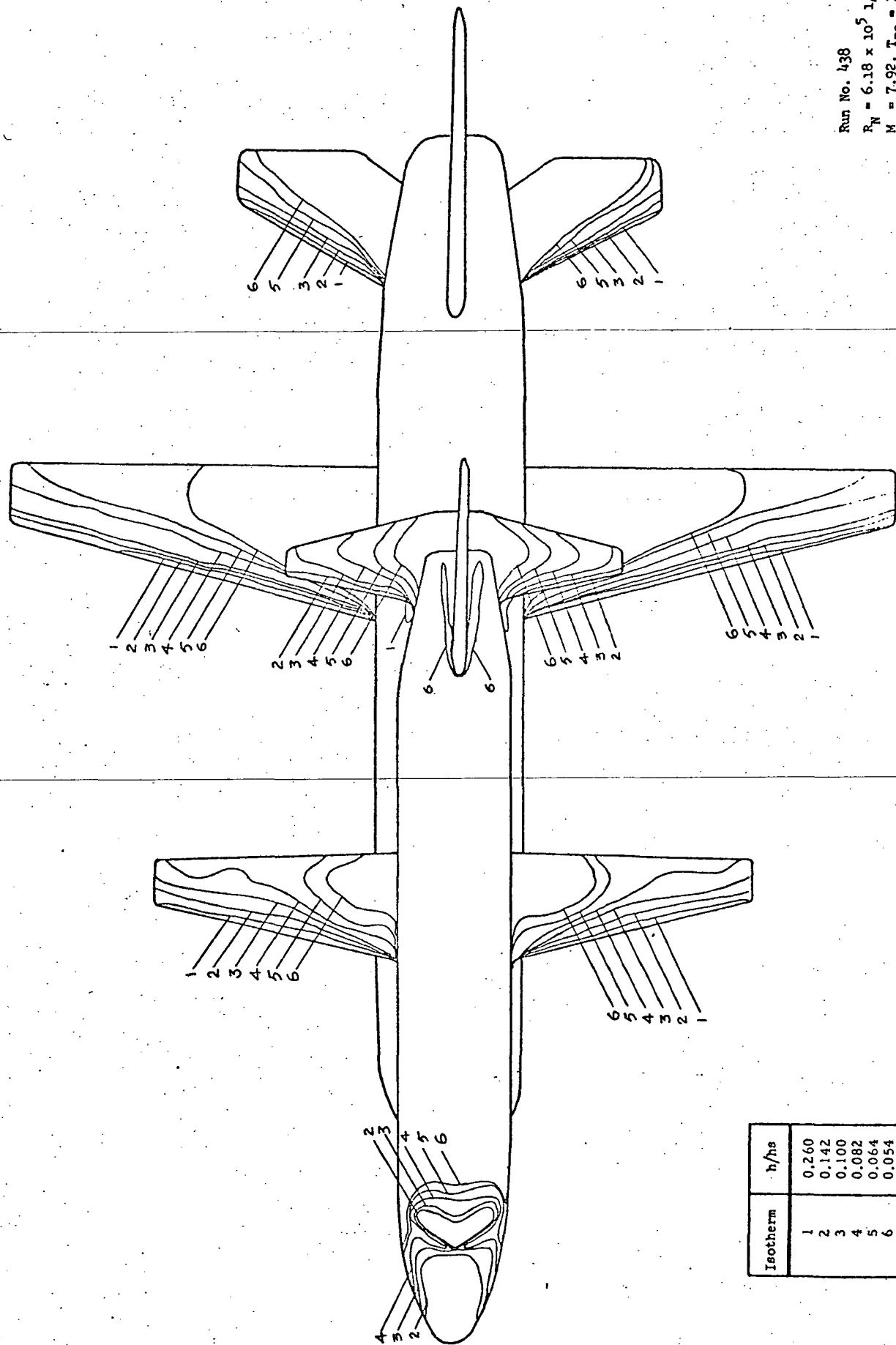
Run No. 436
 $R_N = 6.18 \times 10^5 \text{ 1/ft}$
 $M = 7.92, T_{PC} = 150^\circ\text{F}$
 $\text{Roll} = 0^\circ, \alpha = -10^\circ$
 Booster, Top View

Fig. 5 - Upper Surface Local to Stagnation Point Heat Transfer Coefficients



Run No. 437
 $R_N = 6.10 \times 10^5$ 1/Ft
 $M = 7.92$, $T_{PC} = 150^\circ\text{F}$
 $\text{Roll} = 0^\circ$, $\alpha = 10^\circ$
 Orbiter, Bottom View

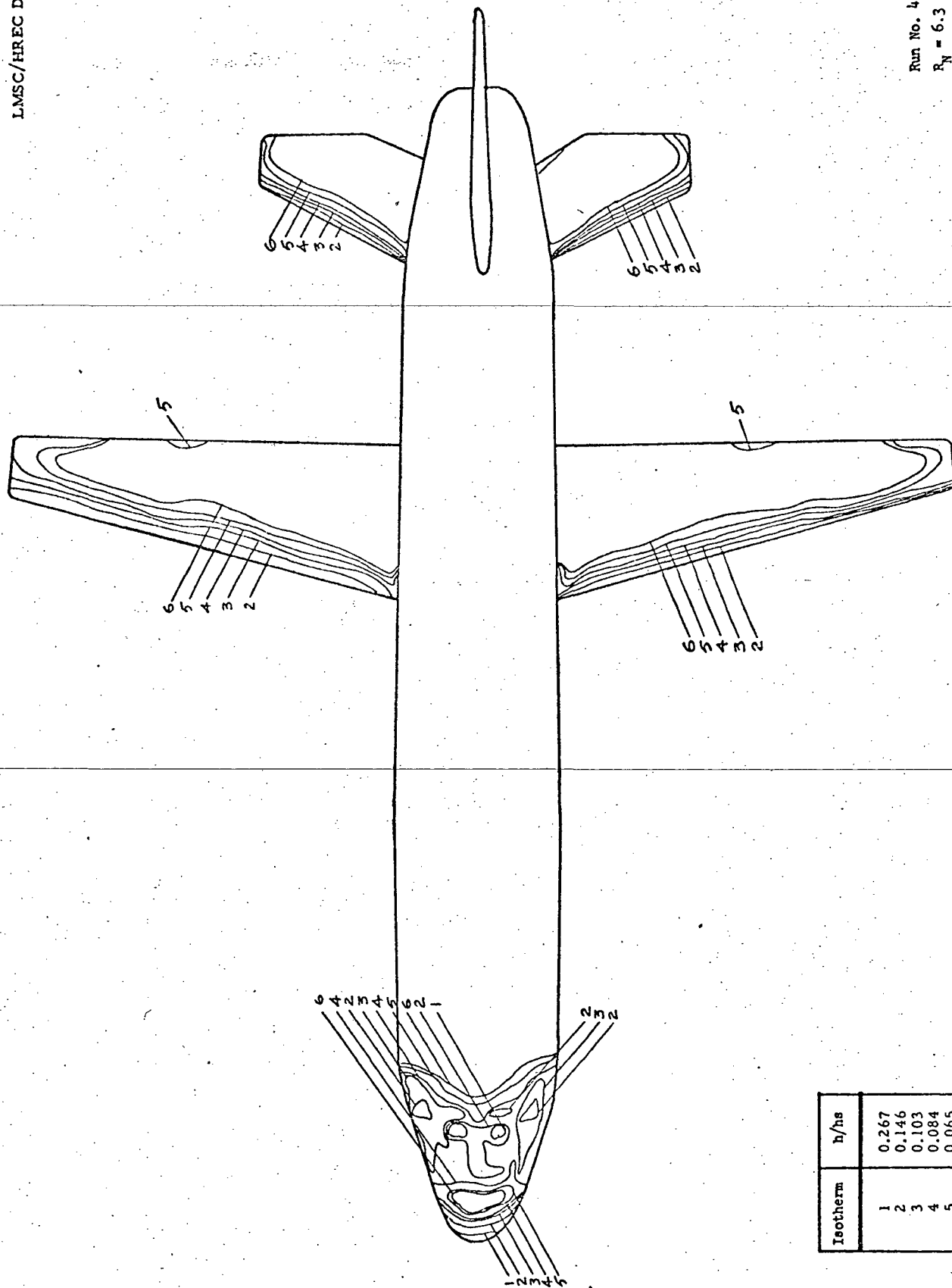
Fig. 6 - Lower Surface Local to Stagnation Heat Transfer Coefficients



Isotherm	h/h_s
1	0.260
2	0.142
3	0.100
4	0.082
5	0.064
6	0.054

Run No. 438
 $R_N = 6.18 \times 10^5 \text{ 1/Ft.}$
 $M = 7.92, T_{PC} = 150^\circ\text{F}$
 $\text{Roll} = 0^\circ, \alpha = -10^\circ$
 Launch Config., Top View

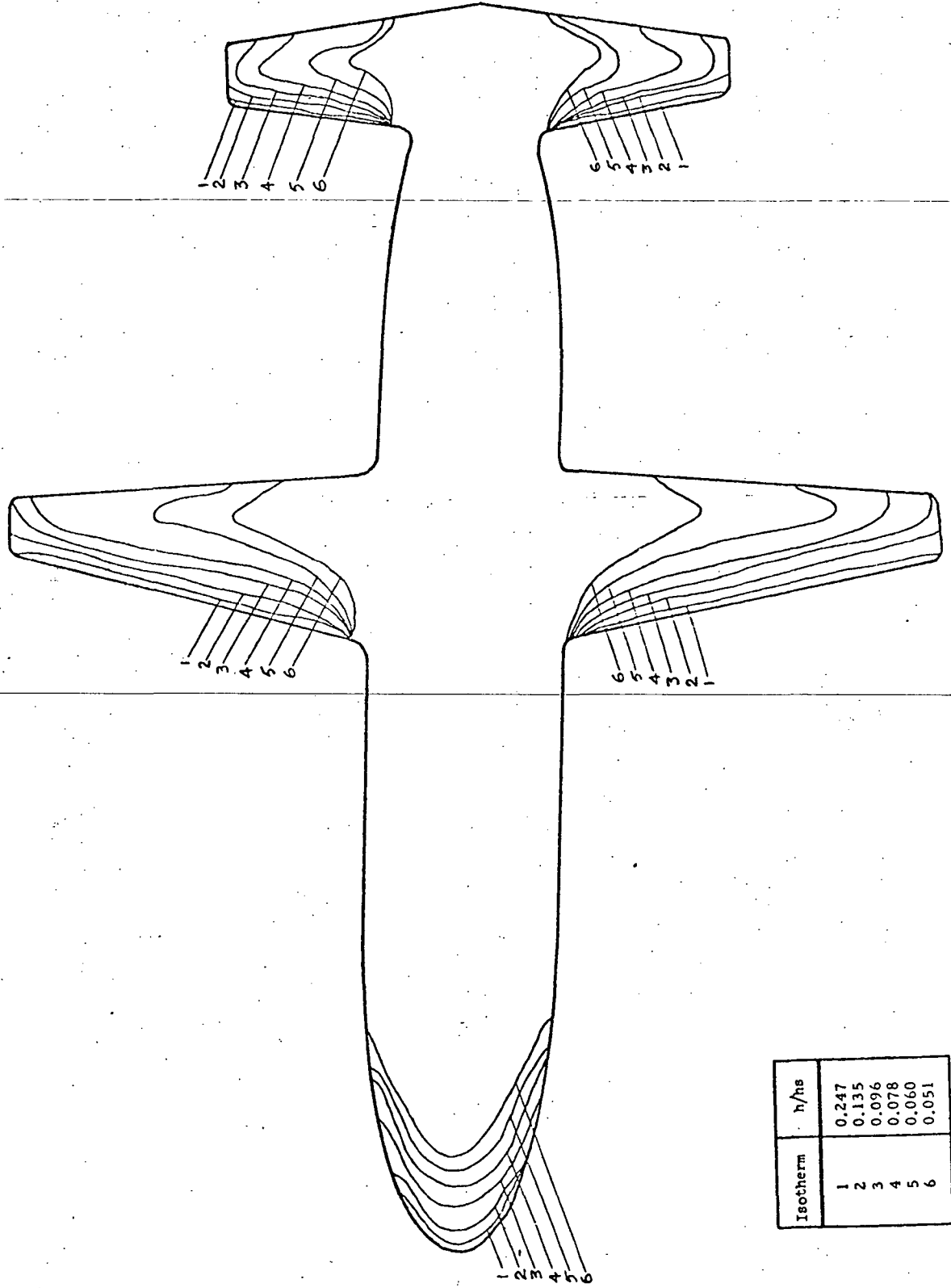
Fig. 7 - Upper Surface Local to Stagnation Point Heat Transfer Coefficients



Isotherm	h/h_s
1	0.267
2	0.146
3	0.103
4	0.084
5	0.065
6	0.056

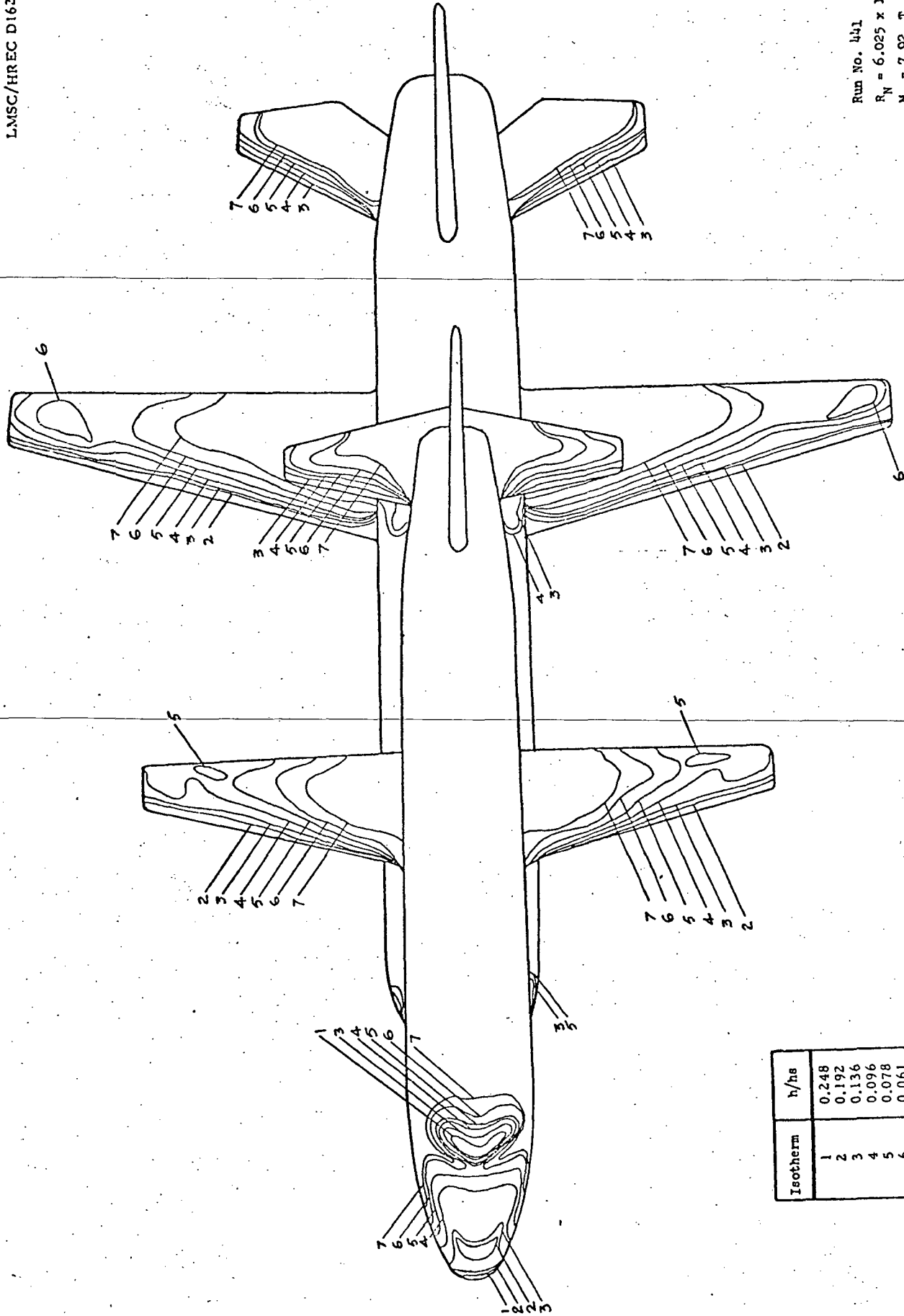
Run No. 439
 $P_N = 6.3 \times 10^5 \text{ l/Ft}$
 $M = 7.92, T_{PC} = 150^\circ\text{F}$
 $\text{Roll} = 0^\circ, \alpha = 0^\circ$
 Booster, Top View

Fig. 8 - Upper Surface Local to Stagnation Point Heat Transfer Coefficients



Run No. 440
 $R_N = 6.14 \times 10^5 \text{ 1/Ft}$
 $M = 7.92, T_{PC} = 150^\circ F$
 $\text{Roll} = 180^\circ, \alpha = 0^\circ$
 Orbiter, Bottom View

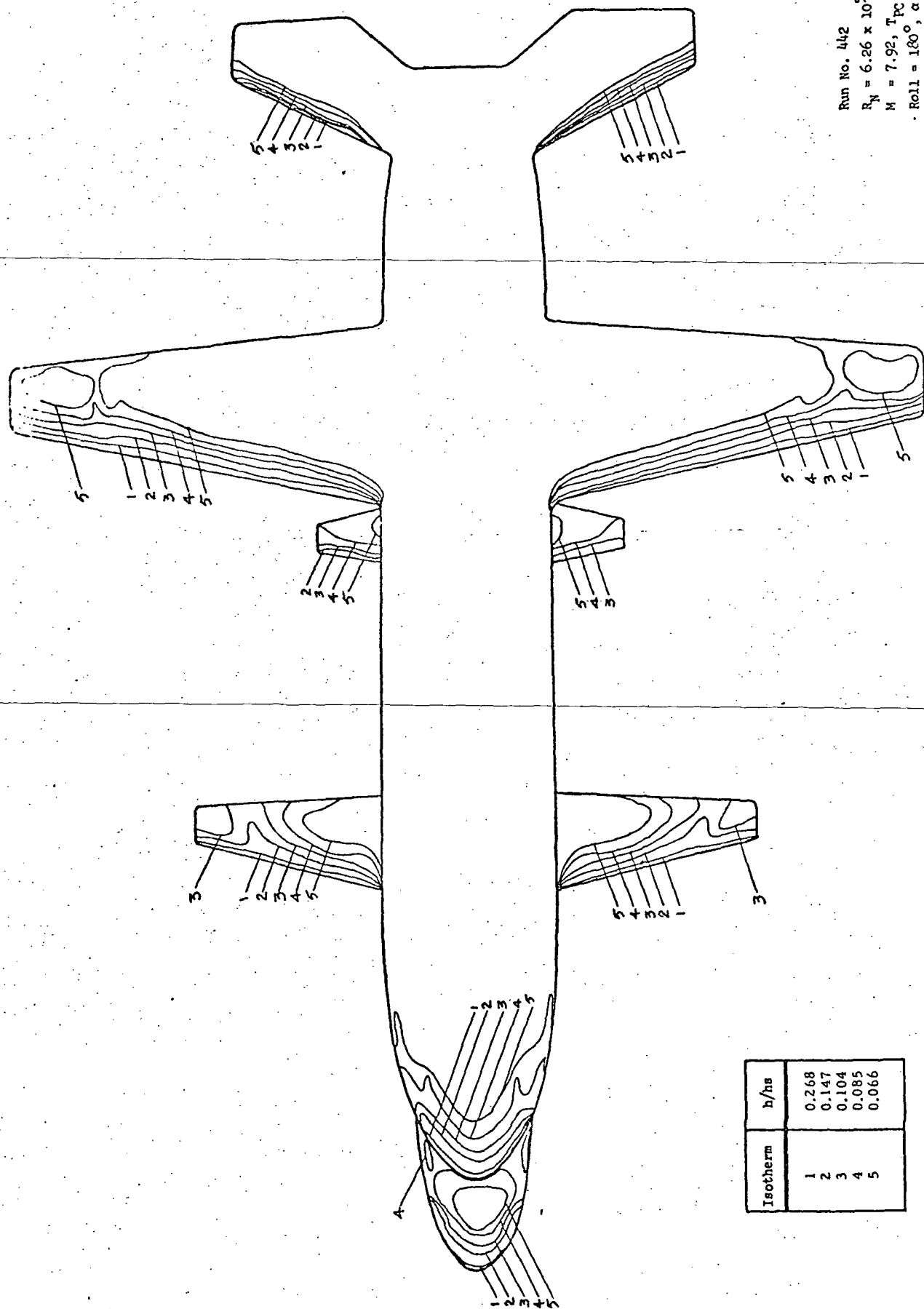
Fig. 9 - Lower Surface Local to Stagnation Point Heat Transfer Coefficients



Isotherm	h/h_s
1	0.248
2	0.192
3	0.136
4	0.096
5	0.078
6	0.061
7	0.052

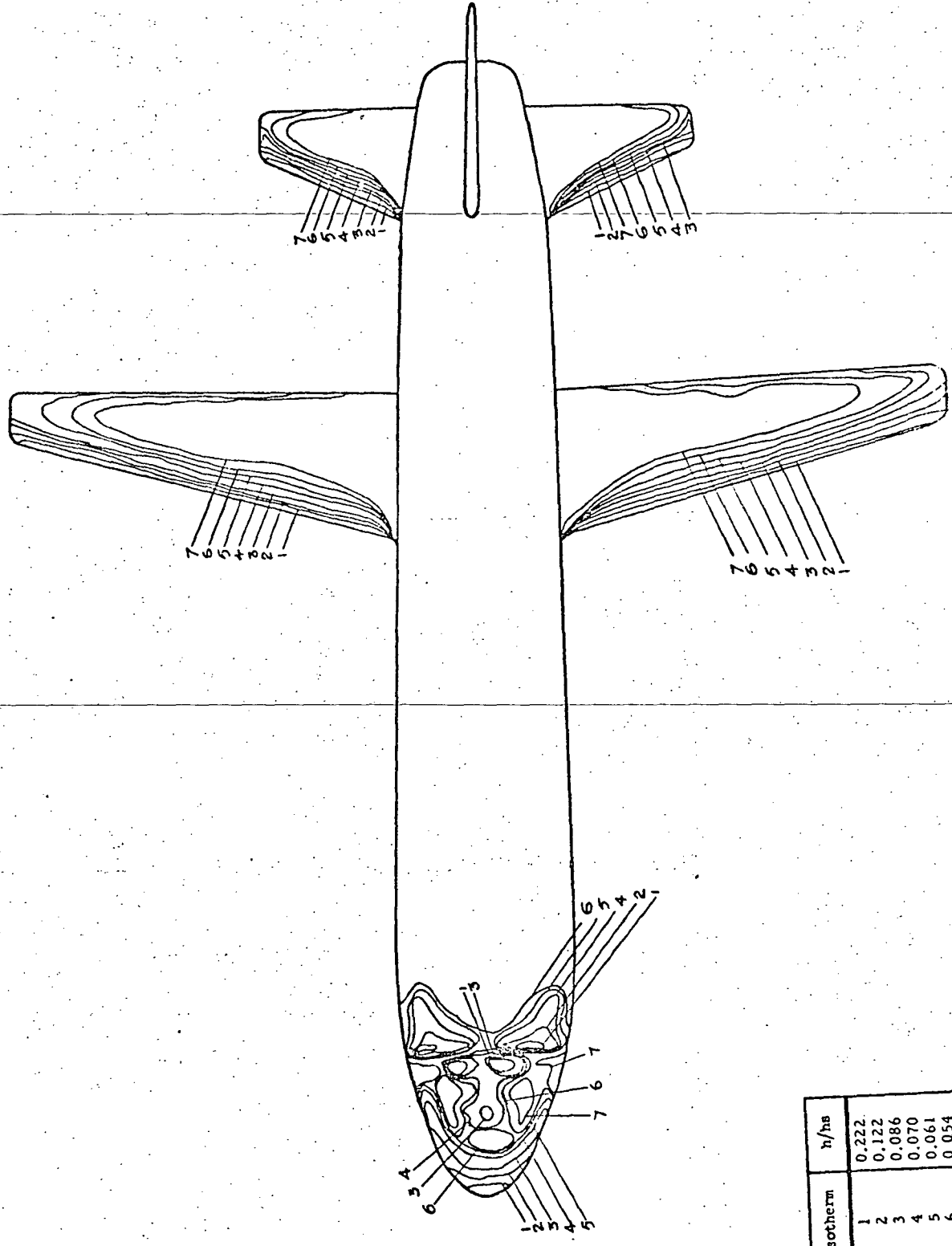
Run No. 441
 $R_N = 6.025 \times 10^5 \text{ 1/ft}$
 $M = 7.92, T_{PC} = 150^\circ\text{F}$
 $\text{Roll} = 0^\circ, \alpha = 0^\circ$
 Launch Config., Top View

Fig. 10 - Upper Surface Local to Stagnation Point Heat Transfer Coefficient



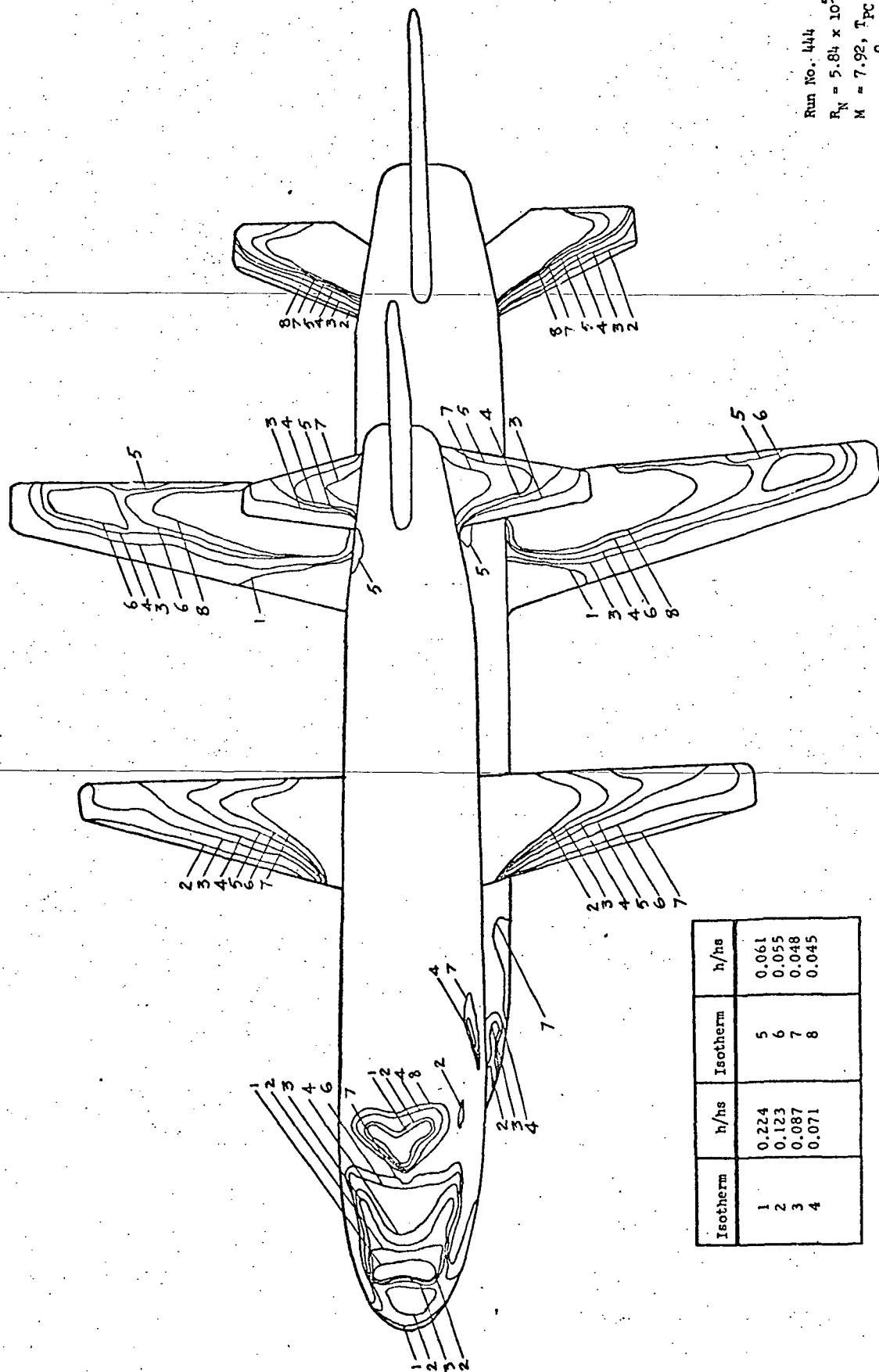
Run No. 442
 $R_N = 6.26 \times 10^5$ 1/ft
 $M = 7.92$, $T_{PC} = 150^\circ\text{F}$
 Roll = 180° , $\alpha = 0^\circ$
 Launch Config., Bottom View

Fig. 11 - Lower Surface Local to Stagnation Point Heat Transfer Coefficients



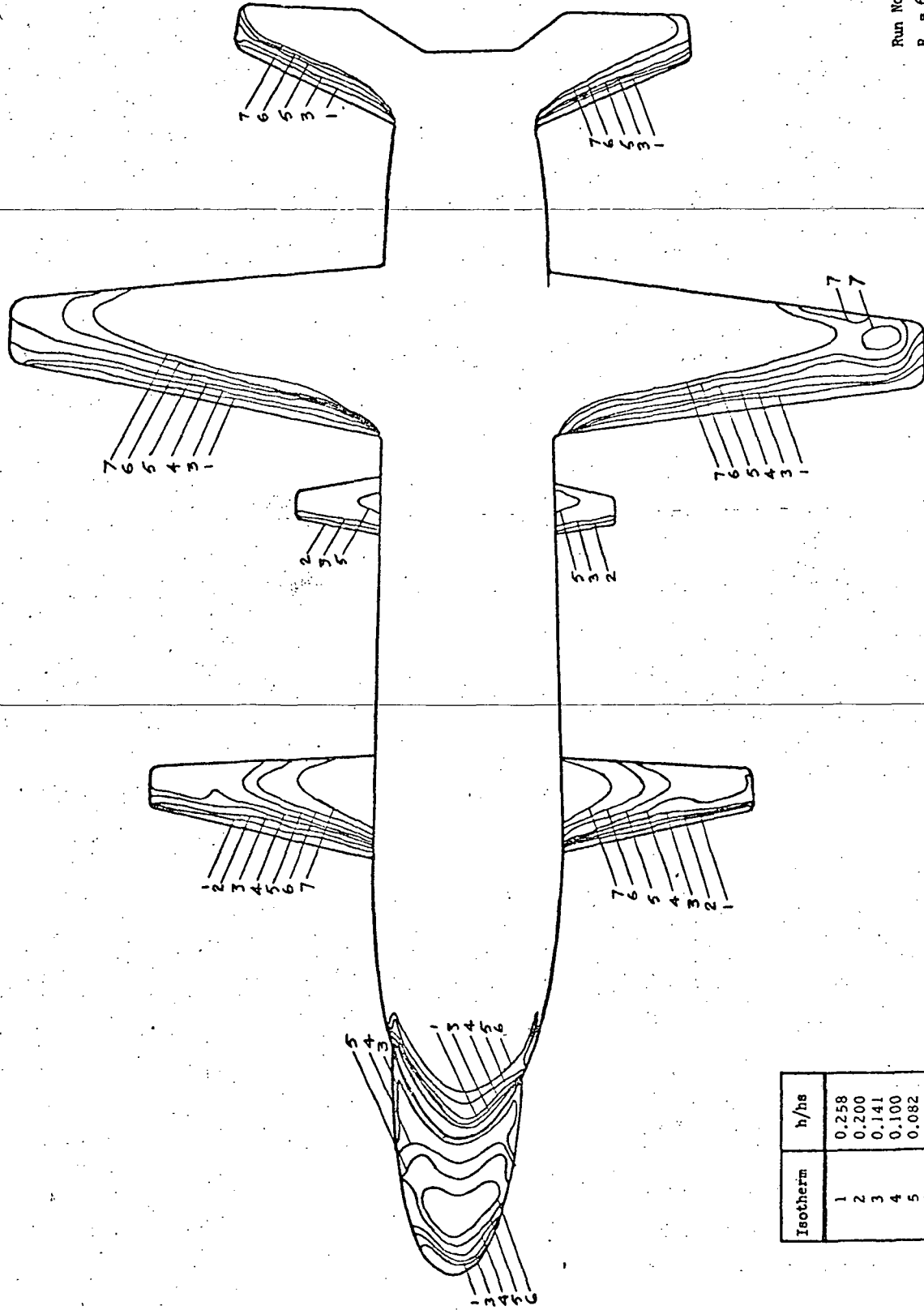
Run No. 443
 $R_N = 5.8 \times 10^5$
 $M = 7.92$, $T_{PC} = 150^\circ F$
 Roll = 0° , $\alpha = 10^\circ$
 Booster, Top View

Fig 12 - Inner Surface Local to Stagnation Point Heat Transfer Coefficients



Run No. 444
 $R_N = 5.84 \times 10^5$ 1/Ft
 $M = 7.92$, $T_{PC} = 150^\circ F$
 $Roll = 0^\circ$, $\alpha = 10^\circ$
 Launch Config., Top View

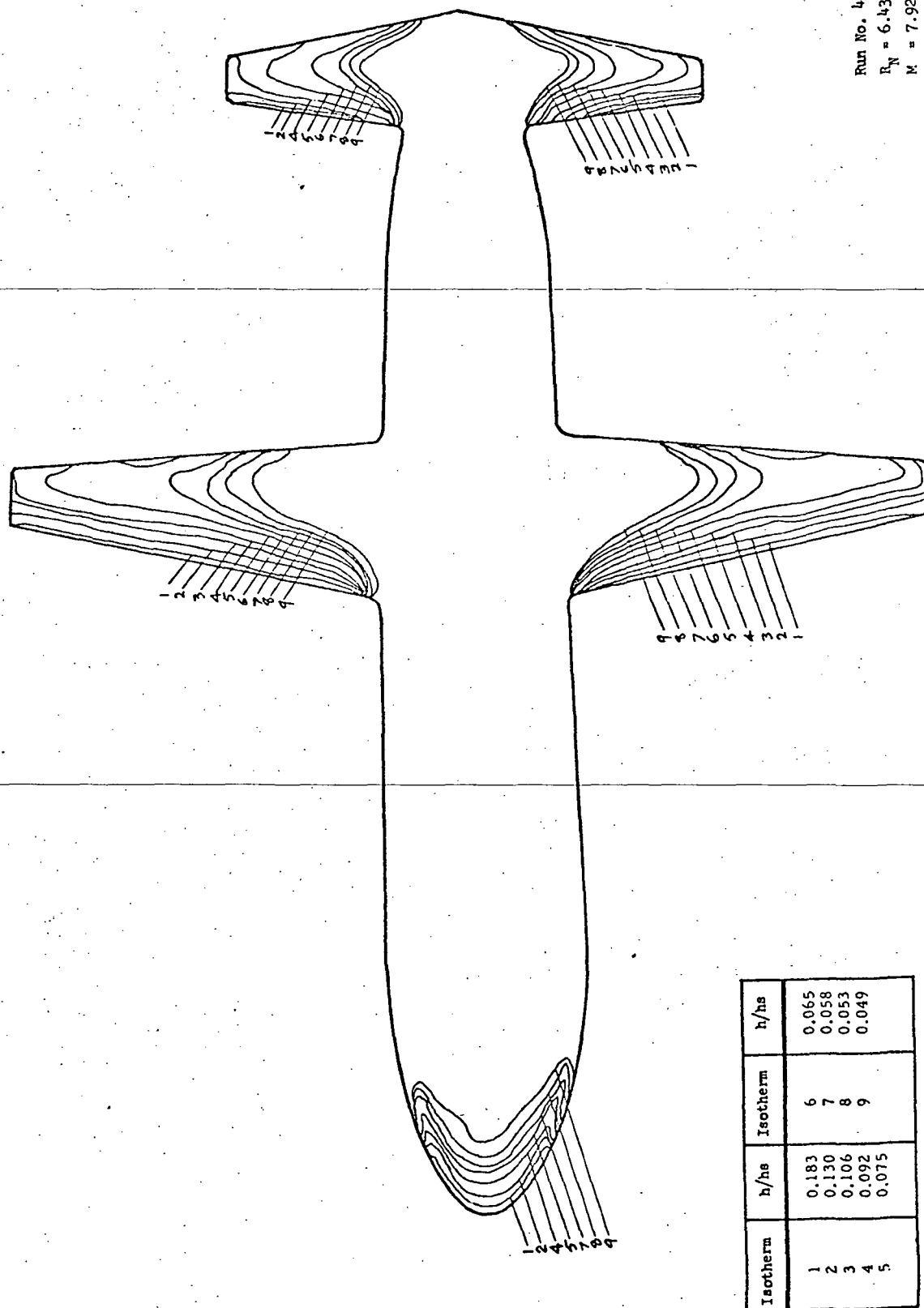
Fig. 13 - Upper Surface Local to Stagnation Point Heat Transfer Coefficients



Isotherm	h/h_s
1	0.258
2	0.200
3	0.141
4	0.100
5	0.082
6	0.071
7	0.058

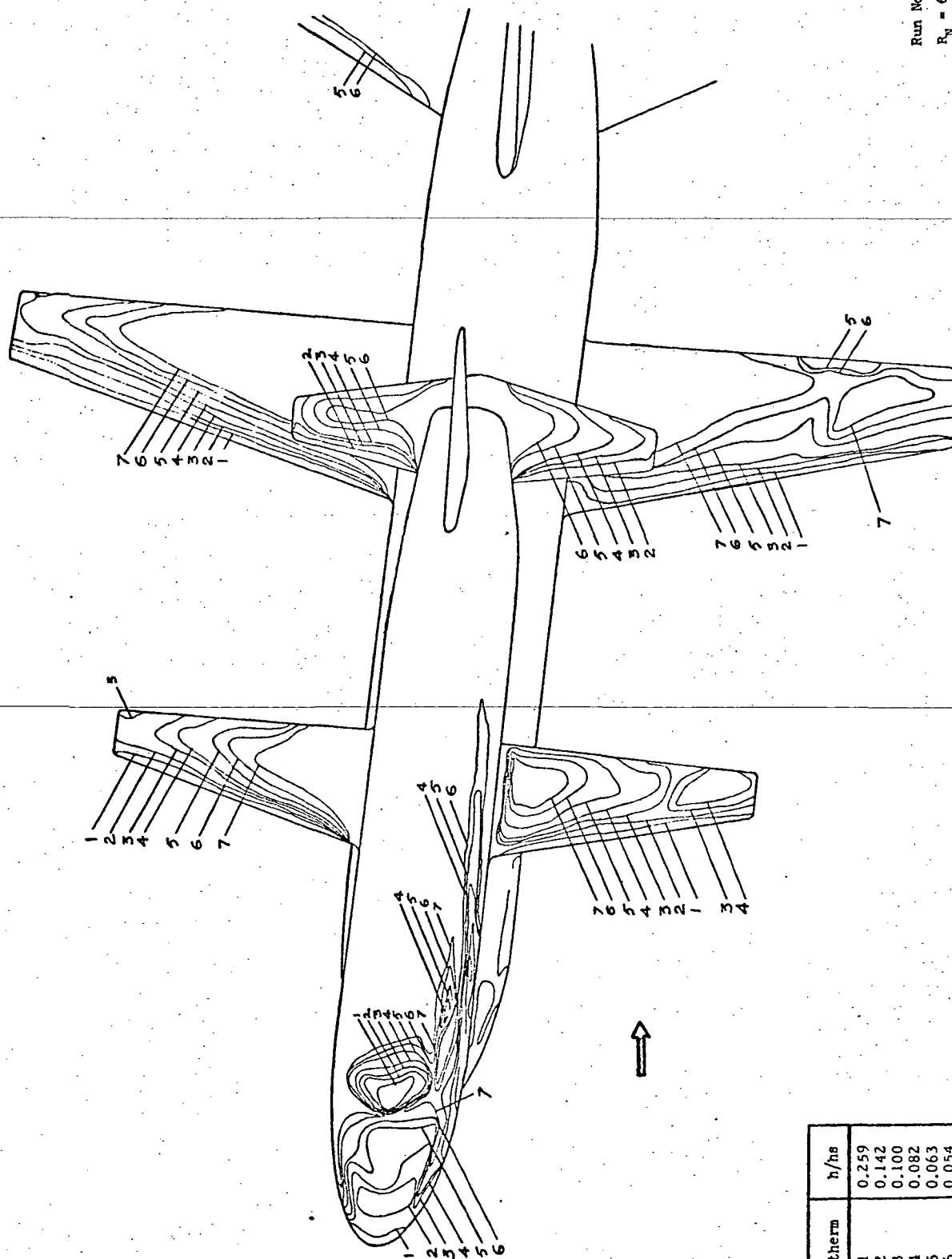
Run No. 445
 $R_N = 6.43 \times 10^5 \text{ 1/ft}$
 $M = 7.92, T_{PC} = 150^\circ\text{F}$
 $\text{Roll} = 180^\circ, \alpha = -10^\circ$
 Launch Config., Bottom View

Fig. 14 - Lower Surface Local to Stagnation Point Heat Transfer Coefficients



Run No. 446
 $R_N = 6.43 \times 10^5 \text{ l/ft}$
 $M = 7.92, T_{PC} = 150^\circ P$
 $\text{Roll} = 180^\circ, \alpha = -10^\circ$
 Orbiter, Bottom View

Fig. 15 - Lower Surface Local to Stagnation Point Heat Transfer Coefficients



Isotherm	h/h_s
1	0.259
2	0.142
3	0.100
4	0.082
5	0.063
6	0.054
7	0.052

Run No. 447
 $P_N = 6.3 \times 10^5$ l/Ft
 $M = 7.92$, $T_{PC} = 150^\circ F$
 Roll = 0° , $\alpha = 0^\circ$, Yaw = $+6^\circ$
 Launch Config., Top View

Fig. 16 - Upper Surface Local to Stagnation Point Heat Transfer Coefficients

Isotherm	h/hs	Isotherm	h/hs
1	0.254	5	0.080
2	0.197	6	0.062
3	0.139	7	0.053
4	0.098	8	0.051

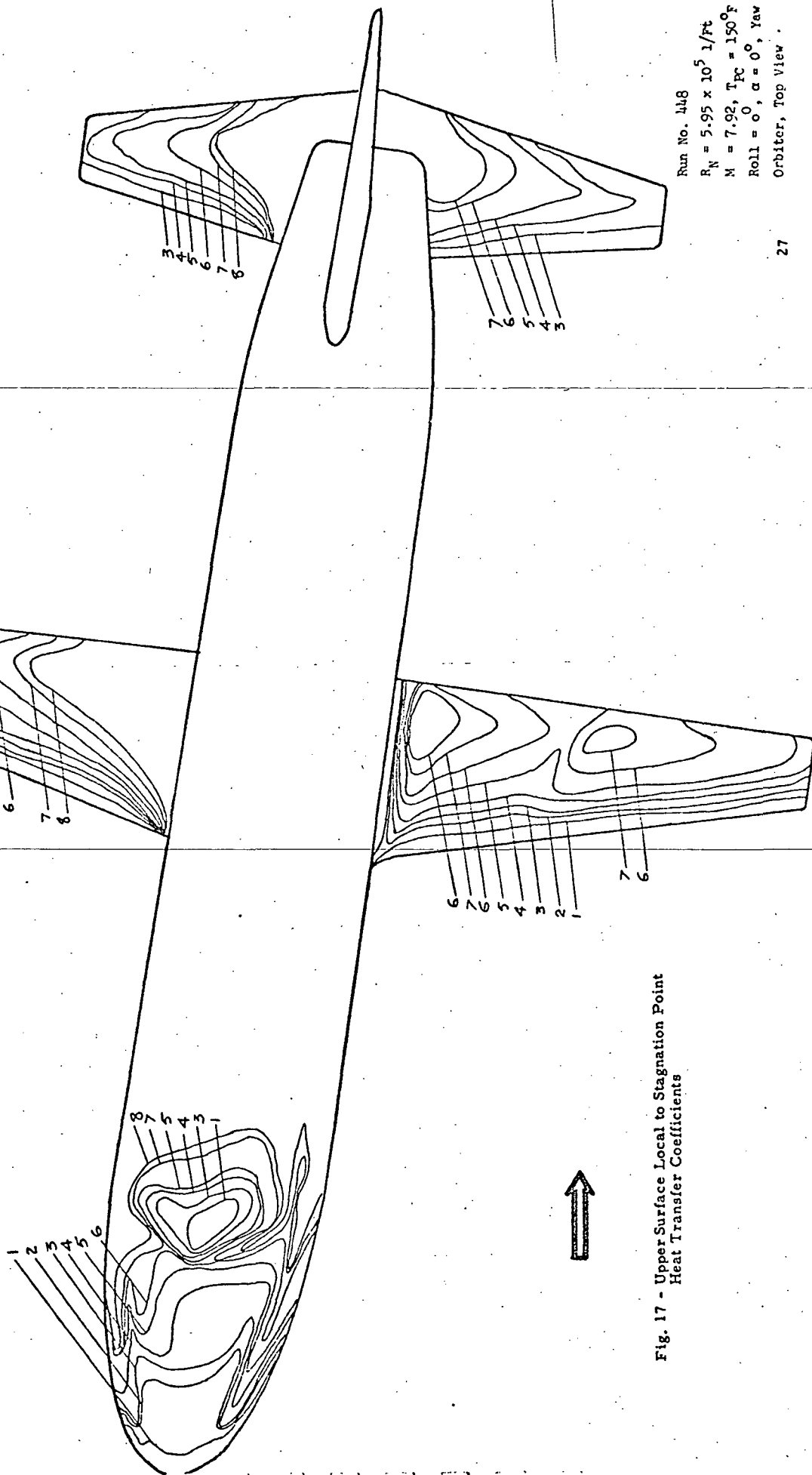
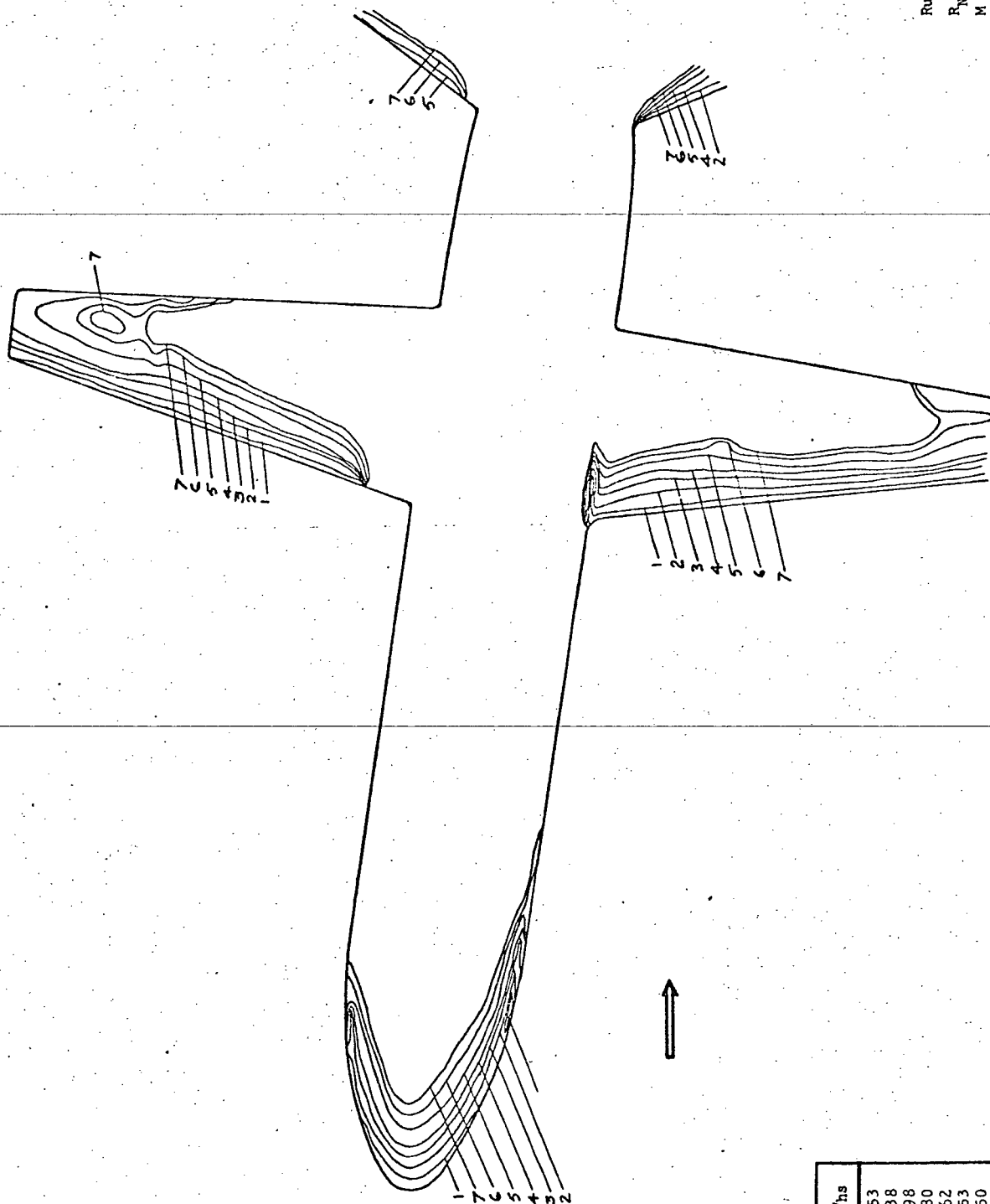


Fig. 17 - Upper Surface Local to Stagnation Point
Heat Transfer Coefficients

Run No. 448

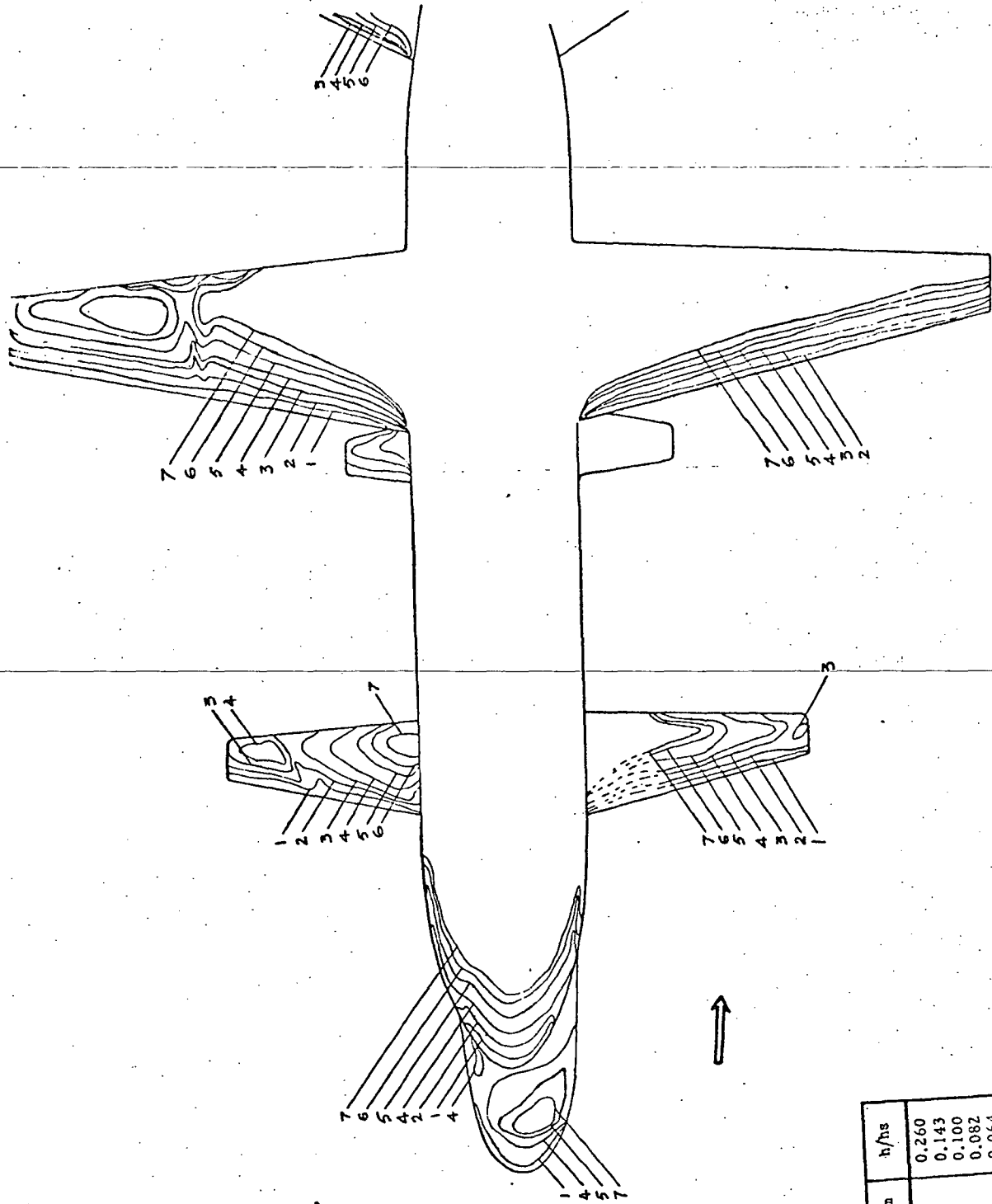
$R_N = 5.95 \times 10^5 \text{ l/Ft}$
 $M = 7.92, T_{PC} = 150^\circ\text{F}$
 $\text{Roll} = 0, \alpha = 0^\circ, \text{Yaw} = +6^\circ$
 Orbiter, Top View



Isotherm	h/h_s
1	0.253
2	0.138
3	0.098
4	0.080
5	0.062
6	0.053
7	0.050

Run No. 449
 $R_N = 5.988 \times 10^5 \text{ 1/Ft}$
 $M = 7.92, T_{FC} = 150^\circ\text{F}$
 $\text{Roll} = 0^\circ, \alpha = 0^\circ, \text{Yaw} = +6^\circ$
 Booster, Bottom View

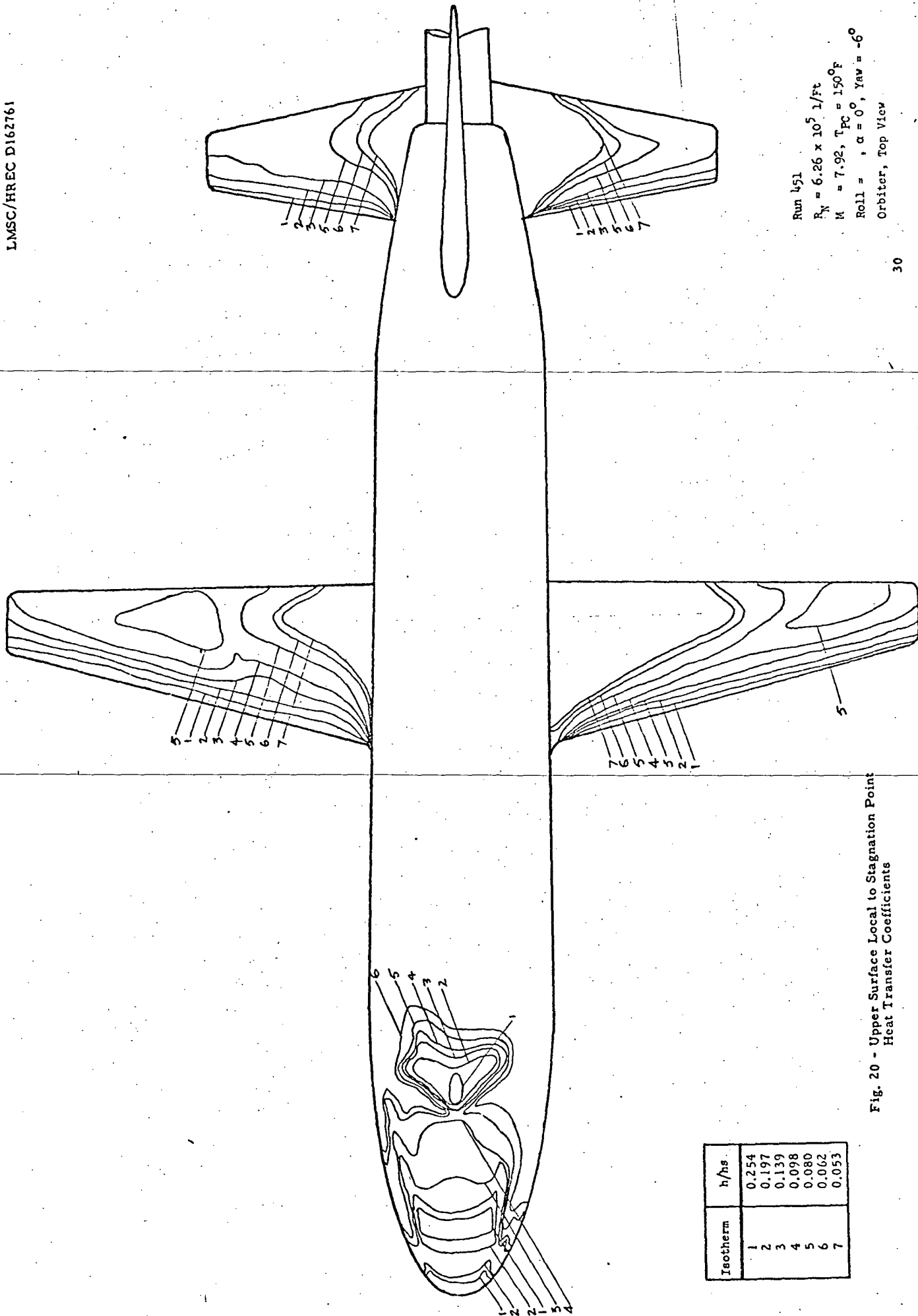
Fig. 18 - Lower Surface Local to Stagnation Point Heat Transfer Coefficients



Isotherm	h/h_s
1	0.260
2	0.143
3	0.100
4	0.082
5	0.064
6	0.058
7	0.052

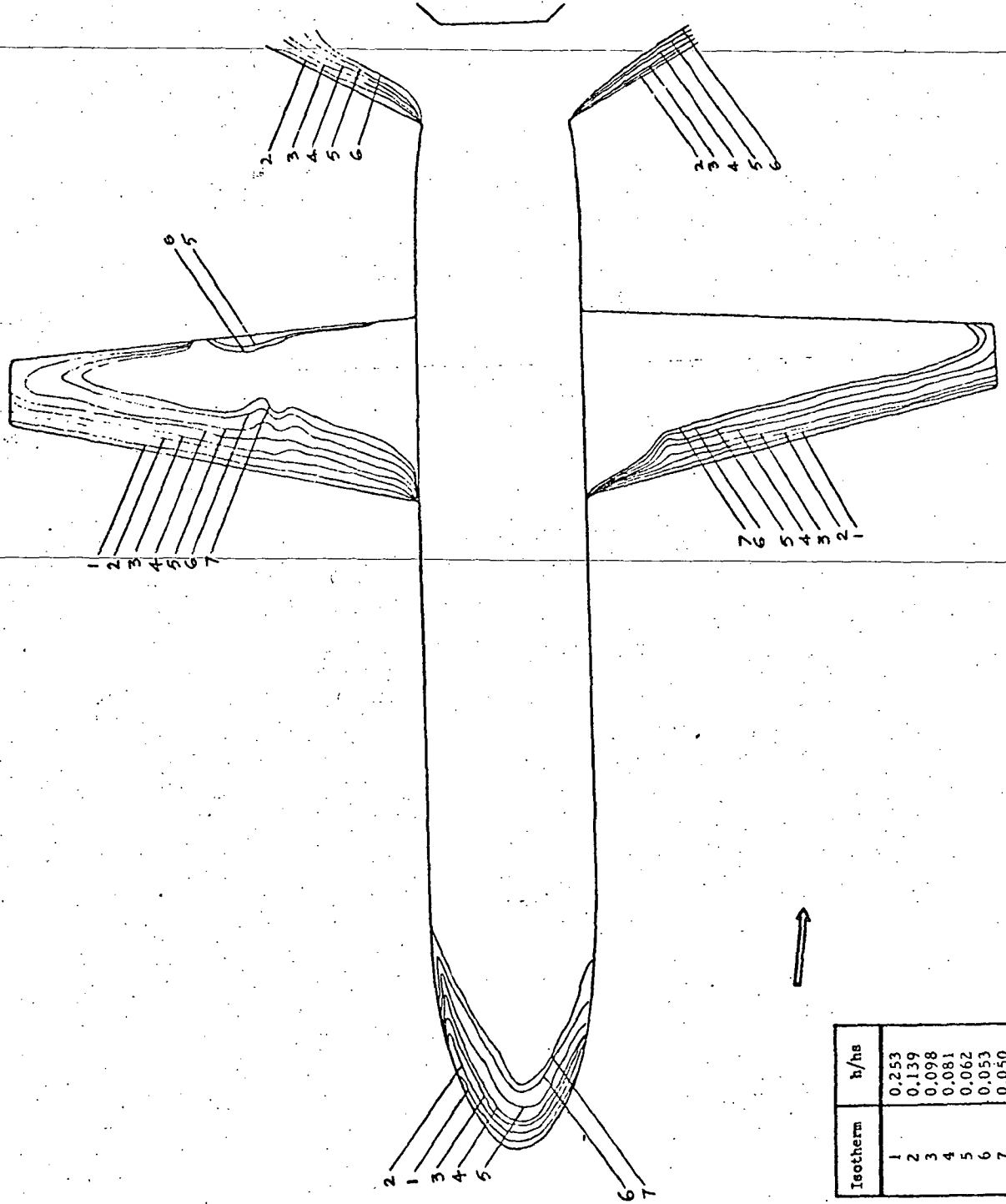
Run No. 450
 $R_N = 6.26 \times 10^5$ l/Ft
 $M = 7.92$, $T_{PG} = 150^\circ\text{F}$
 Roll = 0° , $\alpha = 0^\circ$, Yaw = -6°
 Launch Config., Bottom View

Fig. 19 - Lower Surface Local to Stagnation Point Heat Transfer Coefficients



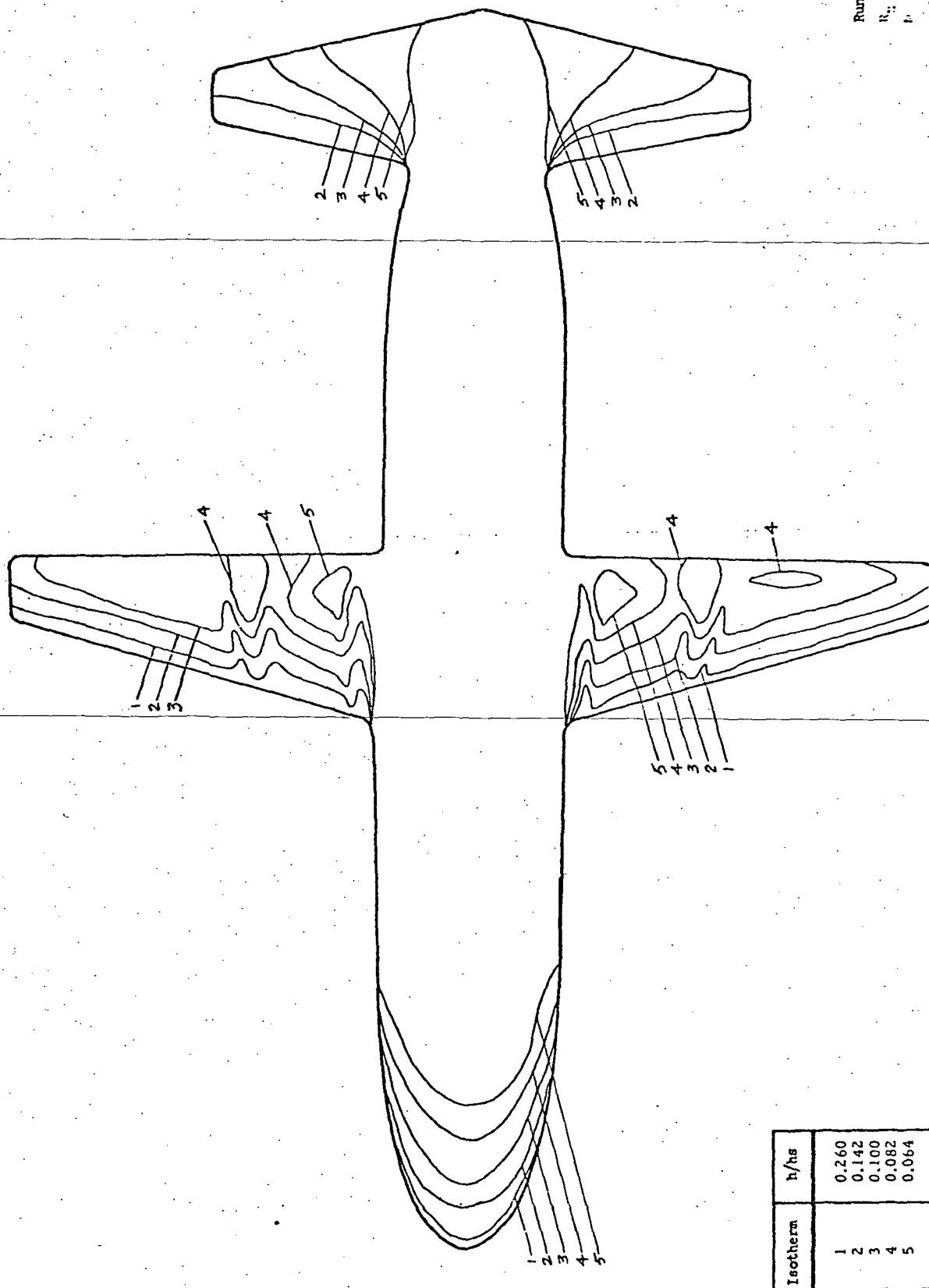
Run 451
 $R_N = 6.26 \times 10^5 \text{ l/Ft}$
 $M = 7.92, T_{PC} = 150^\circ\text{F}$
 $\text{Roll} = 0^\circ, \alpha = 0^\circ, \gamma_{av} = -6^\circ$
 Orbiter, Top View

Fig. 20 - Upper Surface Local to Stagnation Point
 Heat Transfer Coefficients



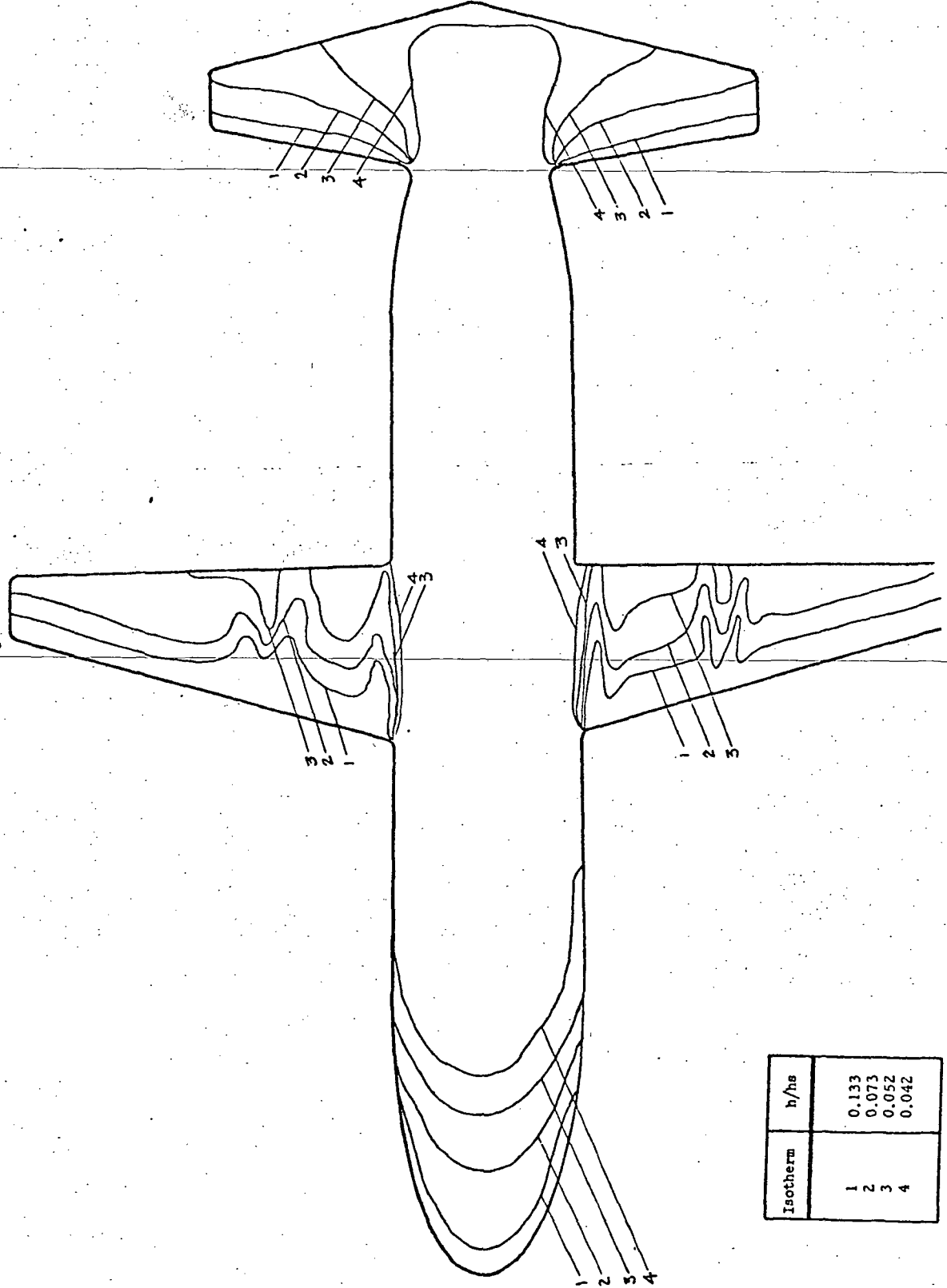
Run No. 452
 $R_N = 6.26 \times 10^5$ 1/Ft
 $M = 7.92$, $T_{PC} = 150^\circ\text{F}$
 Roll = 0° , $\alpha = 0^\circ$, Yaw = -6°
 Booster, Bottom View

Fig. 21 - Lower Surface Local to Stagnation Point Heat Transfer Coefficients



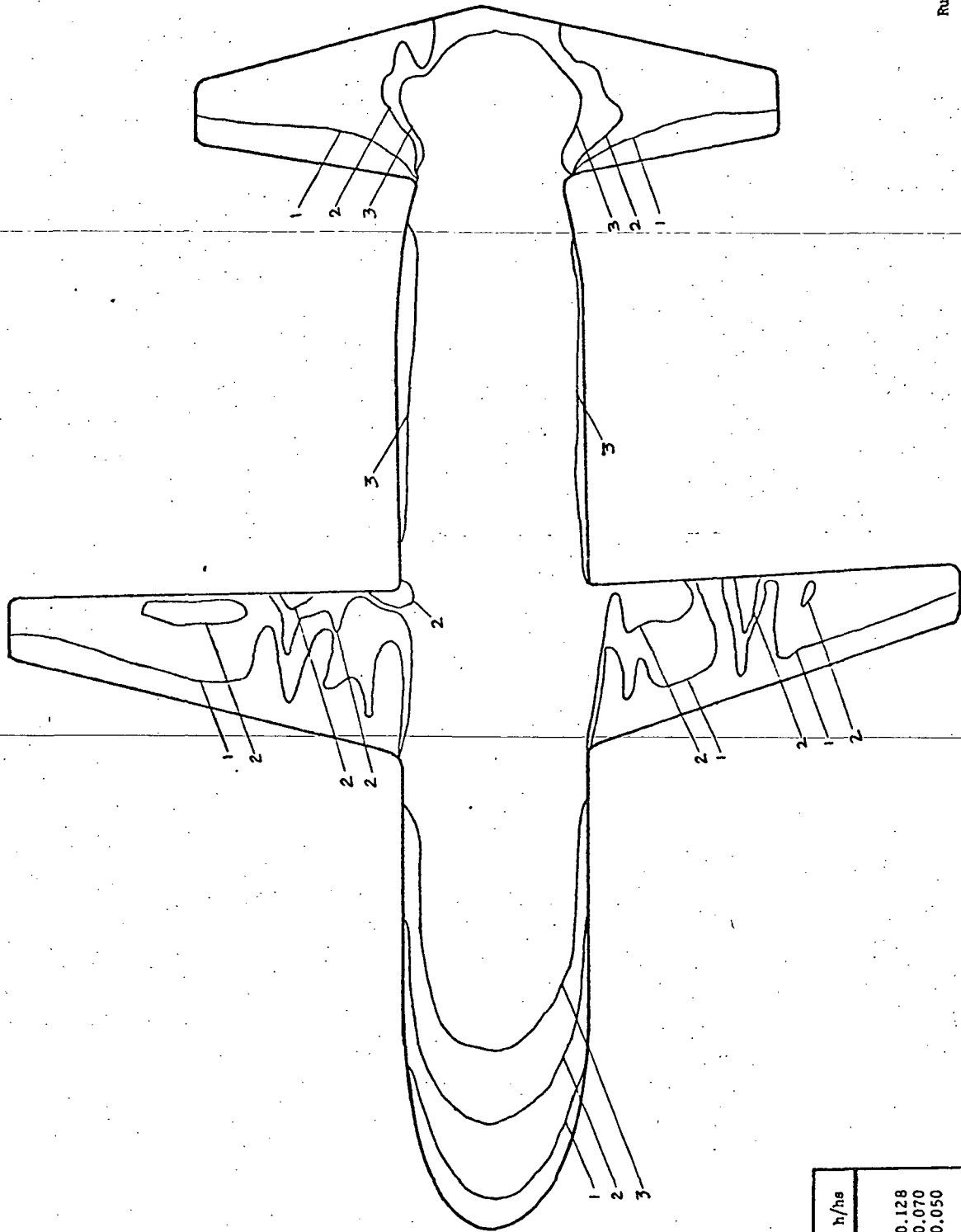
Run No. 453
 $R_{\infty} = 6.31 \times 10^5$ 1/Ft.
 $P_r = 7.00$, $T_{\infty} = 1.0^\circ\text{C}$
 $\theta_{\text{coll}} = 0^\circ$, $\alpha = 20^\circ$
 Orbiter, Bottom View

Fig. 22 - Lower Surface Local to Stagnation Point Heat Transfer Coefficients



Run No. 454
 $R_N = 2.04 \times 10^6 \text{ l/Ft}$
 $M = 7.98, T_{PC} = 150^\circ\text{F}$
 $\text{Roll} = 0^\circ, \alpha = 20^\circ$
 Orbiter, Bottom View

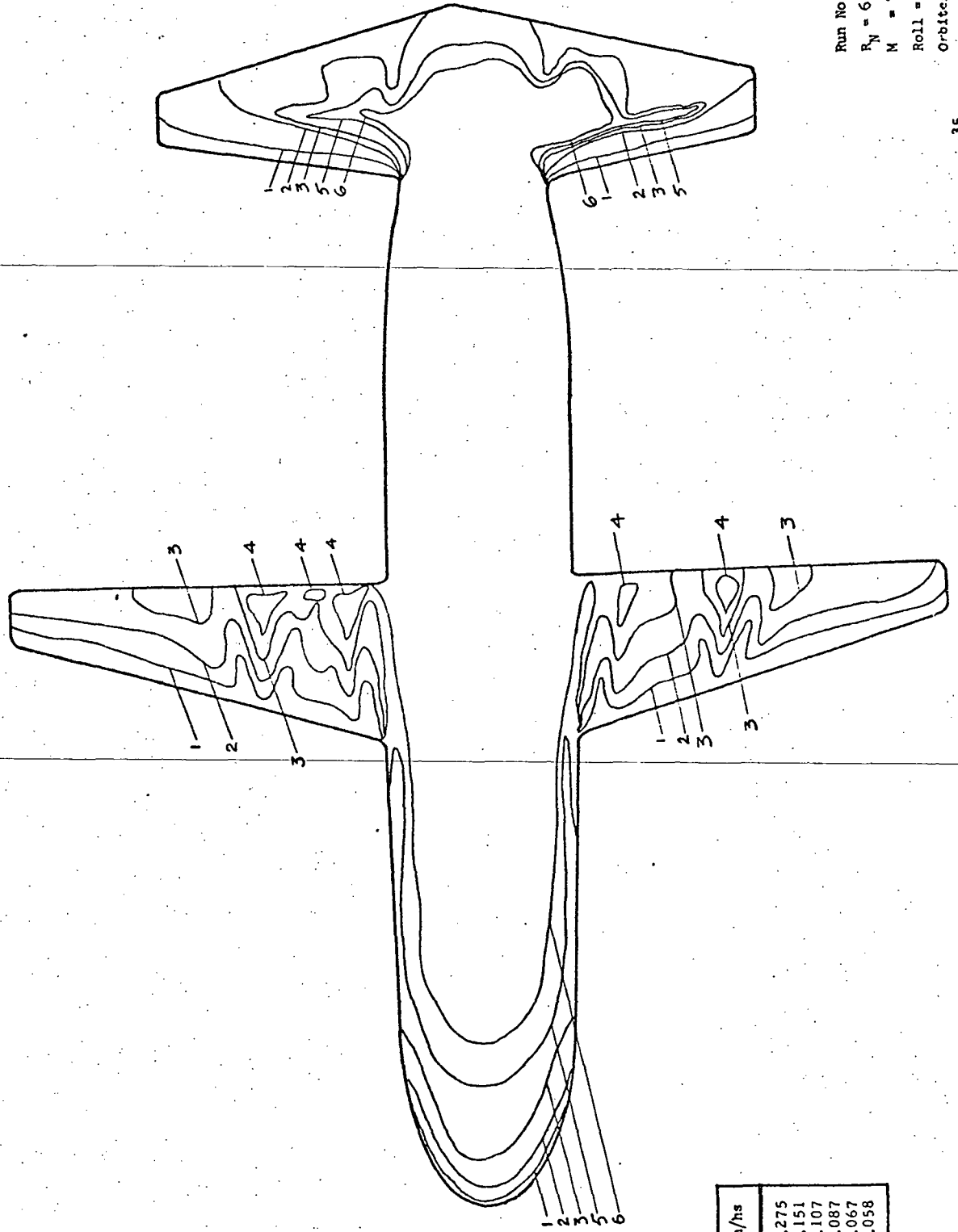
Fig. 23 - Lower Surface Local to Stagnation Point Heat Transfer Coefficients



Isotherm	h/h_s
1	0.128
2	0.070
3	0.050

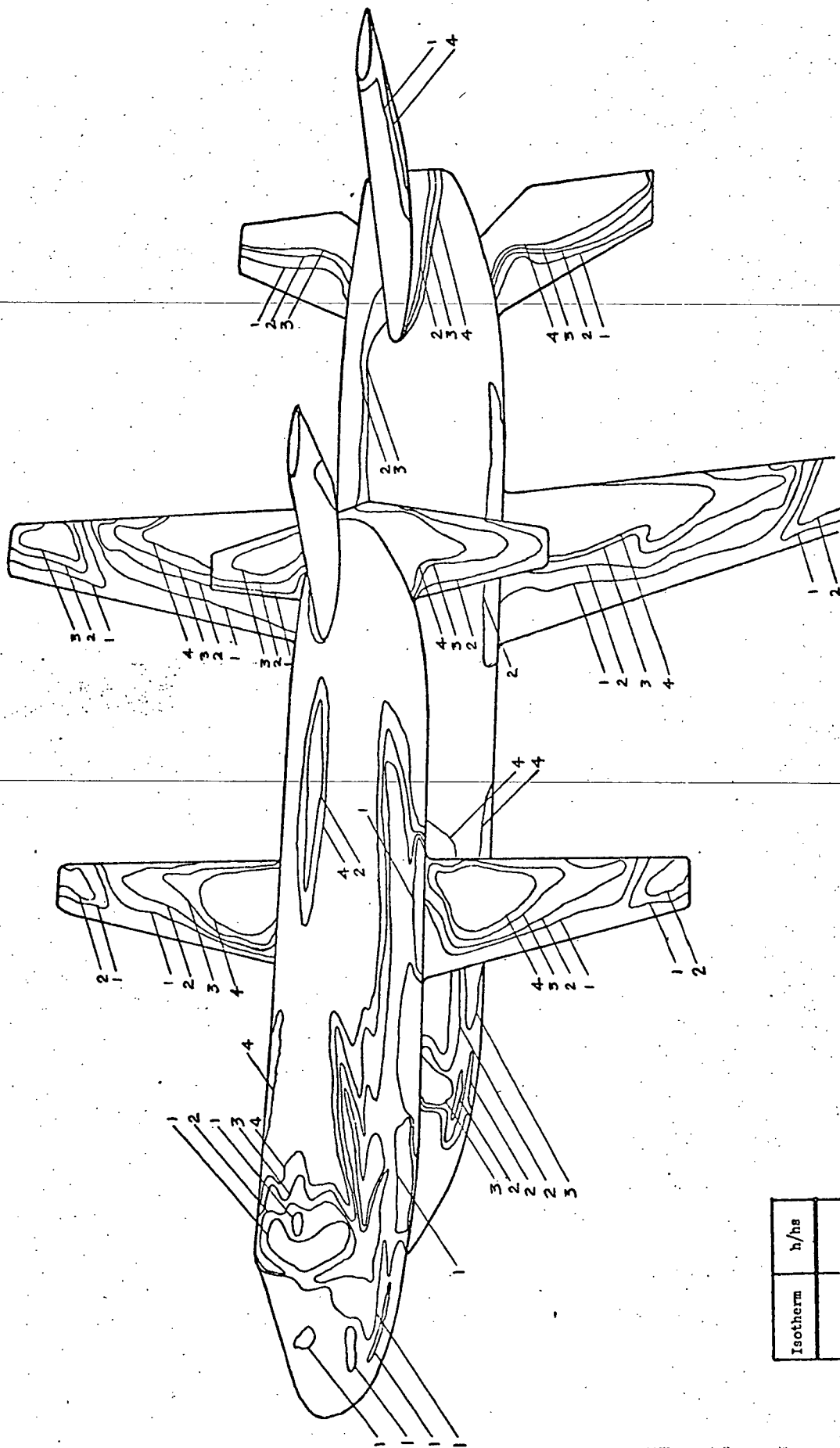
Run No. 455
 $R_N = 2.36 \times 10^6 \text{ 1/ft}$
 $M = 7.92, T_{PC} = 150^\circ\text{F}$
 $\text{Roll} = 0^\circ, \alpha = 30^\circ$
 Orbiter, Bottom View

Fig. 24 - Lower Surface Local to Stagnation Point Heat Transfer Coefficients



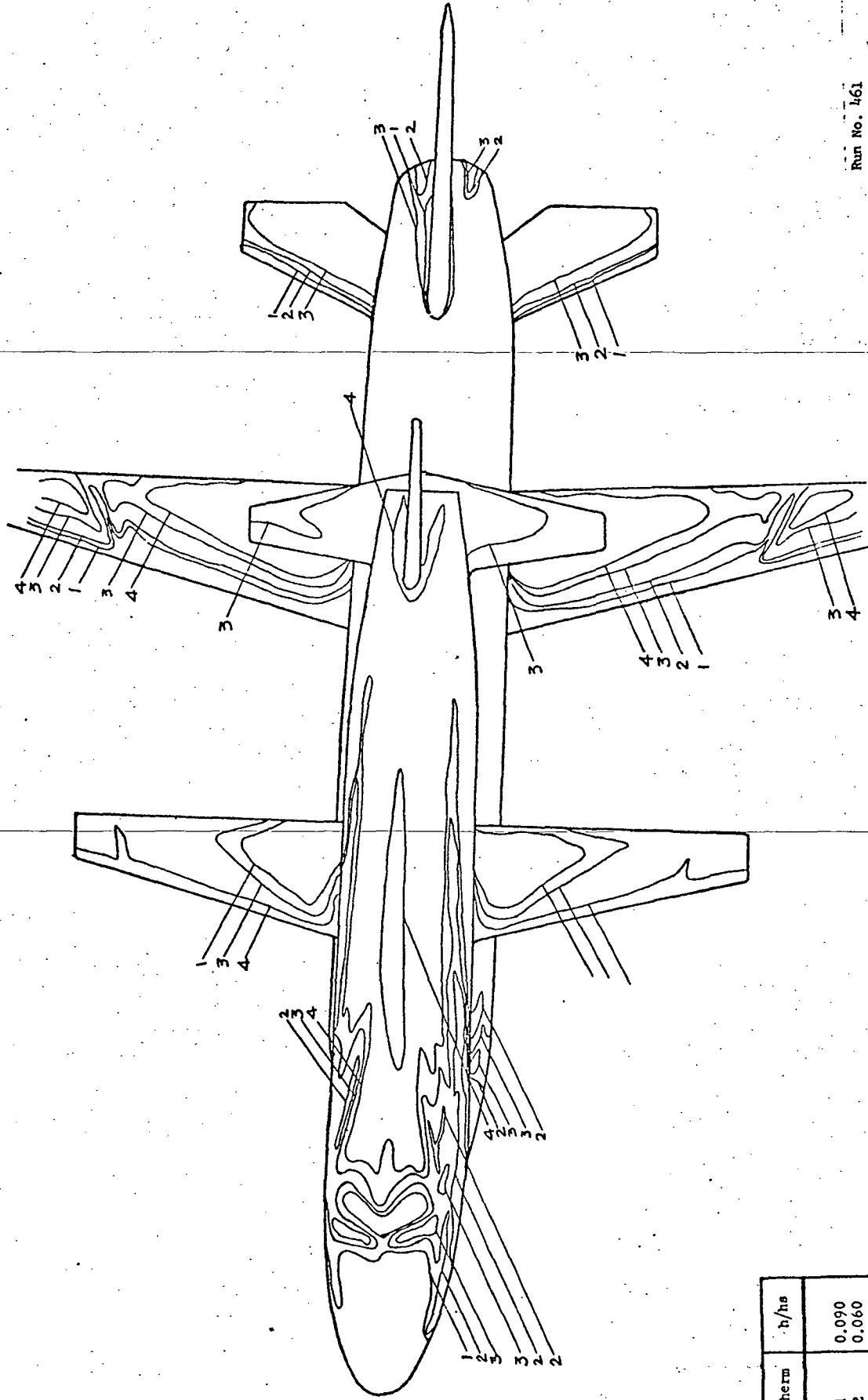
Run No. 456
 $R_N = 6.38 \times 10^5$ 1/ft
 $M = 7.92$, $T_{PC} = 150^\circ\text{F}$
 Roll = 0° , $\alpha = 30^\circ$
 Orbiter, Bottom View

Fig. 25 - Lower Surface Local to Stagnation Point Heat Transfer Coefficients



Run No. 460
 $R_N = 3.7 \times 10^6 \text{ 1/Ft}$
 $M = 7.92, T_{PC} = 150^\circ \text{F}$
 $\text{Roll} = 15^\circ, \alpha = 0^\circ$
 Launch Config., Top View

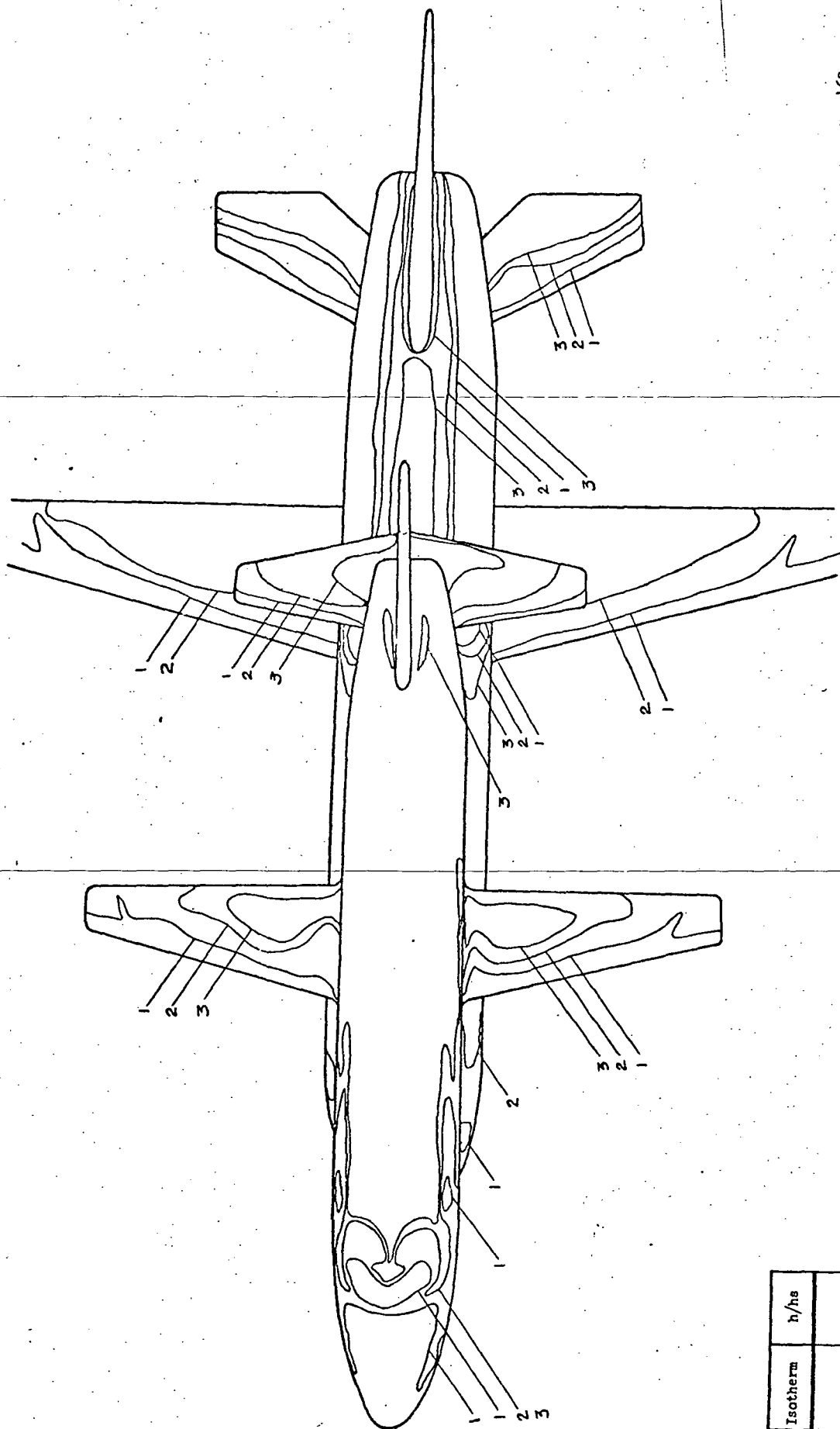
Fig. 26 - Upper Surface Local to Stagnation Point Heat Transfer Coefficients



Isotherm	h/h_s
1	0.090
2	0.060
3	0.035
4	0.028

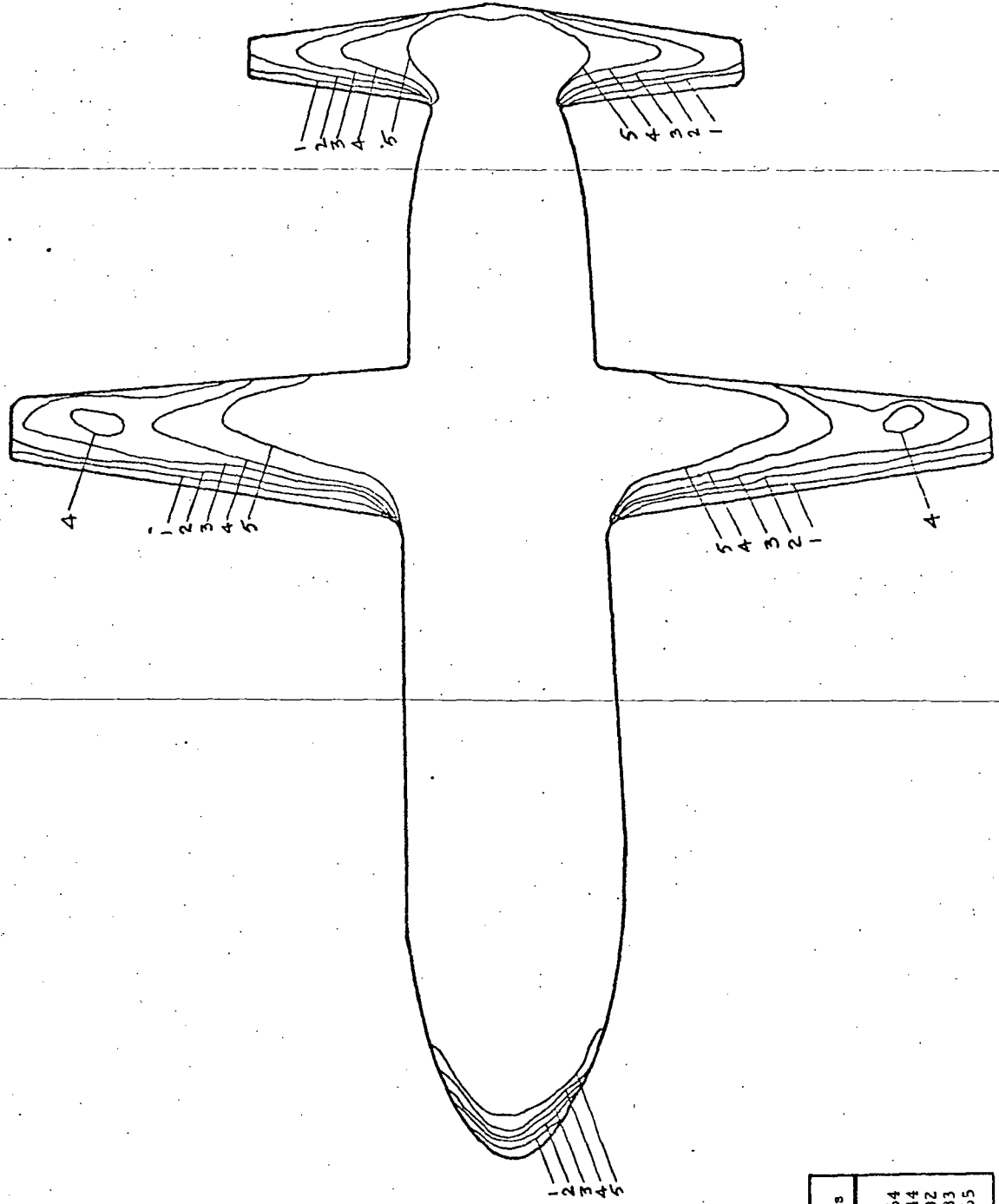
Run No. 461
 $R_N = 3.747 \times 10^6 \text{ 1/ft}$
 $M = 7.92, T_{PC} = 150^\circ\text{F}$
 $\text{Roll} = 0^\circ, \alpha = 5^\circ$
 Launch Config., Top View

Fig. 27 - Upper Surface Local to Stagnation Point Heat Transfer Coefficients



Run No. 462
 $R_N = 3.776 \times 10^6 \text{ 1/Ft}$
 $M = 7.92, T_N = 1.00^\circ\text{F}$
 $\text{Roll} = 0^\circ, \alpha = -5^\circ$
 Launch Config., Top View

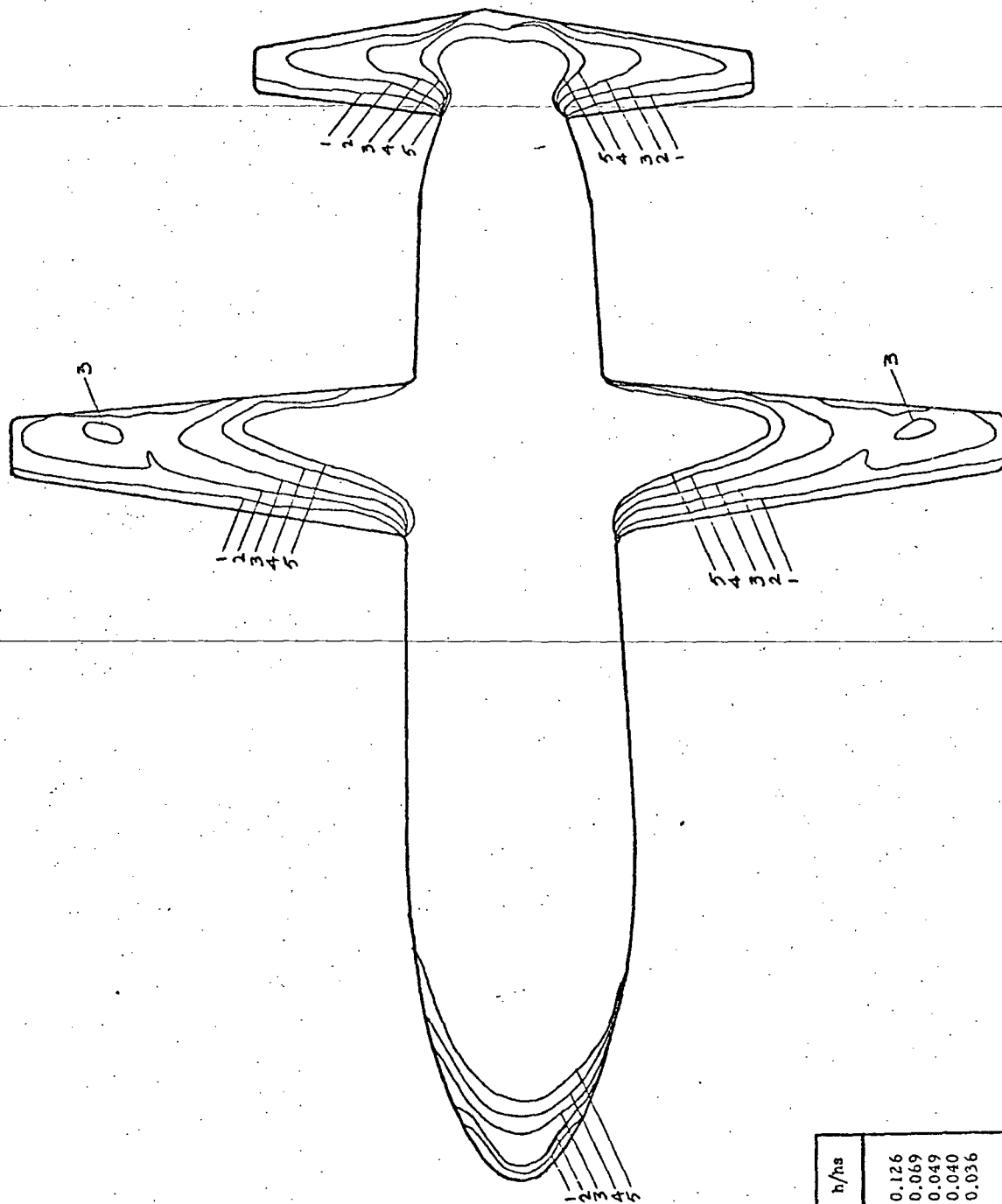
Fig. 28 - Upper Surface Local to Stagnation Point Heat Transfer Coefficients



Isotherm	h/h_s
1	0.264
2	0.144
3	0.102
4	0.083
5	0.065

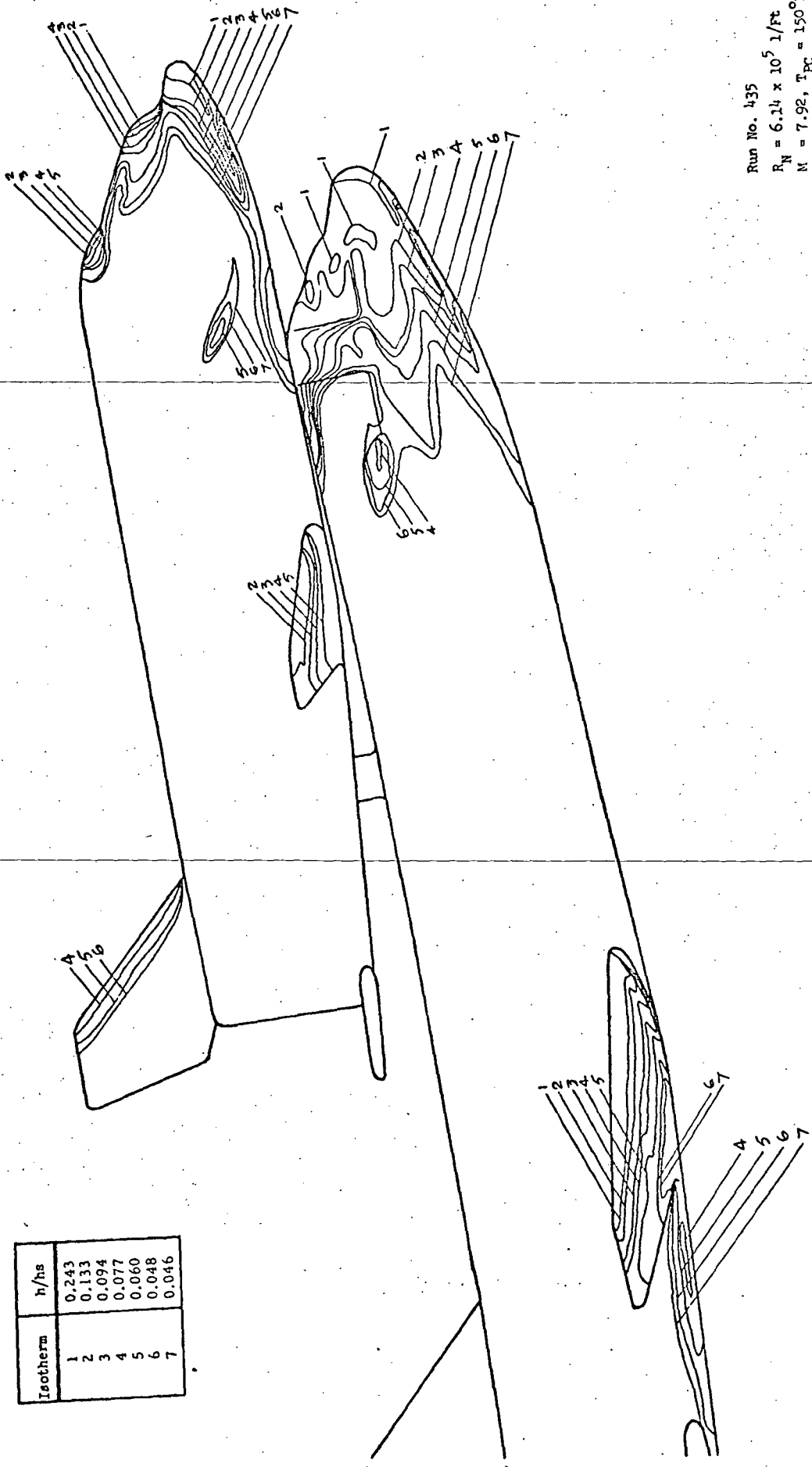
Run No. 463
 $R_N = 6.38 \times 10^5 \text{ 1/ft}$
 $M = 7.92, T_{FC} = 150^\circ\text{F}$
 $\text{Roll} = 0^\circ, \alpha = -20^\circ$
 Orbiter, Bottom View

Fig. 29 - Lower Surface Local to Stagnation Point Heat Transfer Coefficients



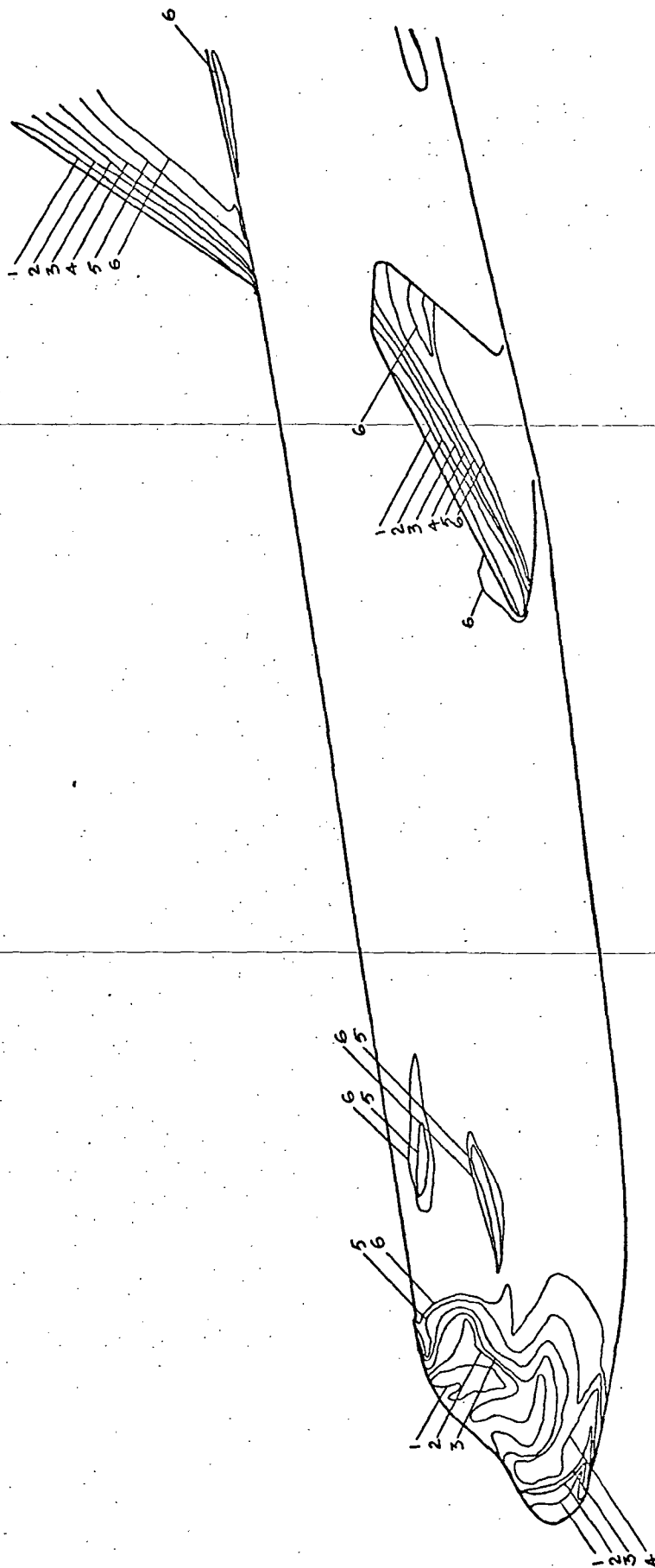
Run No. 164
 $R_N = 1.975 \times 10^6$ 1/ft
 $N = 7.52$, $T_p = 100^\circ\text{F}$
 $\text{Re} = 10^6$, $\alpha = 20^\circ$
 Orbiter, Bottom View

Fig. 30 - Lower Surface Local to Stagnation Point Heat Transfer Coefficients



Run No. 135
 $R_N = 6.14 \times 10^5 \text{ l/Ft}$
 $M = 7.92, T_{PC} = 150^\circ\text{F}$
 $\text{Roll} = 180^\circ, \alpha = 10^\circ$
 Launch Config., Side View

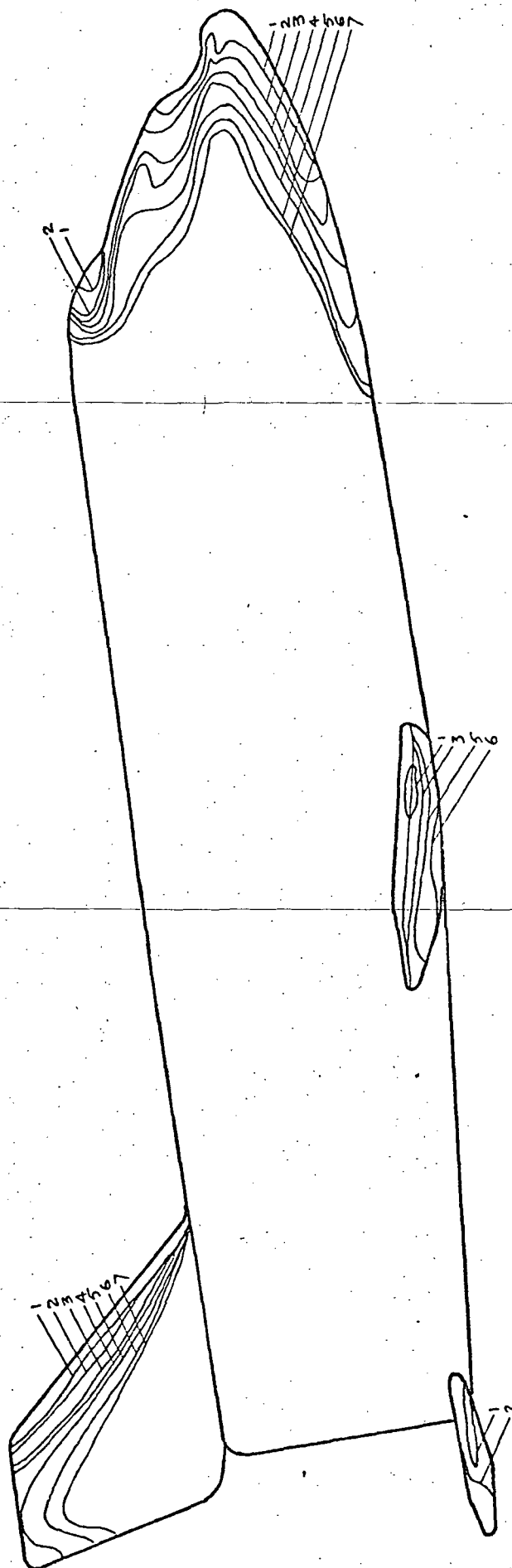
Fig. 31 - Side Panel Local to Stagnation Point Heat Transfer Coefficients



Isotherm	h/h_s
1	0.250
2	0.136
3	0.096
4	0.079
5	0.061
6	0.050

Run No. 436
 $R_N = 6.18 \times 10^5 \text{ l/ft}$
 $M = 7.92, T_{pc} = 150^\circ\text{F}$
 $\text{Roll} = 0^\circ, \alpha = -10^\circ$
 Booster, Side View

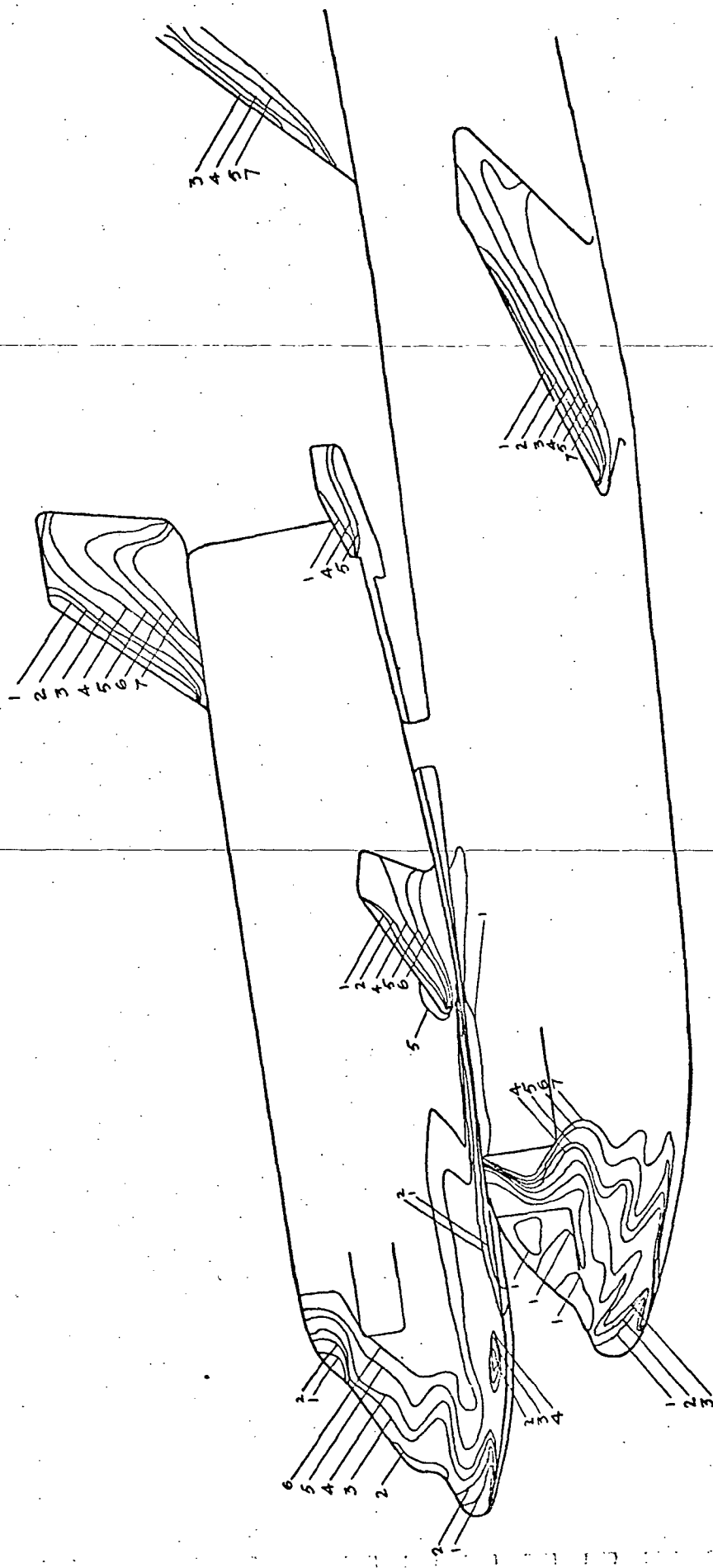
Fig. 32 - Side Panel Local to Stagnation Point Heat Transfer Coefficients



Isotherm	h/h_s
1	0.248
2	0.136
3	0.096
4	0.078
5	0.061
6	0.052
7	0.050

Run No. 437
 $R_N = 6.10 \times 10^5$ 1/Ft
 $M = 7.92$, $T_{PC} = 150^\circ\text{F}$
 Roll = 0° , $\alpha = 10^\circ$
 Orbiter, Side View

Fig. 33 - Side Panel Local to Stagnation Point Heat Transfer Coefficients



Run No. 438
 $R_N = 6.18 \times 10^5 \text{ 1/ft.}$
 $M = 7.92, T_{PC} = 150^\circ\text{F}$
 $\text{Roll} = 0^\circ, \alpha = -10^\circ$
 Launch Config., Side View

Fig. 34 - Side Panel Local to Stagnation Point Heat Transfer Coefficients

2
3
4
5

5
4
4
4
3
2
1

1
2
3
4
5
6

Isotherm	h/hs
1	0.267
2	0.146
3	0.103
4	0.084
5	0.065
6	0.057

Run No. 439
 $R_N = 6.3 \times 10^4$ 1/ft
 $M = 7.02$, $T_{\infty} = 100^\circ\text{F}$
 $Re_{11} = 0.0$, $\alpha = 10$
 Isotherm, 11.0 View

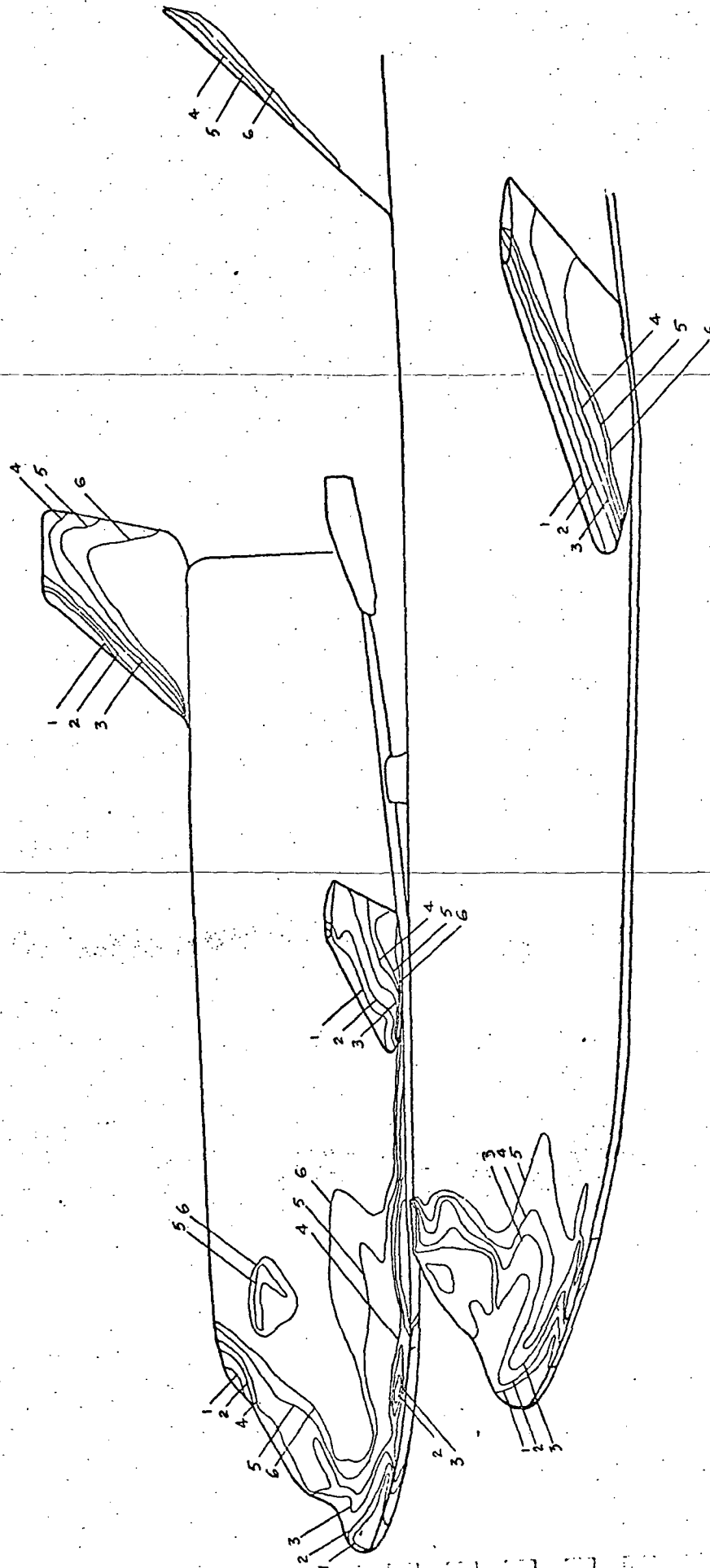
Fig. 35 - Side Panel Local to Stagnation Point Heat Transfer Coefficients



Isotherm	h/h_s
1	0.247
2	0.135
3	0.096
4	0.078
5	0.068
6	0.060
7	0.052

Run No. 440
 $R_N = 6.14 \times 10^5$ 1/Ft
 $M = 7.92$, $T_{FC} = 150^\circ\text{F}$
 $\text{Roll} = 180^\circ$, $\alpha = 0^\circ$
 Orbiter, Side View

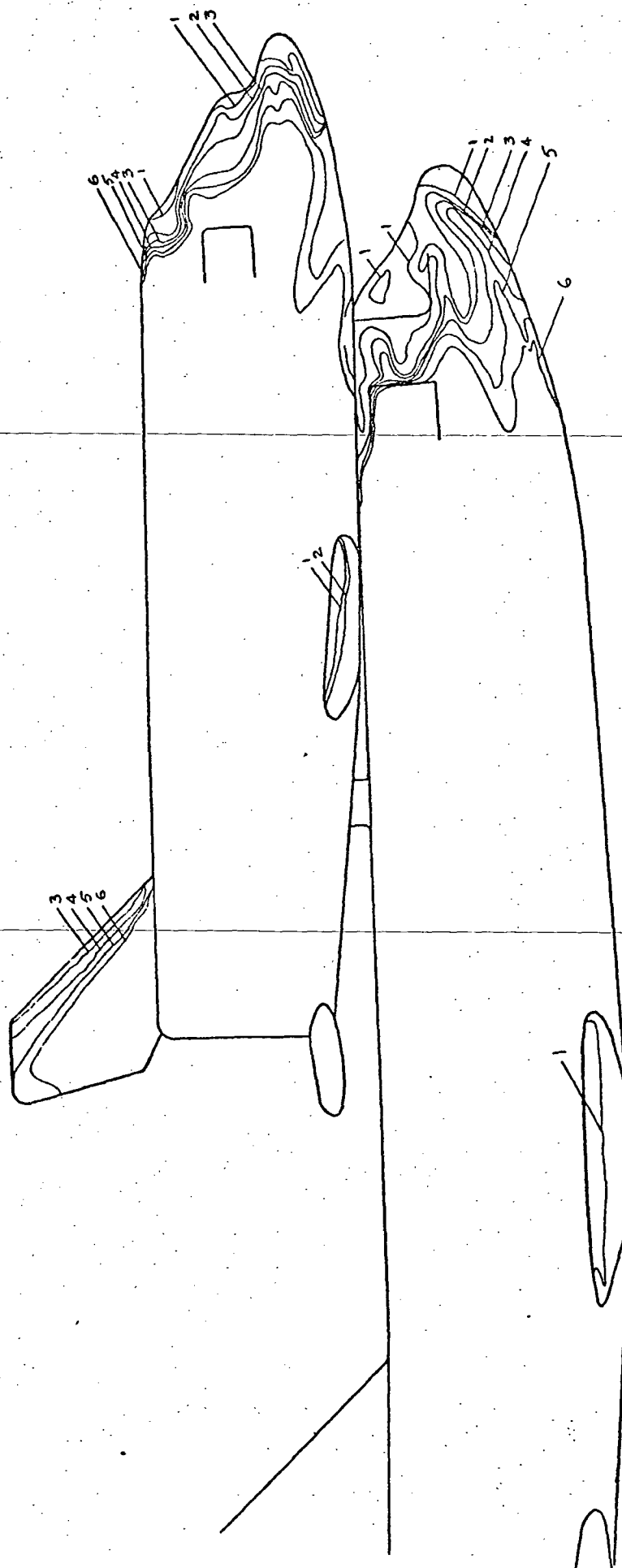
Fig. 36.- Side Panel Local to Stagnation Point Heat Transfer Coefficients



Isotherm	h/h_s
1	0.247
2	0.136
3	0.096
4	0.078
5	0.060
6	0.049

Run No. 441
 $R_N = 6.025 \times 10^5 \text{ l/Ft}$
 $M = 7.92, T_{PC} = 150^\circ\text{F}$
 $\text{Roll} = 0^\circ, \alpha = 0^\circ$
 Launch Config., Side View

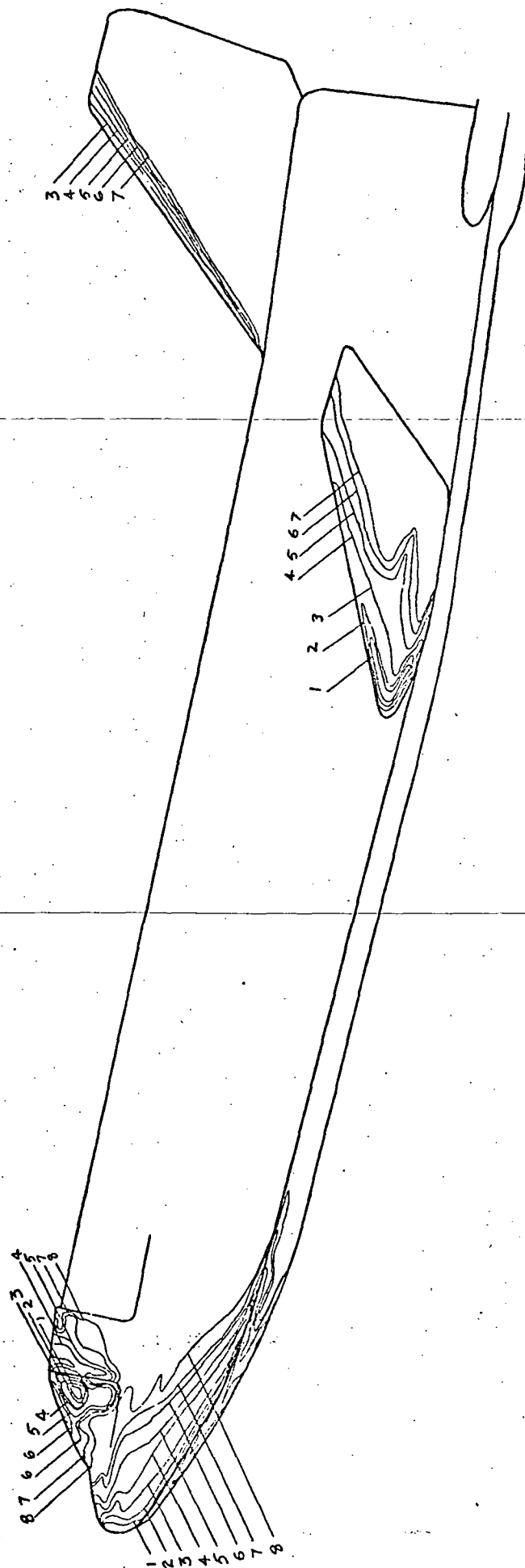
Fig. 37 - Side Panel Local to Stagnation Point Heat Transfer Coefficients



Isotherm	h/h_s
1	0.268
2	0.147
3	0.104
4	0.085
5	0.066
6	0.055

Run No. 442
 $R_N = 6.26 \times 10^5 \text{ 1/Ft}$
 $M = 7.92, T_{PC} = 150^\circ\text{F}$
 $\text{Roll} = 180^\circ, \alpha = 0^\circ$
 Launch Config., Side View

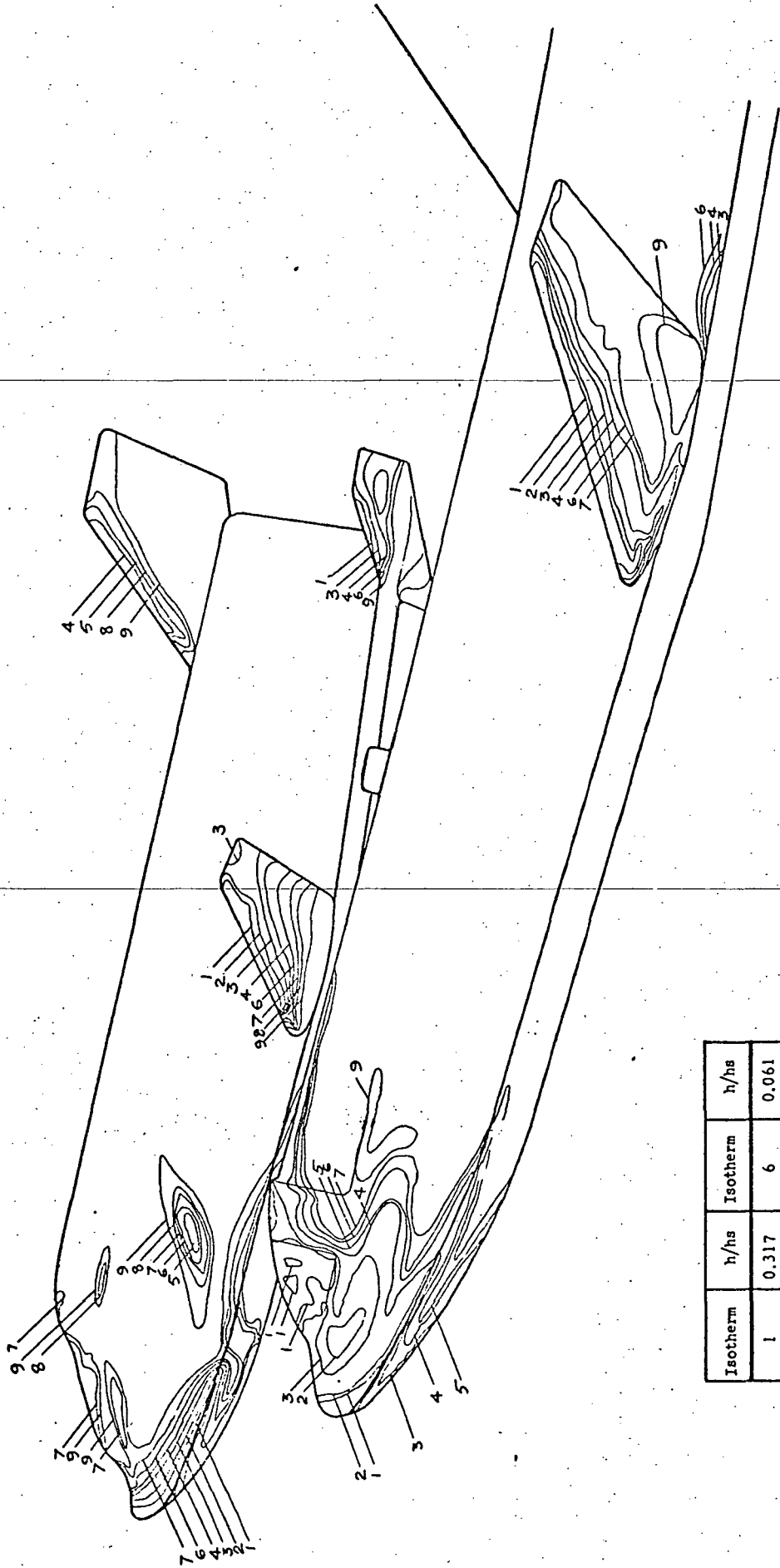
Fig. 38 - Side Panel Local to Stagnation Point Heat Transfer Coefficients



Isotherm	h/h_s	Isotherm	h/h_s
1	0.315	5	0.070
2	0.172	6	0.061
3	0.122	7	0.054
4	0.086	8	0.044

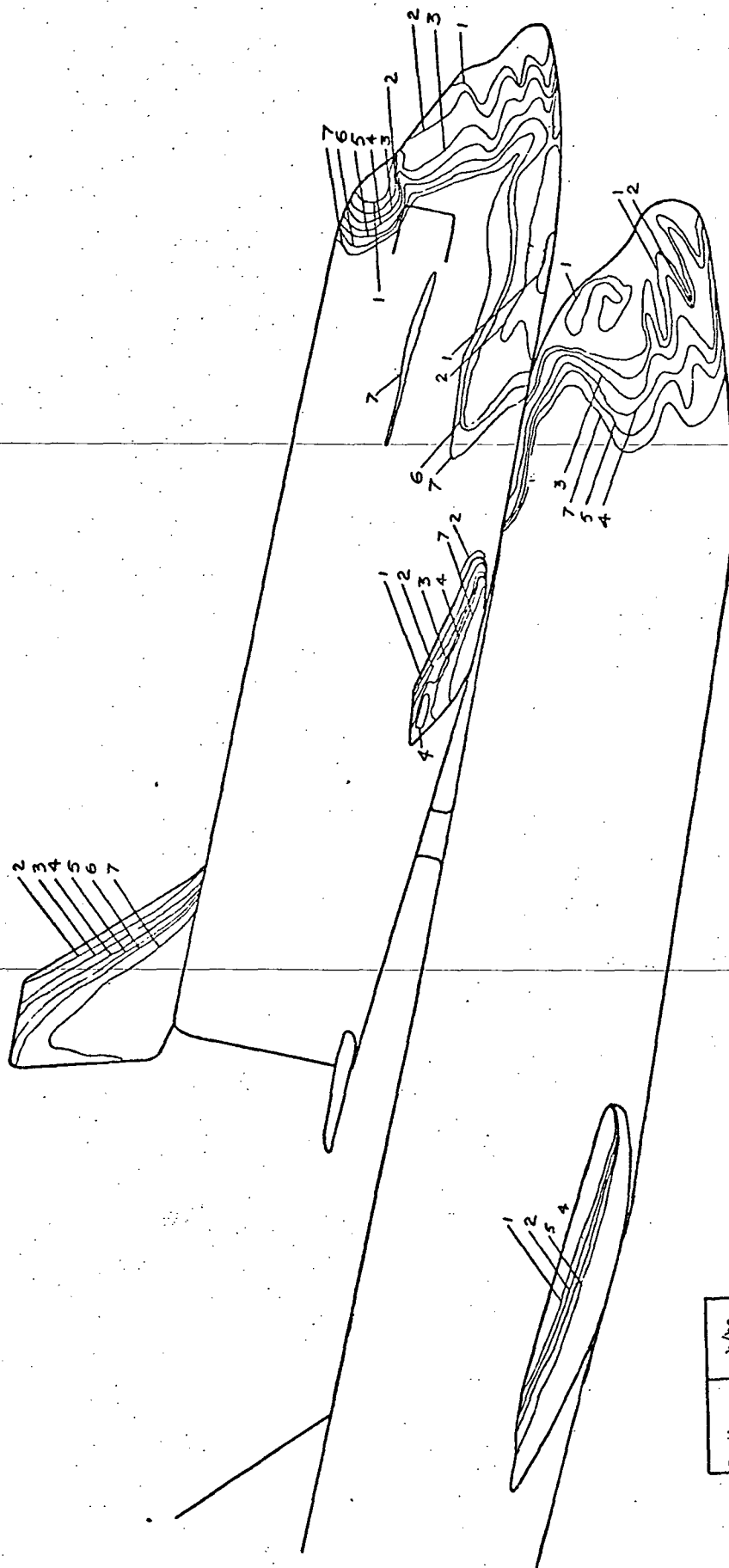
Run No. 443
 $R_N = 5.8 \times 10^5$
 $M = 7.92$, $T_{PC} = 150^\circ F$
 $Roll = 0^\circ$, $\alpha = 10^\circ$
 Booster, Side View

Fig. 39 - Side Panel Local to Stagnation Point Heat Transfer Coefficients



Run No. 1444
 $R_N = 5.84 \times 10^5$ 1/Ft
 $M = 7.92$, $T_{PC} = 150^\circ\text{F}$
 $\text{Roll} = 0^\circ$, $\alpha = 10^\circ$
 Launch Config., Side View

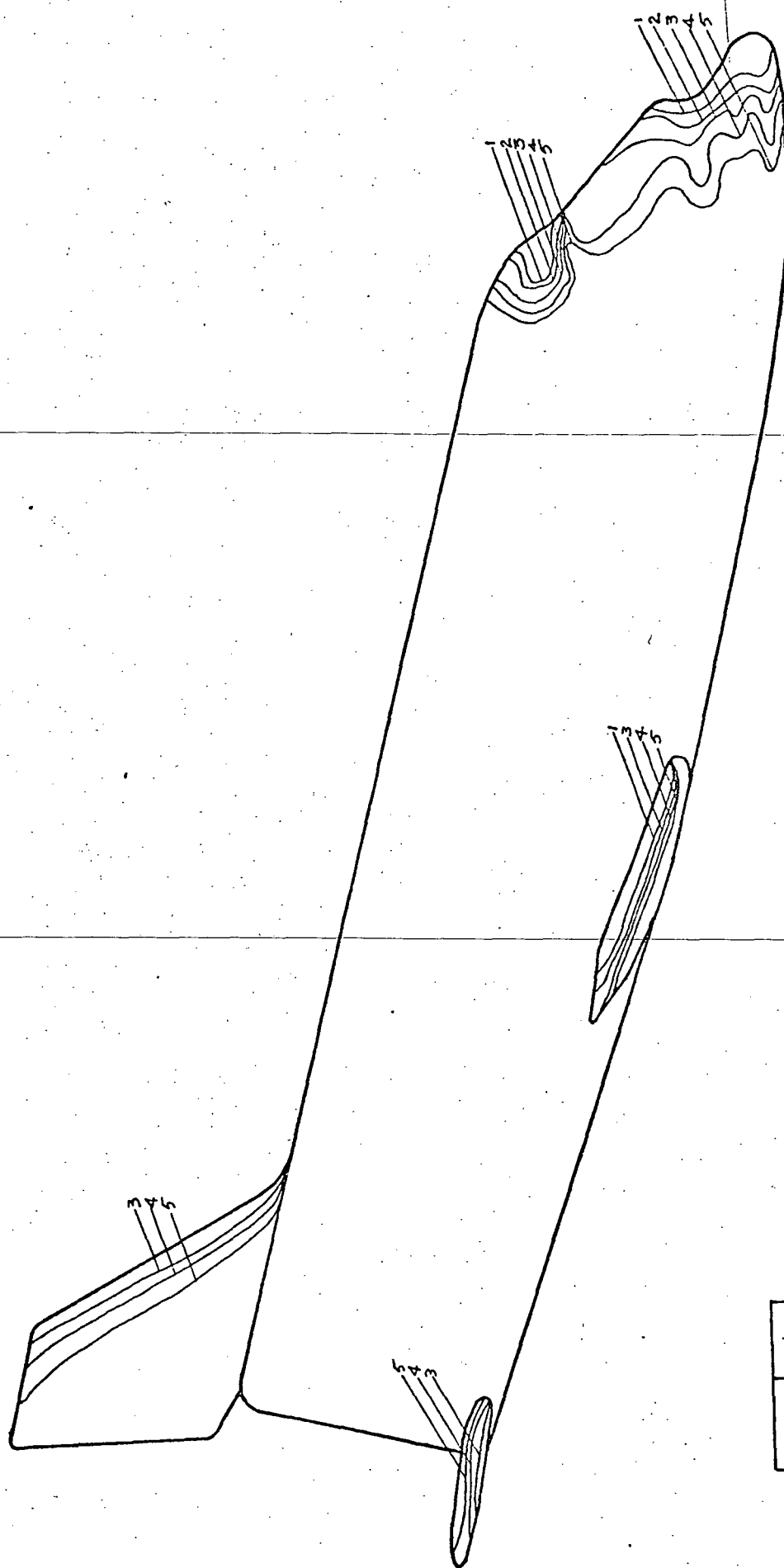
Fig. 40 - Side Panel Local to Stagnation Point Heat Transfer Coefficients



Isotherm	h/h_s
1	0.258
2	0.141
3	0.100
4	0.082
5	0.071
6	0.063
7	0.052

Run No. 445
 $R_H = 6.43 \times 10^5 \text{ l/ft}$
 $M = 7.92, T_{PC} = 150^\circ\text{F}$
 $\text{Roll} = 180^\circ, \alpha = -10^\circ$
 Launch Config., Side View

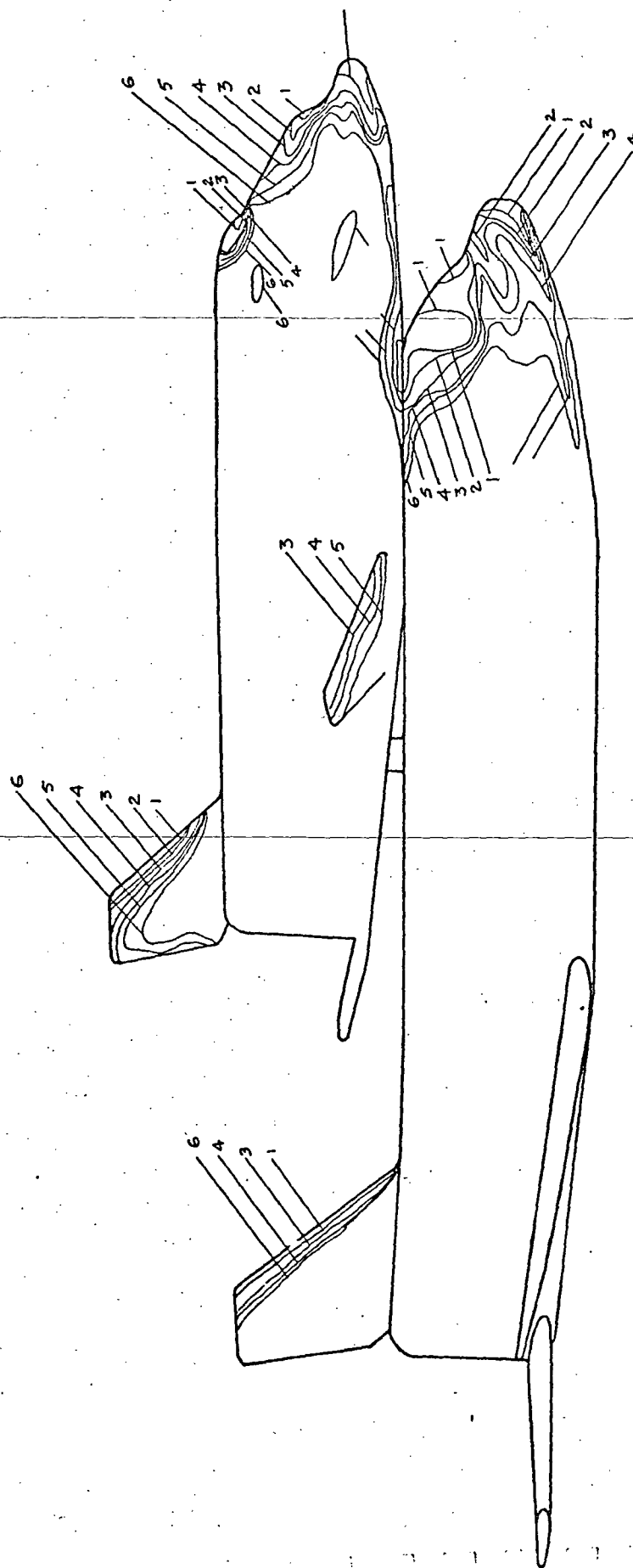
Fig. 41 - Side Panel Local to Stagnation Point Heat Transfer Coefficients



Isotherm	h/h_s
1	0.335
2	0.183
3	0.130
4	0.092
5	0.072

Run No. 446
 $R_N = 6.43 \times 10^5 \text{ 1/Ft}$
 $M = 7.92, T_{PC} = 150^\circ\text{F}$
 $\text{Roll} = 180^\circ, \alpha = -10^\circ$
 Orbiter, Side View

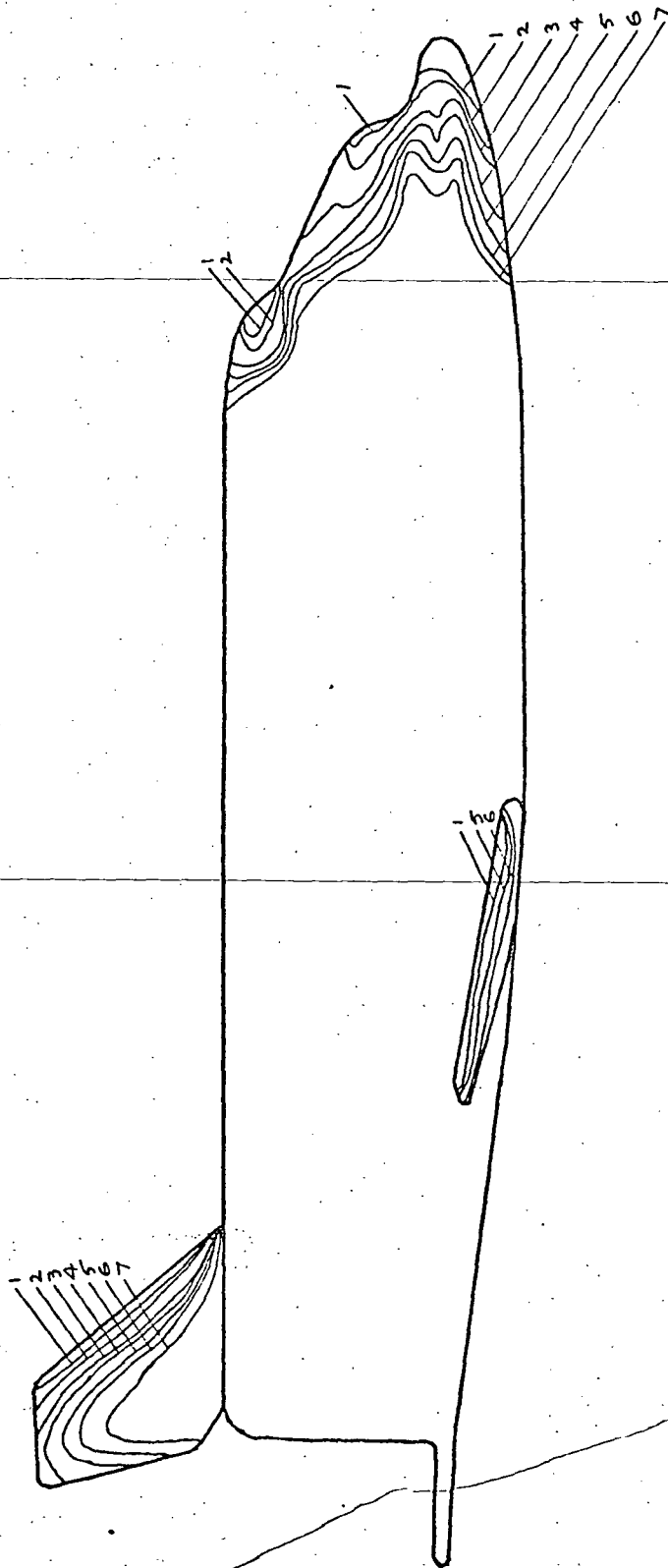
Fig. 42 - Side Panel Local to Stagnation Point Heat Transfer Coefficients



Isotherm	h/h_s
1	0.259
2	0.142
3	0.100
4	0.082
5	0.063
6	0.052

Run No. 447
 $R_N = 6.3 \times 10^5$ 1/Ft
 $M = 7.92$, $T_{PC} = 150^\circ\text{F}$
 Roll = 0° , $\alpha = 0^\circ$, $\gamma_{av} = +6^\circ$
 Launch Config., Side View

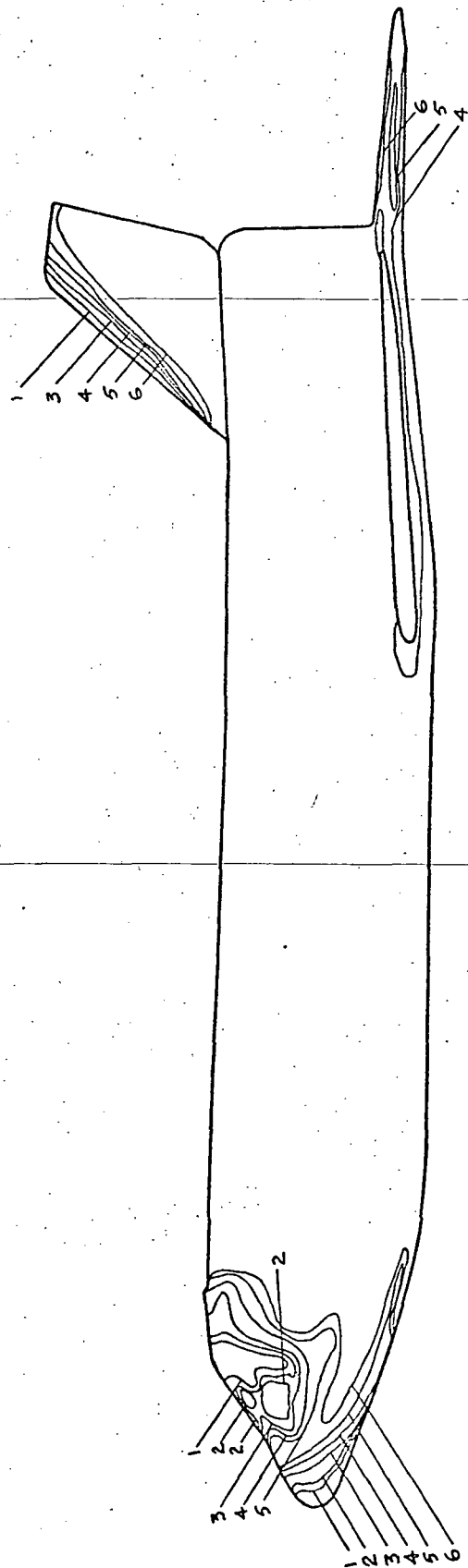
Fig. 43 - Side Panel Local to Stagnation Point Heat Transfer Coefficients



Isotherm	h/h_s
1	0.237
2	0.130
3	0.092
4	0.075
5	0.058
6	0.049
7	0.047

Run No. 448
 $R_N = 5.95 \times 10^5$ 1/Ft
 $M = 7.92$, $T_{FC} = 150^\circ\text{F}$
 Roll = 0° , $\alpha = 0^\circ$, $\gamma_{sw} = +6^\circ$
 Orbiter, Side View

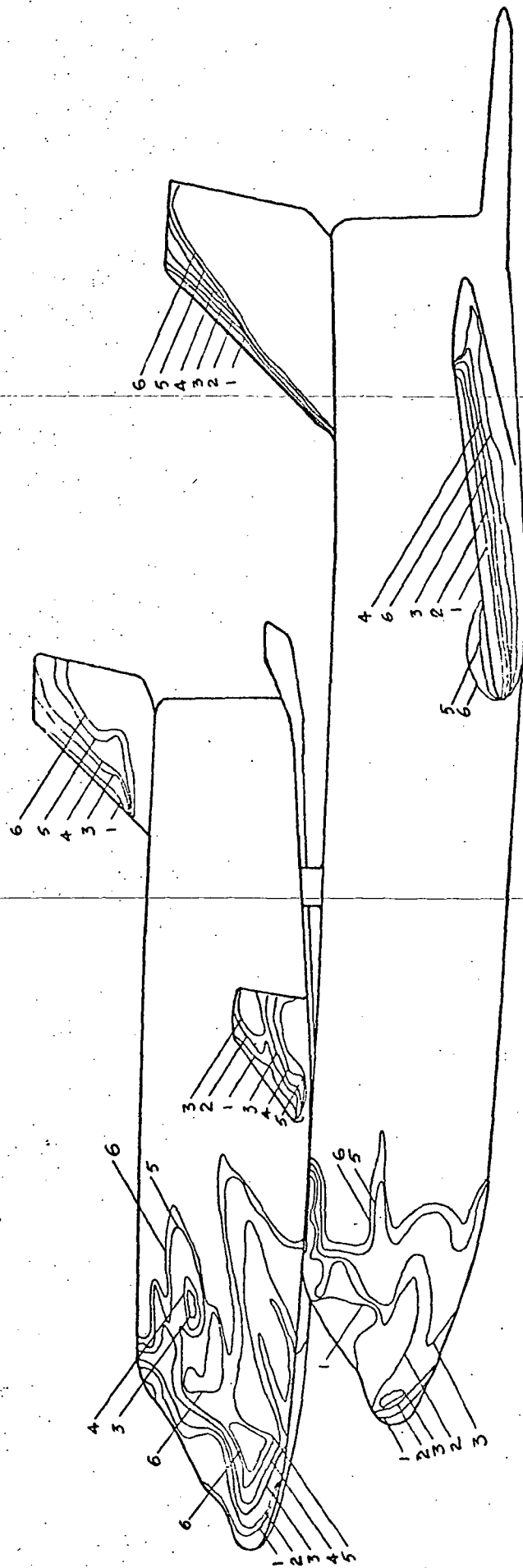
Fig. 44 - Side Panel Local to Stagnation Point Heat Transfer Coefficients



Isotherm	h/h_s
1	0.253
2	0.138
3	0.098
4	0.080
5	0.062
6	0.050

Run No. 449
 $R_N = 5.988 \times 10^5 \text{ 1/Ft}$
 $M = 7.92, T_{FC} = 150^\circ\text{F}$
 $\text{Roll} = 0^\circ, \alpha = 0^\circ, \gamma_{AW} = +6^\circ$
 Booster, Side View

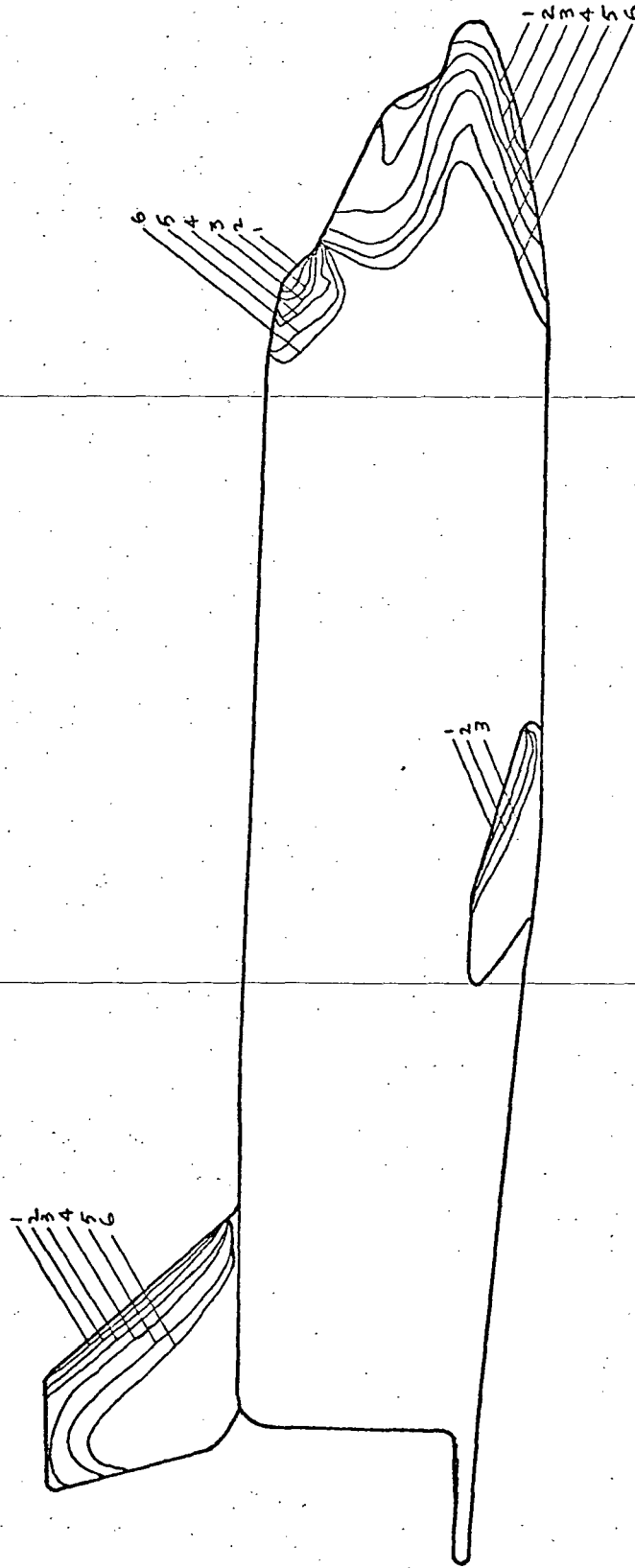
Fig. 45 - Side Panel Local to Stagnation Point Heat Transfer Coefficients



Isotherm	h/h_s
1	0.260
2	0.142
3	0.100
4	0.082
5	0.064
6	0.055

Run No. 450
 $R_N = 6.26 \times 10^5 \text{ 1/Ft}$
 $M = 7.92, T_{\infty} = 150^\circ\text{F}$
 $\text{Roll} = 0^\circ, \alpha = 0^\circ, \gamma_{\text{NW}} = -6^\circ$
 Launch Config., Side View

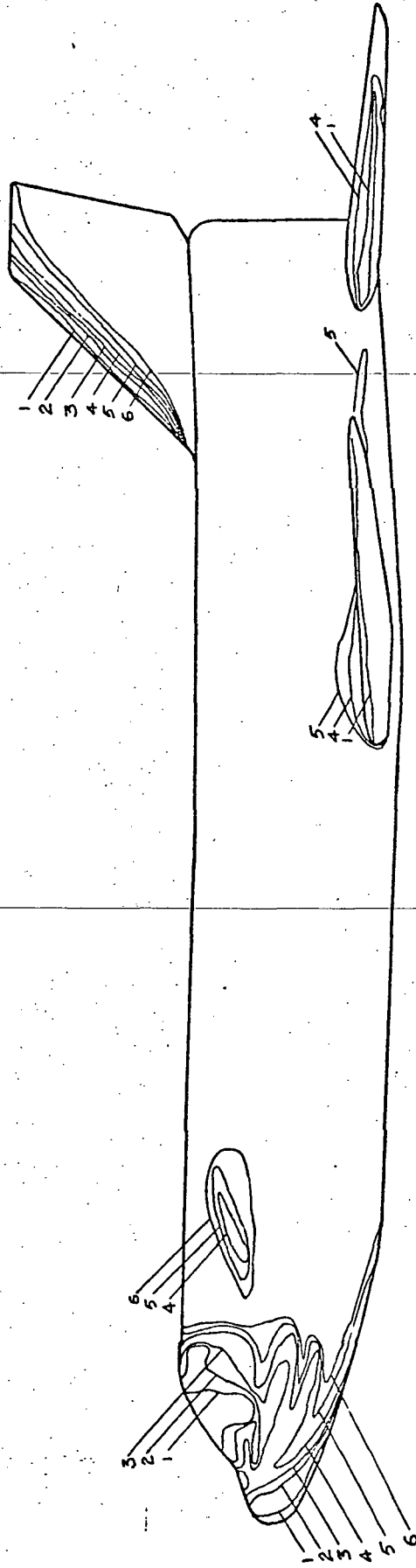
Fig. 46 - Side Panel Local to Stagnation Point Heat Transfer Coefficients



Isotherm	h/h_s
1	0.237
2	0.130
3	0.092
4	0.075
5	0.058
6	0.05

Run 451
 $R_N = 6.26 \times 10^5$ 1/Ft
 $M = 7.92$, $T_{PC} = 150^\circ\text{F}$
 Roll = , $\alpha = 0$, $\gamma_{AV} = -6^\circ$
 Orbiter, Side View

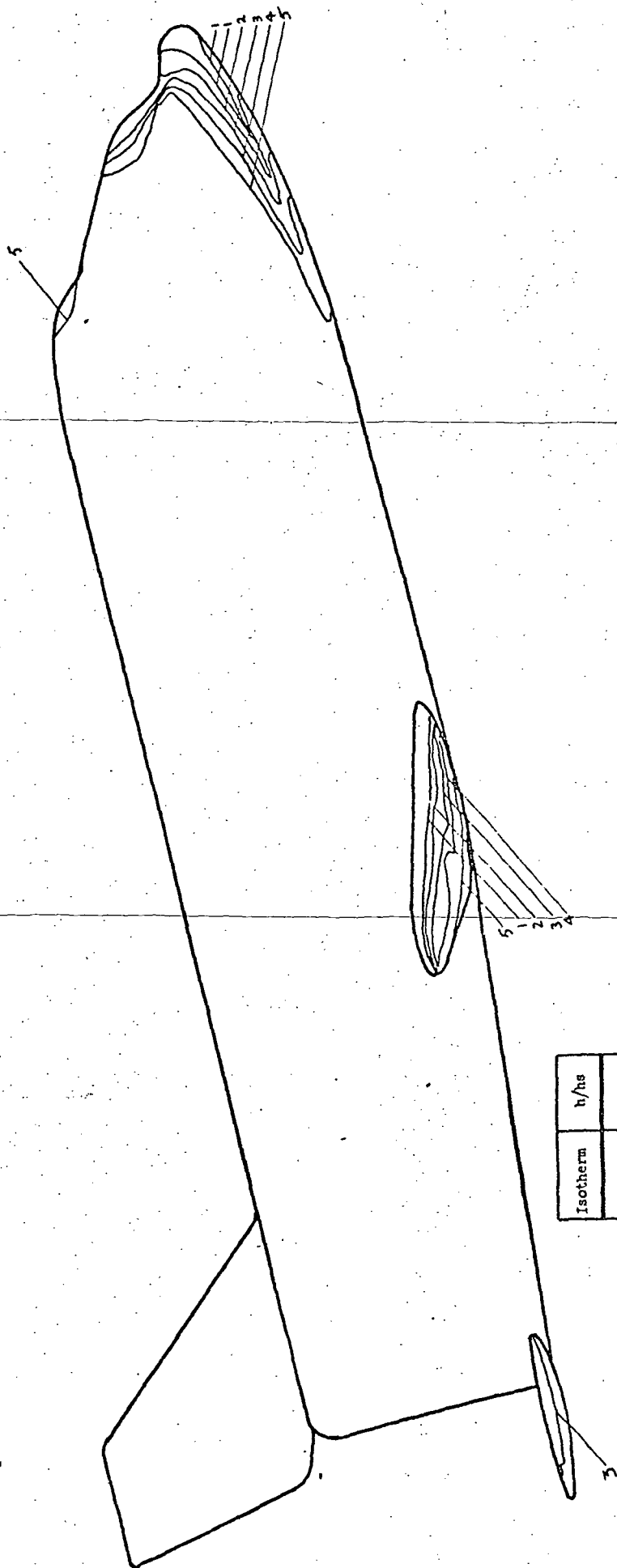
Fig. 47 - Side Panel Local to Stagnation Point Heat Transfer Coefficients



Isotherm	h/h_s
1	0.253
2	0.134
3	0.098
4	0.080
5	0.062
6	0.053

Run No. 452
 $R_N = 6.26 \times 10^5$ 1/Ft
 $M = 7.92$, $T_{PC} = 150^\circ\text{F}$
 $\text{Roll} = 0^\circ$, $\alpha = 0^\circ$, $\text{Yaw} = -6^\circ$
 Booster, Side View

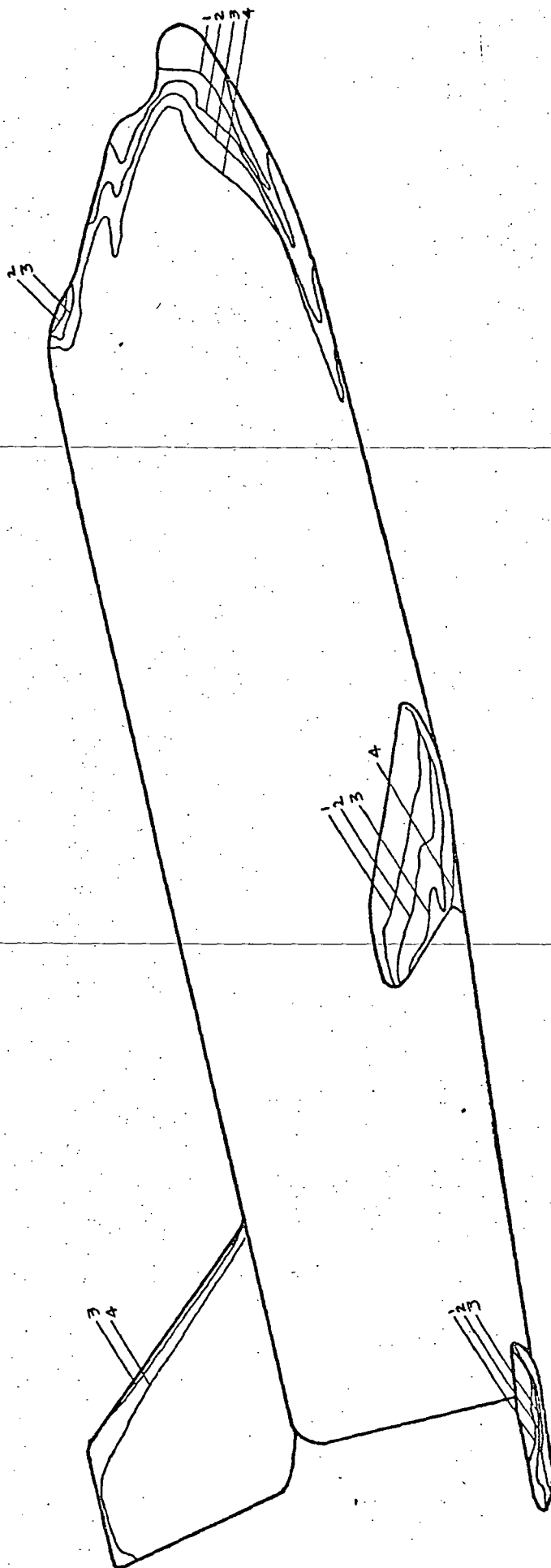
Fig. 48 - Side Panel Local to Stagnation Point Heat Transfer Coefficients



Isotherm	h/h_s
1	0.260
2	0.142
3	0.100
4	0.082
5	0.064

Run No. 453
 $R_N = 6.38 \times 10^5 \text{ 1/Ft}$
 $M = 7.92, T_{PC} = 150^\circ\text{F}$
 $\text{Roll} = 0^\circ, \alpha = 20^\circ$
 Orbiter, Side View

Fig. 49 - Side Panel Total to Stagnation Point Heat Transfer Coefficients

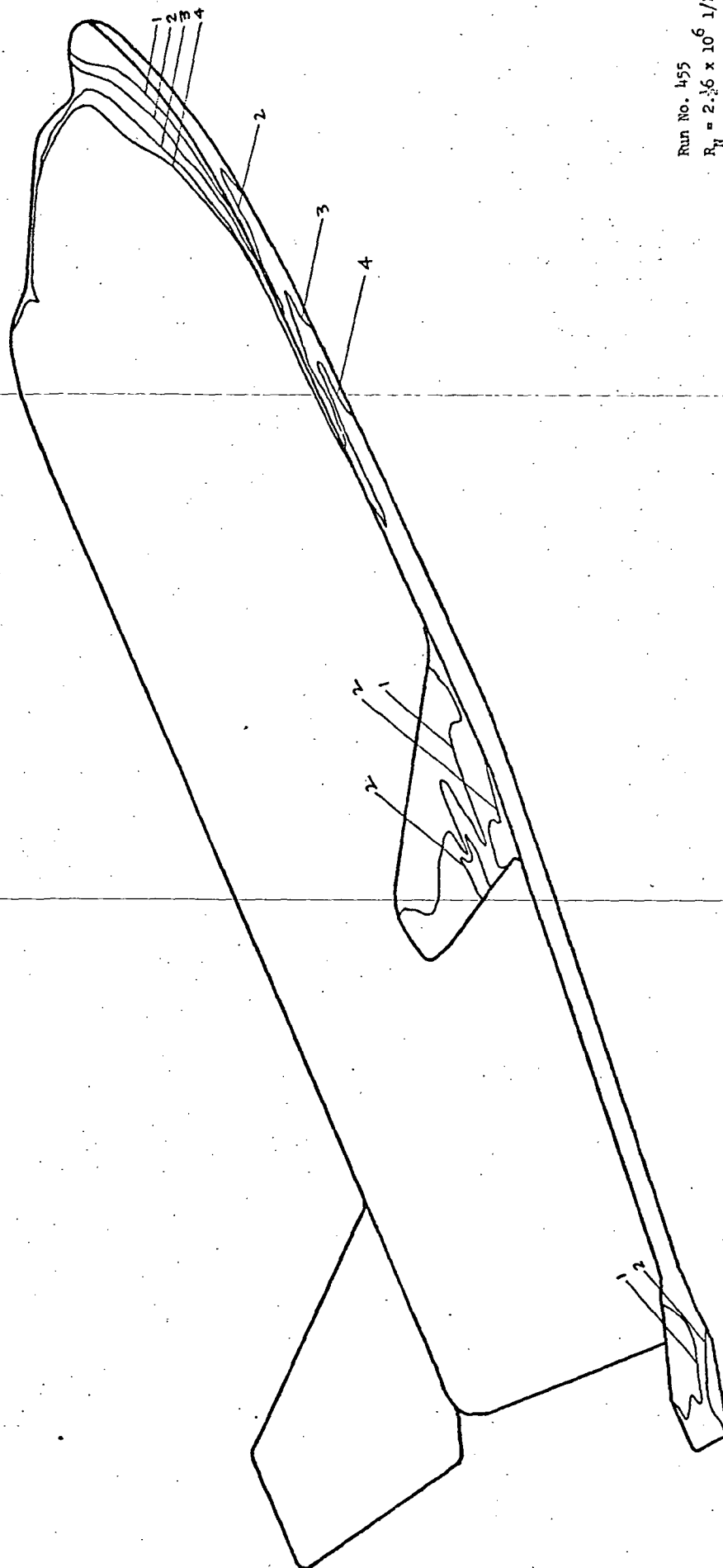


Isotherm	h/h_s
1	0.133
2	0.073
3	0.051
4	0.042

Run No. 454
 $R_N = 2.04 \times 10^6 \text{ 1/ft}$
 $M = 7.92$, $T_{PC} = 150^\circ\text{F}$
 $\text{Roll} = 0^\circ$, $\alpha = 20^\circ$
 Orbiter, Side View

Fig. 50 - Side Panel Local to Stagnation Point Heat Transfer Coefficients

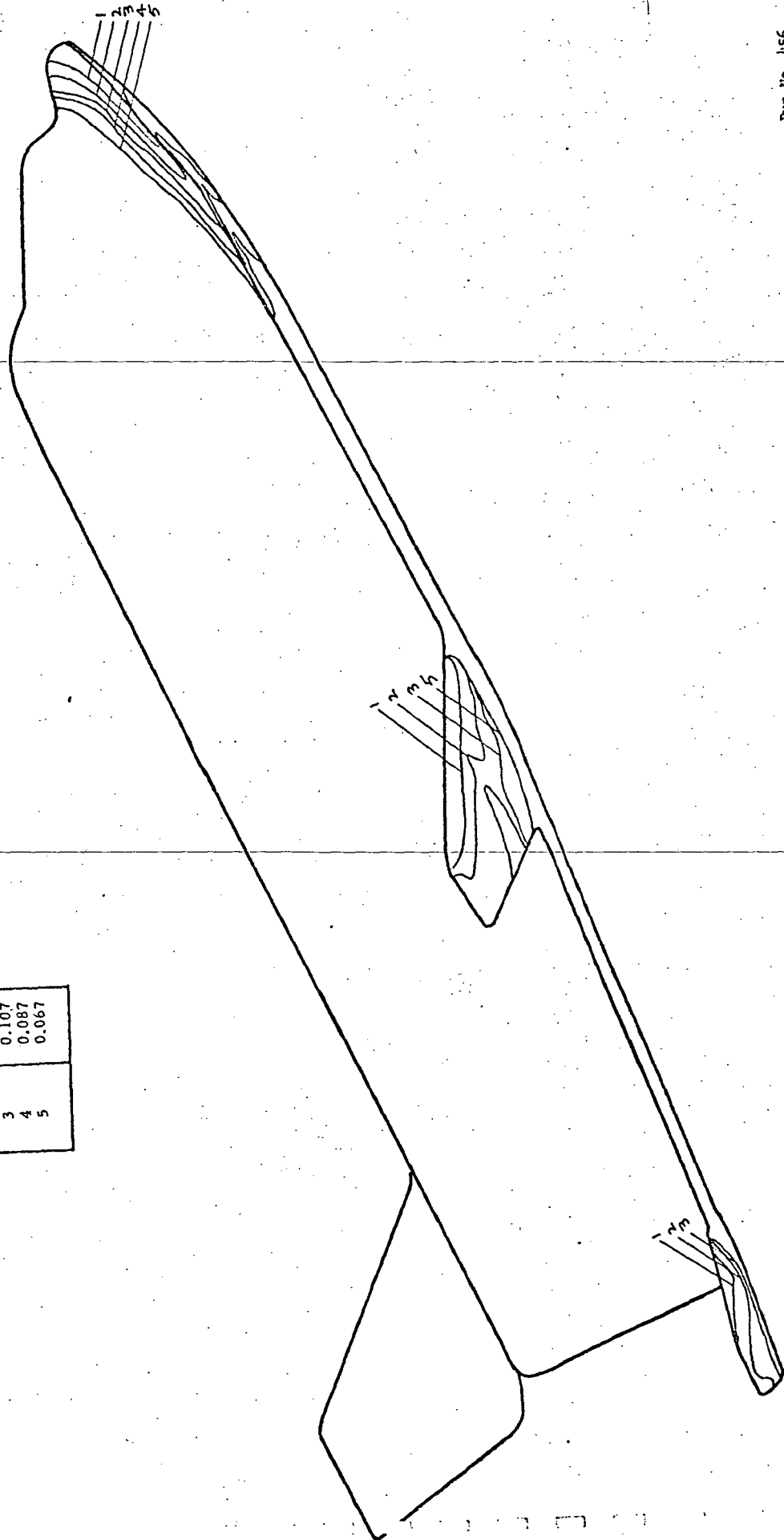
Isotherm	h/h_s
1	0.128
2	0.070
3	0.050
4	0.031



Run No. 455
 $R_H = 2.36 \times 10^6 \text{ 1/Ft}$
 $M = 7.92, T_{PC} = 150^\circ\text{F}$
 $\text{Roll} = 0^\circ, \alpha = 30^\circ$
 Orbiter, Side View

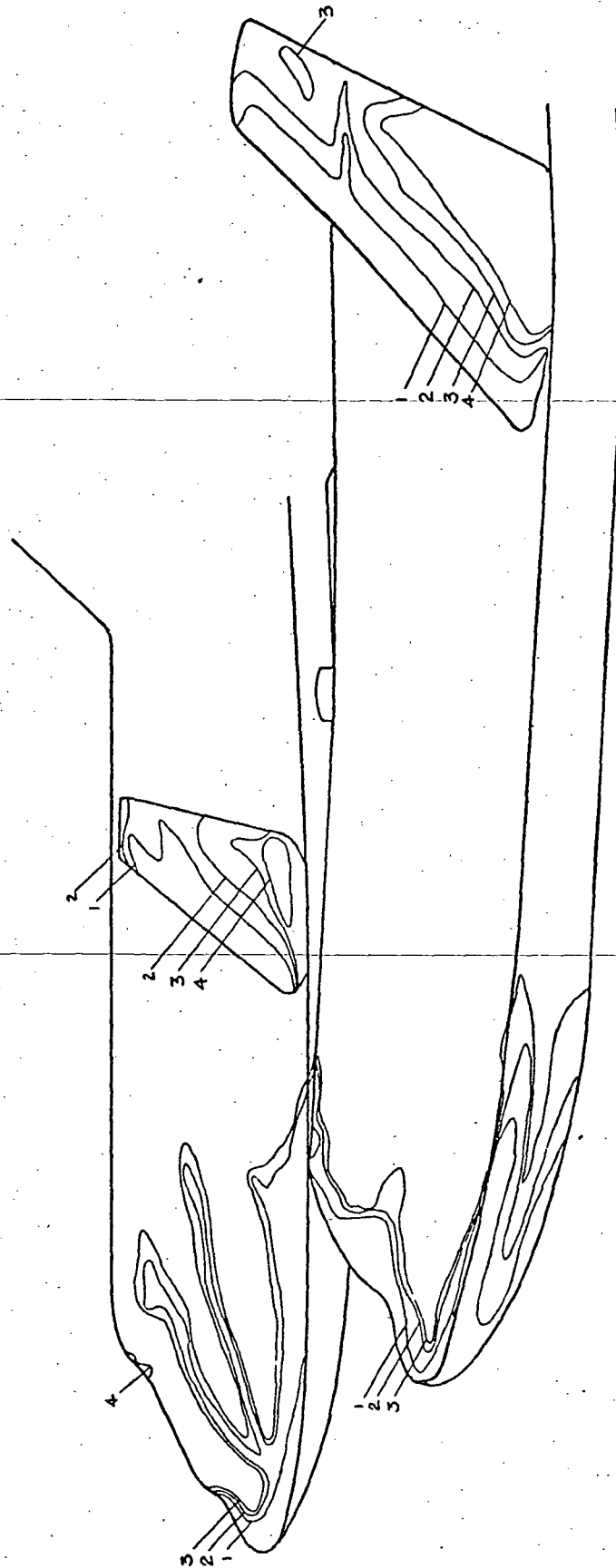
Fig. 51 - Side Panel Local to Stagnation Point Heat Transfer Coefficients

Isotherm	h/h_e
1	0.275
2	0.150
3	0.107
4	0.087
5	0.067



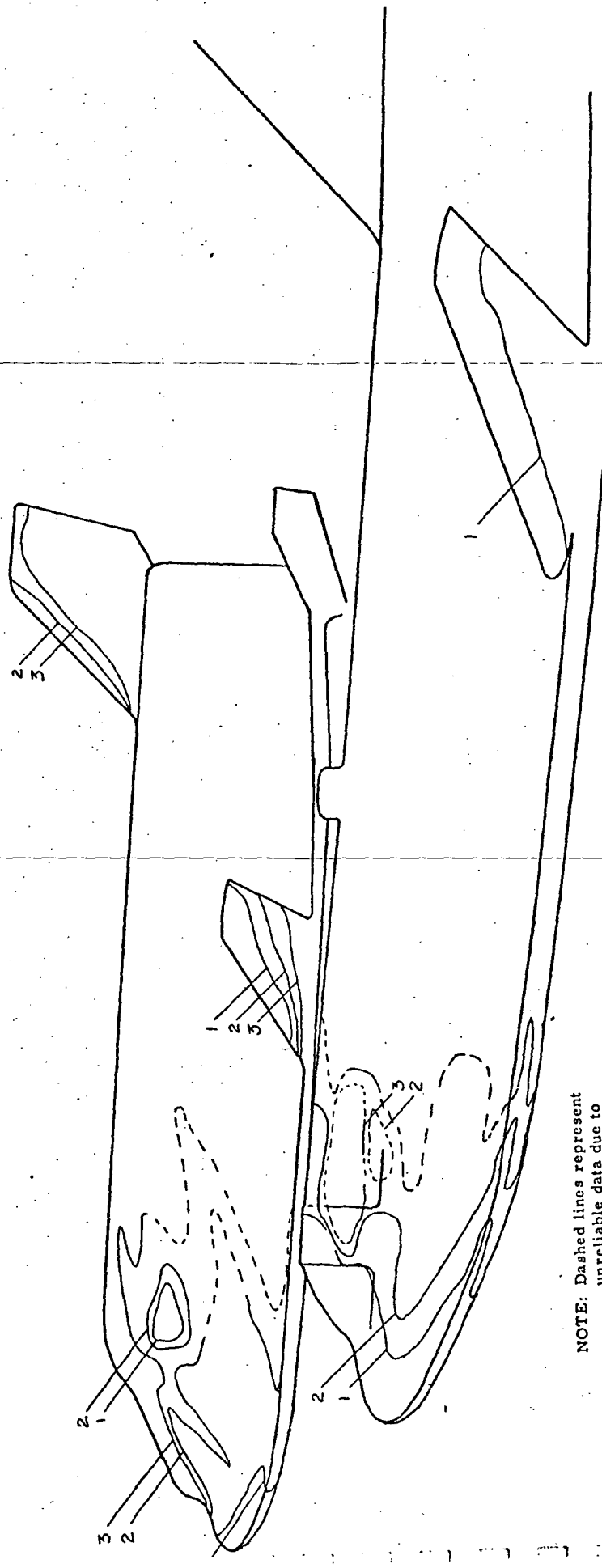
Run No. 456
 $R_N = 6.38 \times 10^5$ 1/Ft.
 $M = 7.92$, $T_{PC} = 150^\circ F$
 $Roll = 0^\circ$, $\alpha = 30^\circ$
 Orbiter, Side View

Fig. 52 - Side Panel Local to Stagnation Point Heat Transfer Coefficients



Run No. 460
 $R_N = 3.7 \times 10^6 \text{ 1/Ft}$
 $N = 7.92, T_K = 150^\circ\text{F}$
 $\text{Roll} = 15^\circ, \alpha = 0^\circ$
 Launch Config.. Side View

Fig. 53 - Side Panel Local to Stagnation Point Heat Transfer Coefficients

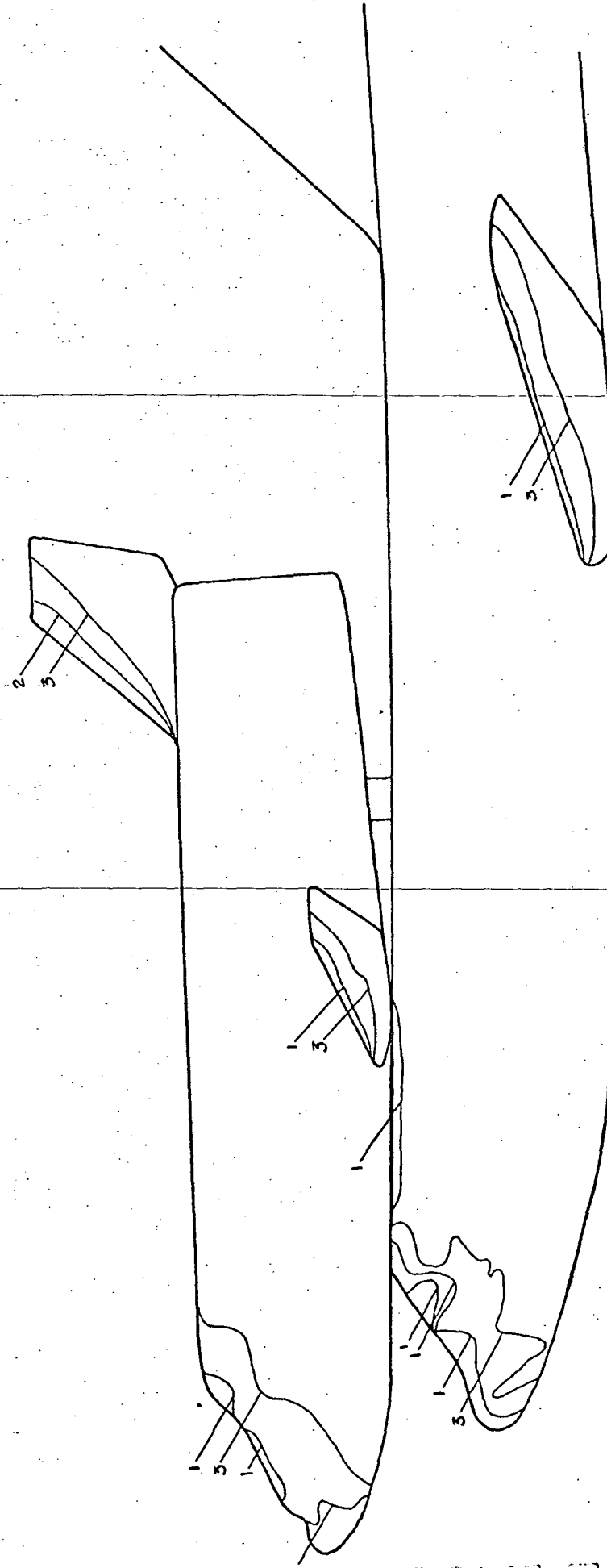


NOTE: Dashed lines represent unreliable data due to poor lighting.

Isotherm	h/h_s
1	0.090
2	0.049
3	0.035

Run No. 461
 $P_N = 3.747 \times 10^6$ l/Ft
 $M = 7.92$, $T_{PC} = 150^\circ\text{F}$
 $\text{Roll} = 0^\circ$, $\alpha = 5^\circ$
 Launch Config., Side View

Fig. 54 - Side Panel Local to Stagnation Point Heat Transfer Coefficients



Isotherm	h/h_s
1	0.088
2	0.048
3	0.034

Run No. 462
 $R_H = 3.726 \times 10^6 \text{ 1/Ft}$
 $M = 7.93, T_{PC} = 150^\circ\text{F}$
 $\text{Roll} = 0^\circ, \alpha = -5^\circ$
 Launch Config., Side View

Fig. 55 - Side Panel Local to Stagnation Point Heat Transfer Coefficients

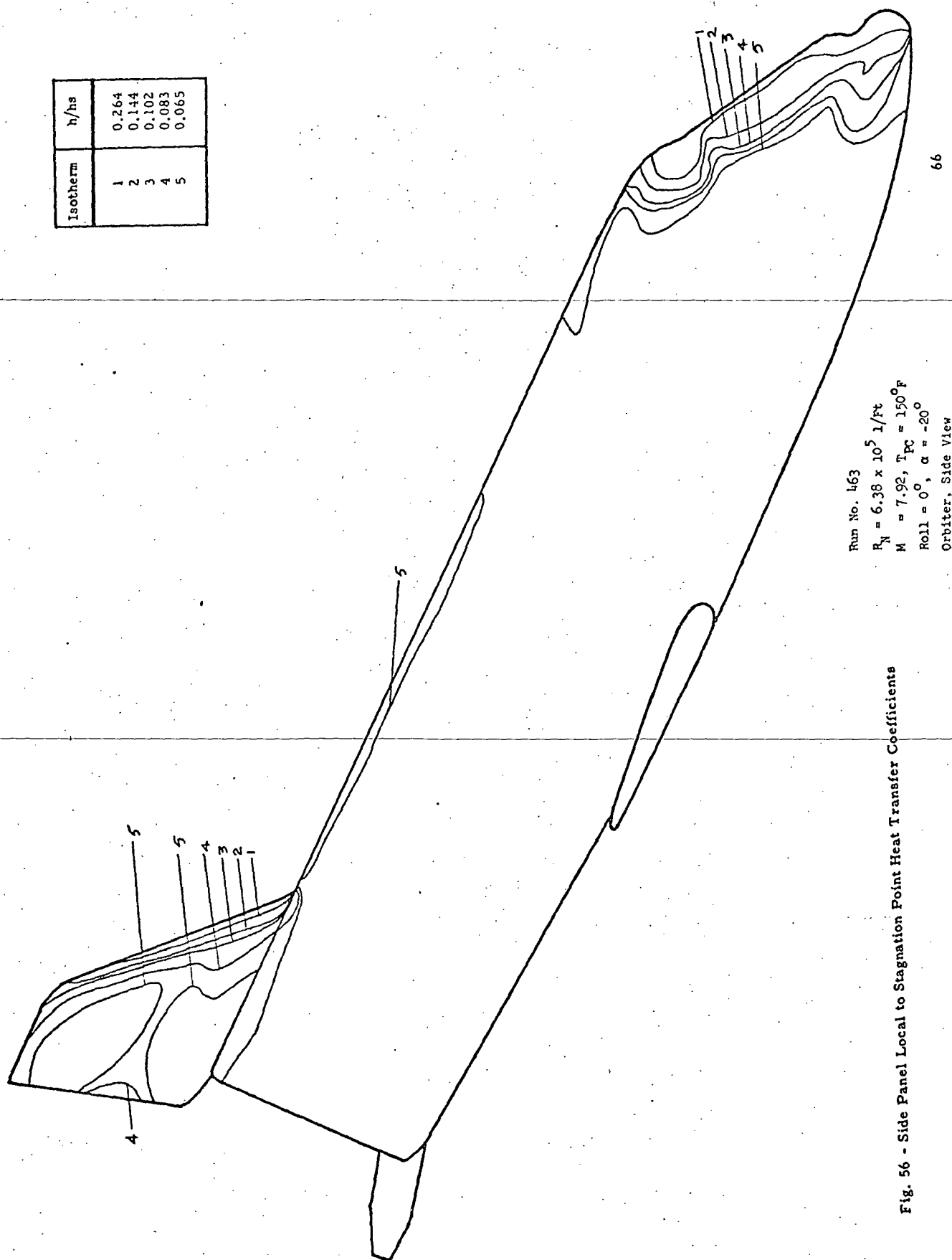
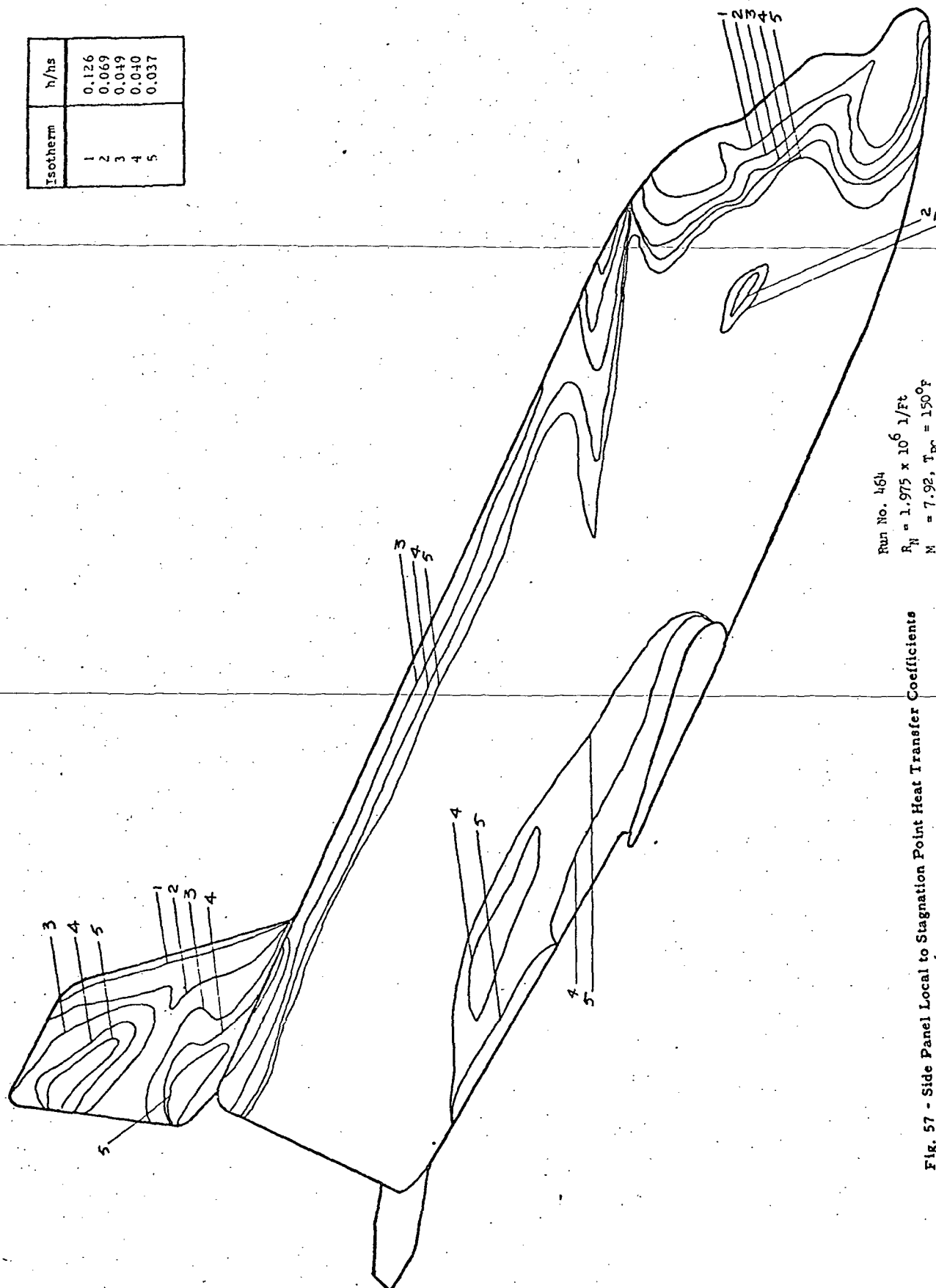


Fig. 56 - Side Panel Local to Stagnation Point Heat Transfer Coefficients

Isotherm	h/h_s
1	0.126
2	0.069
3	0.049
4	0.040
5	0.037



Run No. 464
 $R_H = 1.975 \times 10^6 \text{ l/Ft}$
 $M = 7.92, T_{PC} = 150^\circ\text{F}$
 $\text{Roll} = 0^\circ, \alpha = -20^\circ$
 Orbiter, Side View

Fig. 57 - Side Panel Local to Stagnation Point Heat Transfer Coefficients

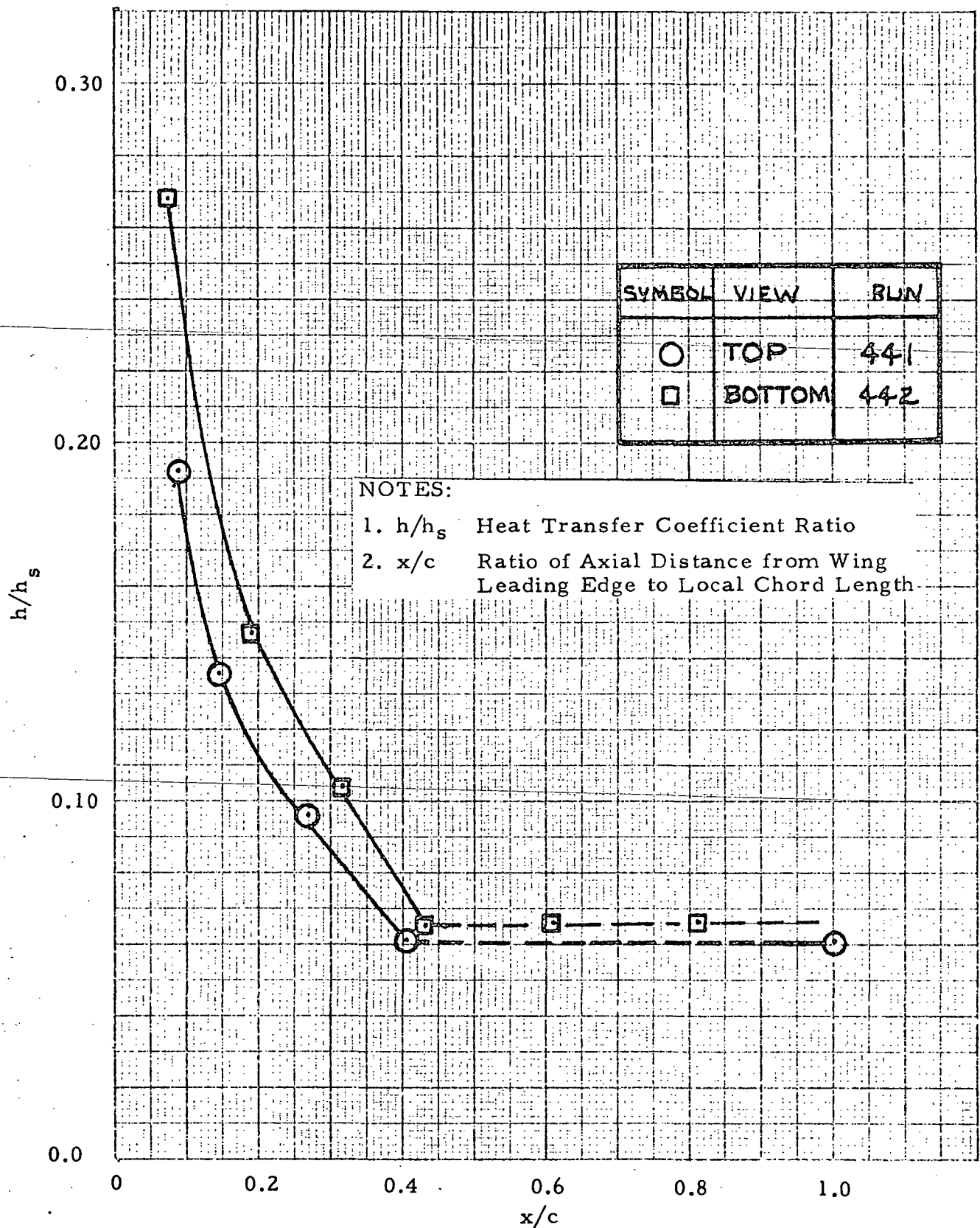


Fig. 58 - NASA-MSC Orbiter/Launch Configuration Wing Chordwise Heat Transfer Distribution at 50% Span, $\alpha = 0^\circ$, $\text{yaw} = 0^\circ$

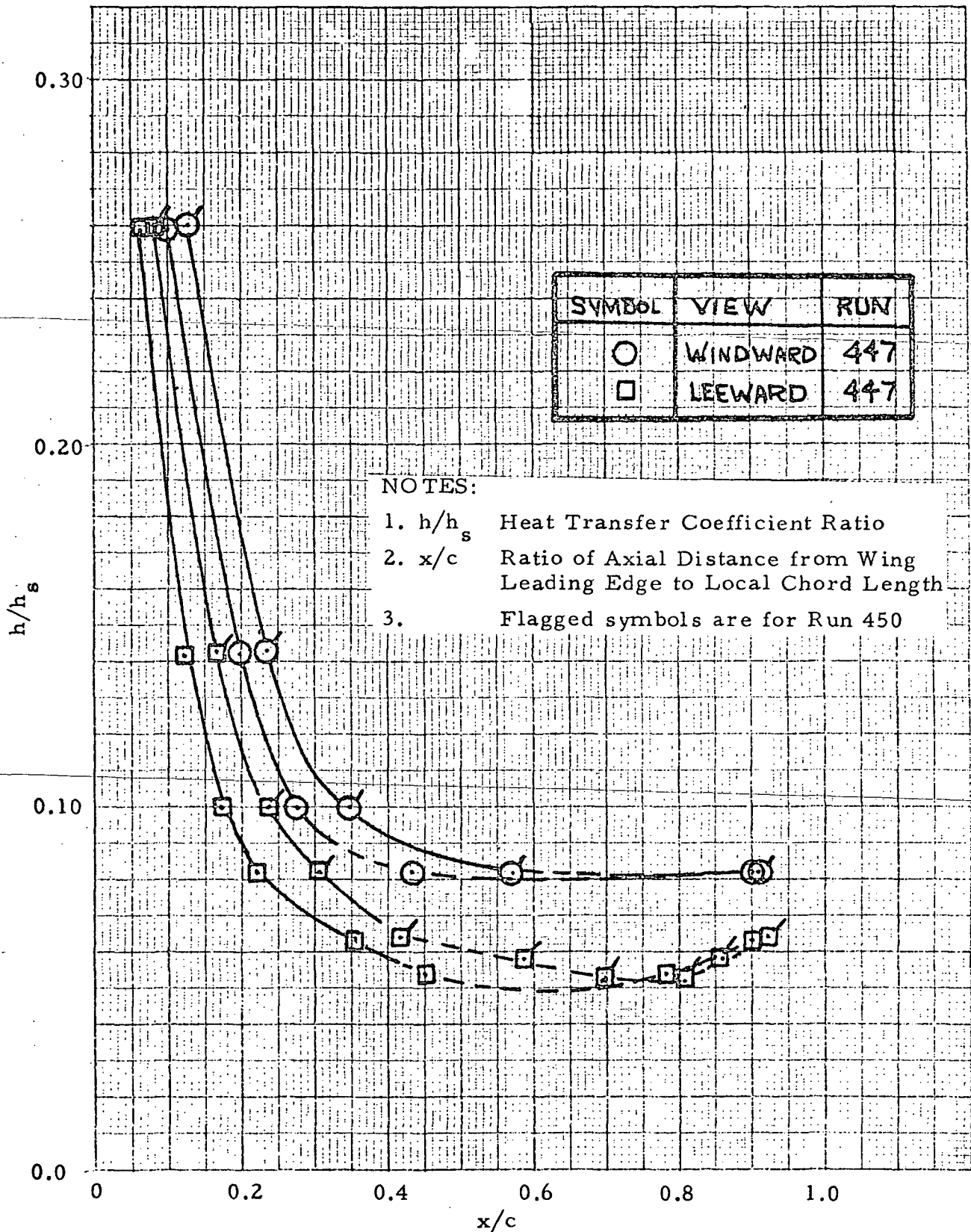


Fig. 59 - NASA-MSC Orbiter/Launch Configuration Wing Chordwise Heat Transfer Distribution at 50% Span, Alpha = 0°, yaw = 6°

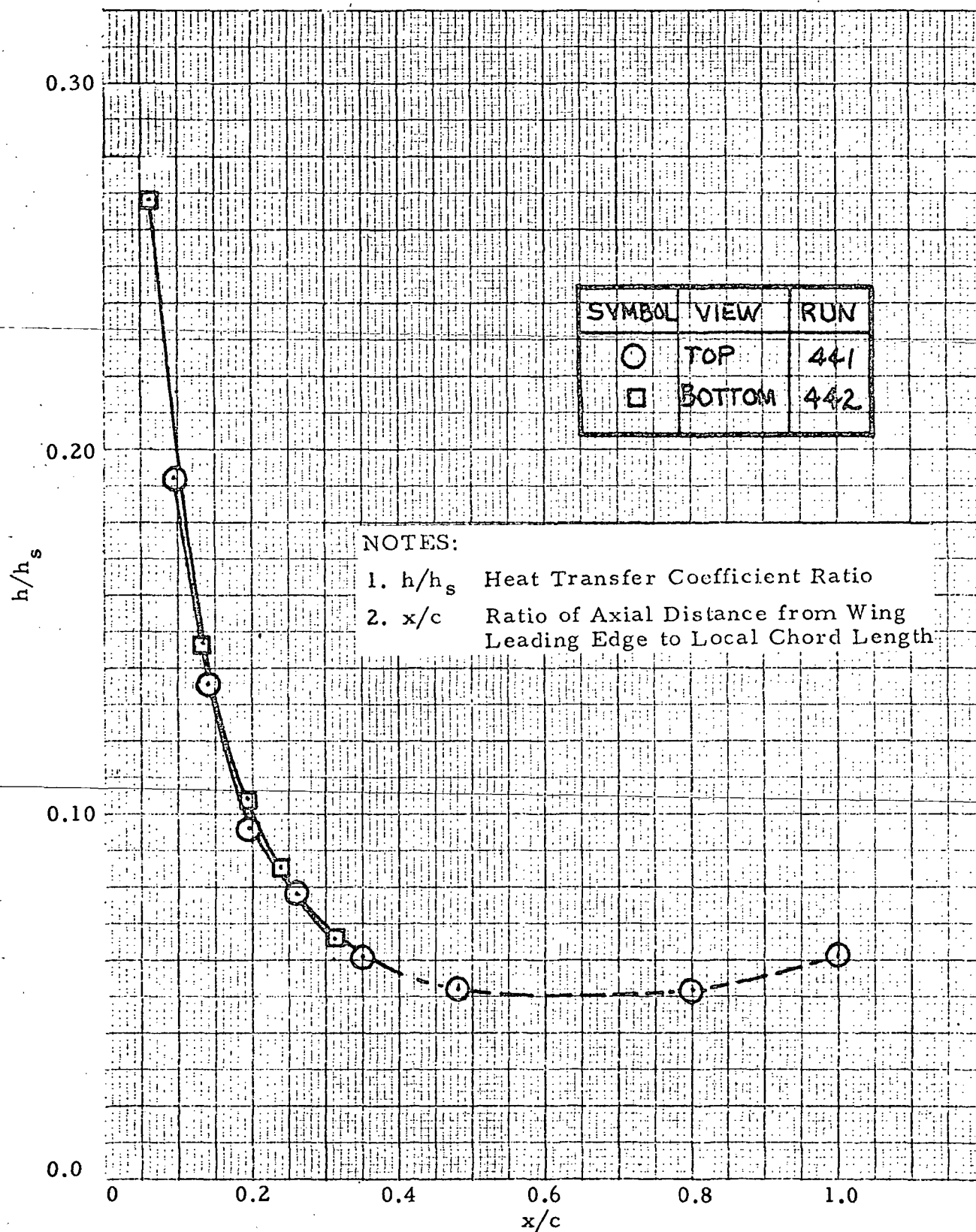


Fig. 60 - NASA-MSC Booster/Launch Configuration Wing Chordwise Heat Transfer Distribution at 50% Span, $\alpha = 0^\circ$, $\text{yaw} = 0^\circ$

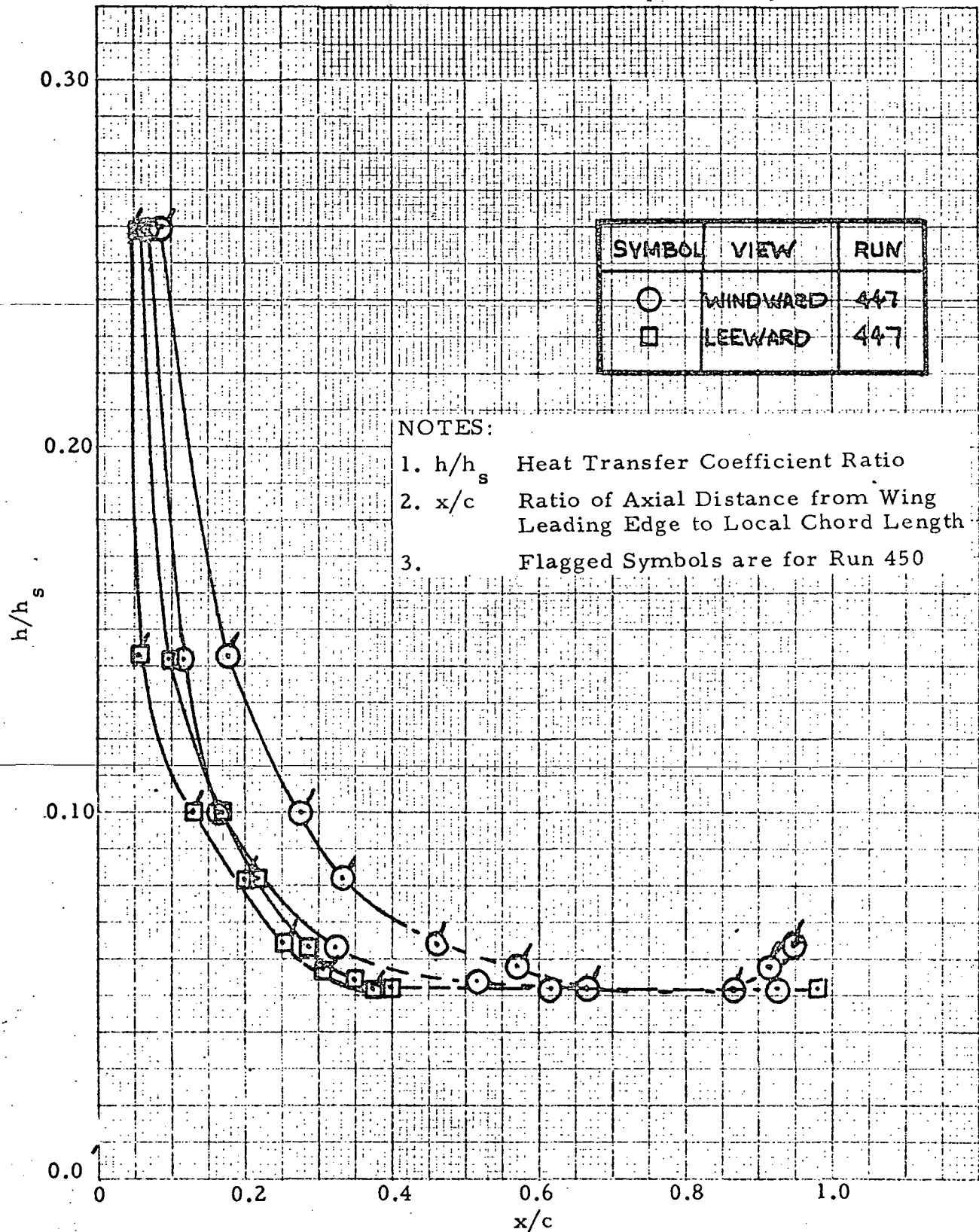


Fig. 61 - NASA-MSC Booster/Launch Configuration Wing Chordwise Heat Transfer Distribution at 50% Span; Alpha = 0°, yaw = 6°

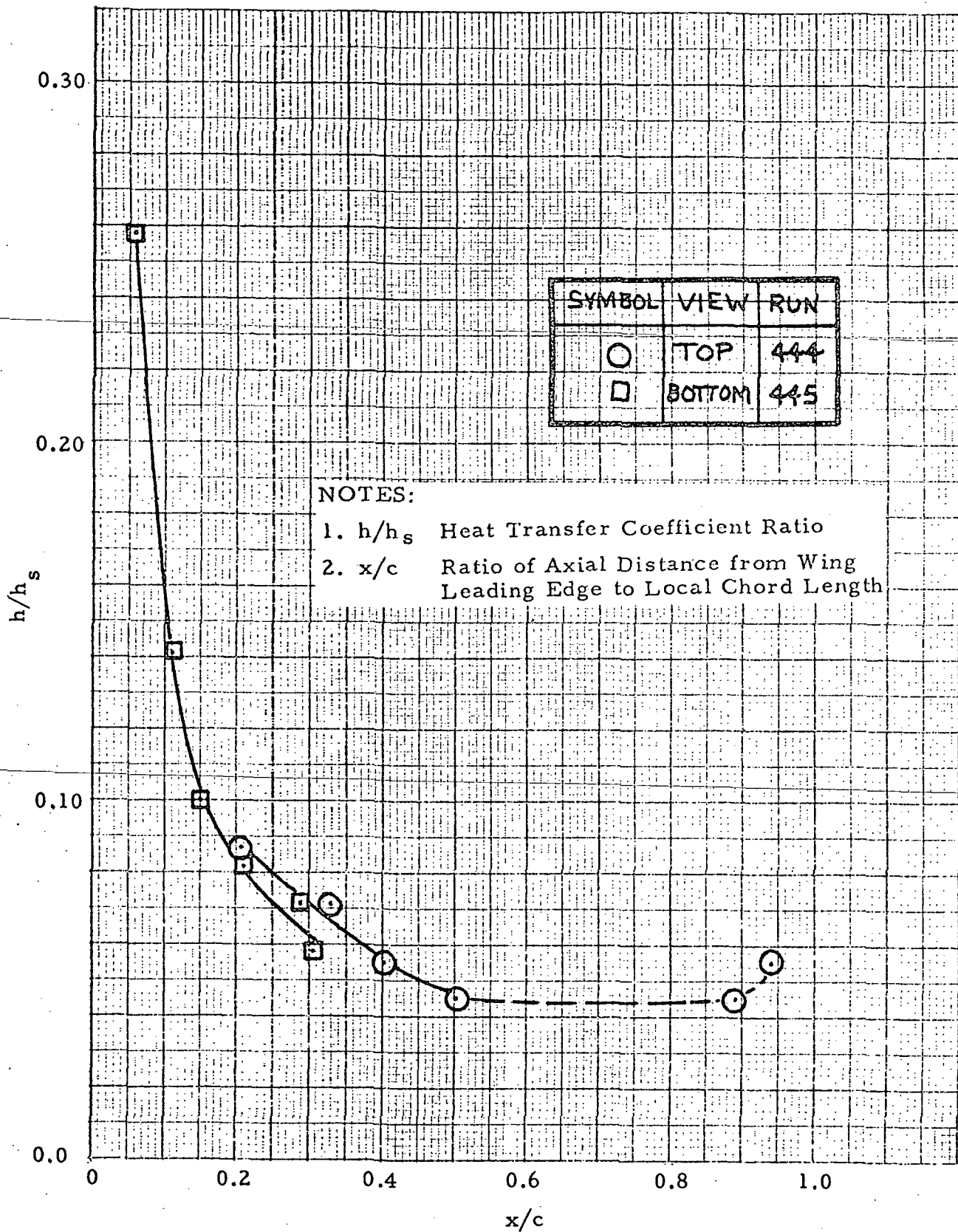


Fig. 62 - NASA-MSC Booster/Launch Configuration Wing Chordwise Heat Transfer Distribution at 50% Span, $\alpha = 10^\circ$, yaw = 0°

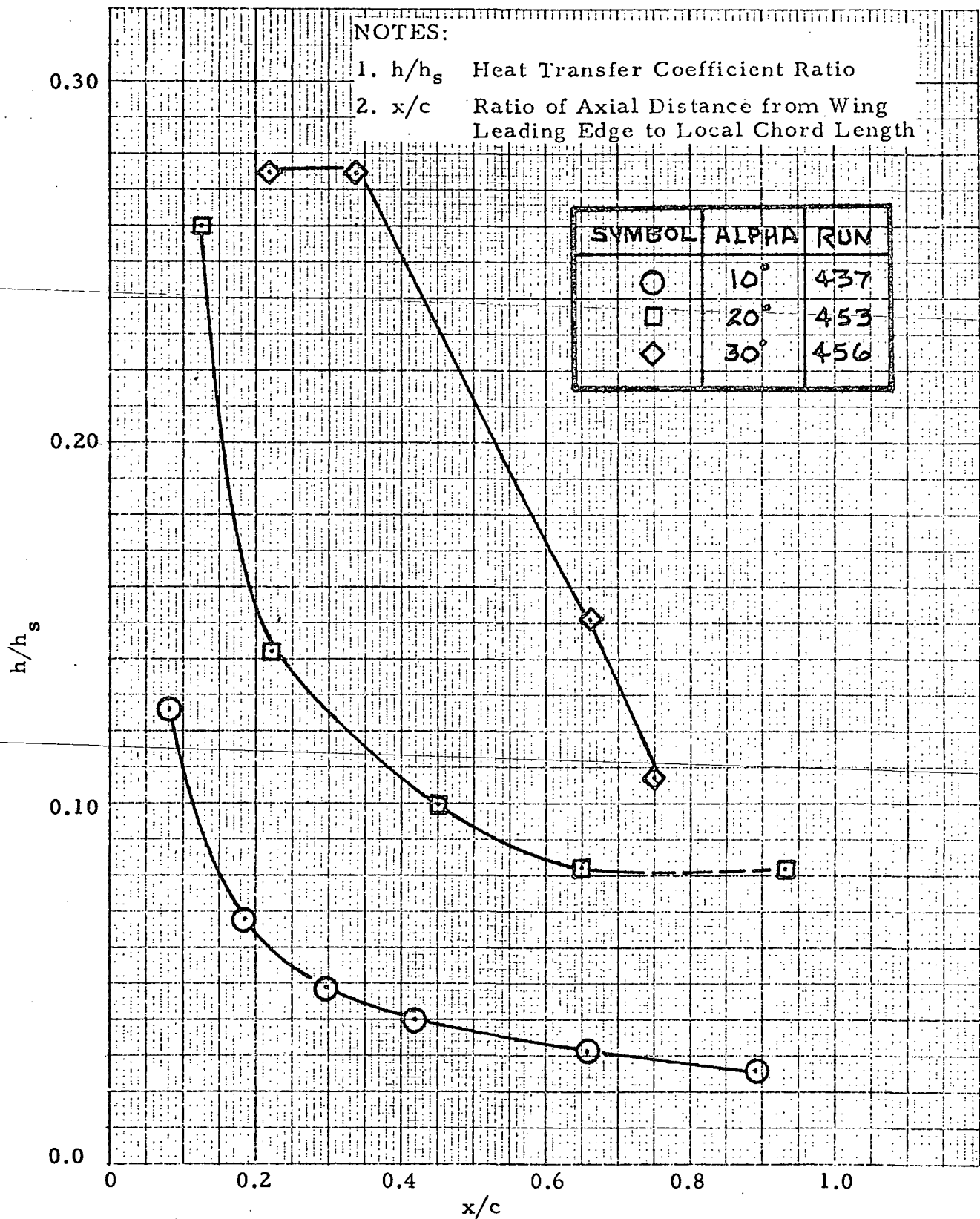


Fig. 63 - NASA-MSC Orbiter Configuration Bottom Wing Chordwise Heat Transfer Distribution at 25% Span

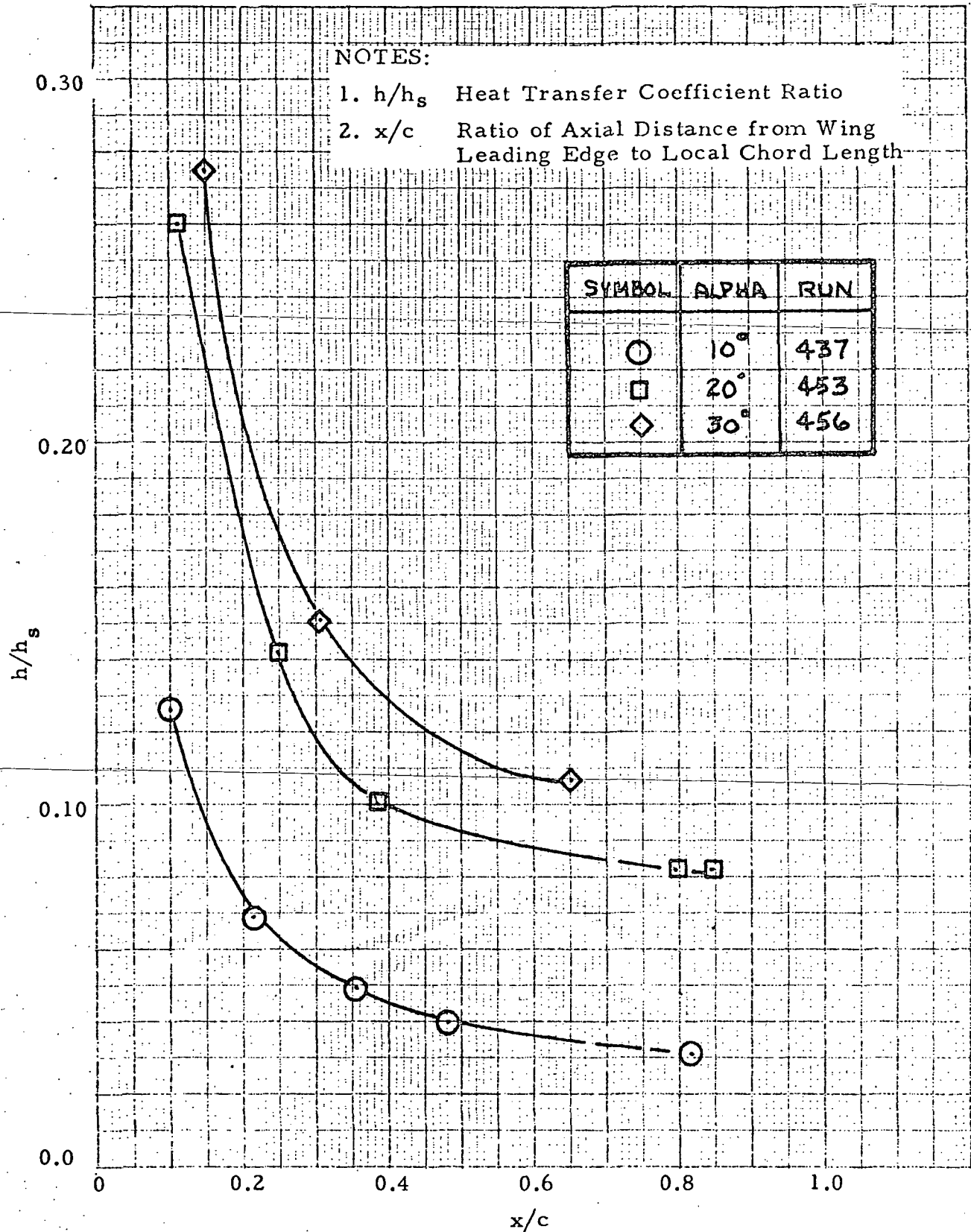


Fig. 64 - NASA-MSC Orbiter Configuration, Bottom Wing Chordwise Heat Transfer Distribution at 50% Span

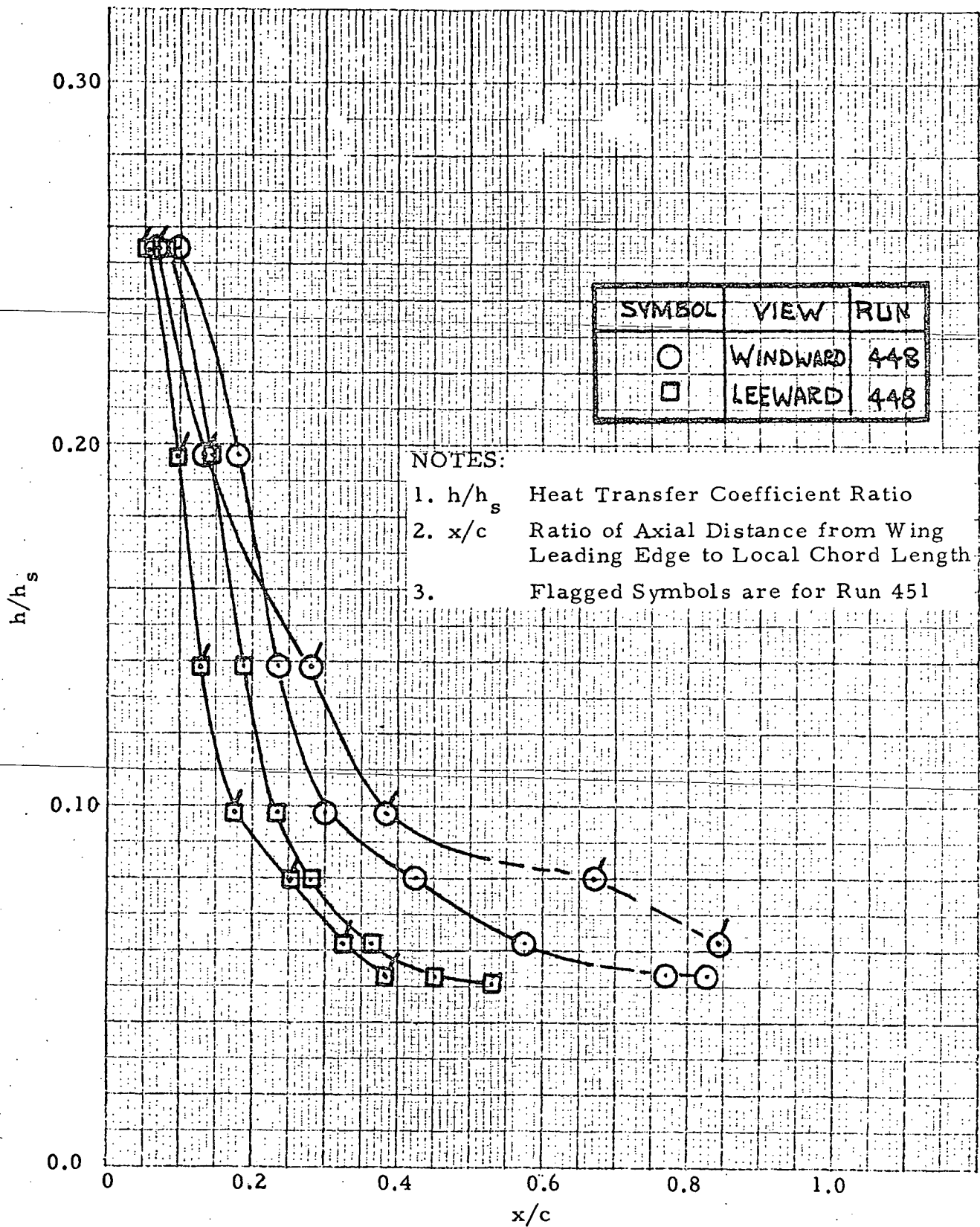


Fig. 65 - NASA-MSC Orbiter Configuration Wing Top Chordwise Heat Transfer Distribution at 25% Span, $\alpha = 0^\circ$, yaw = 6°

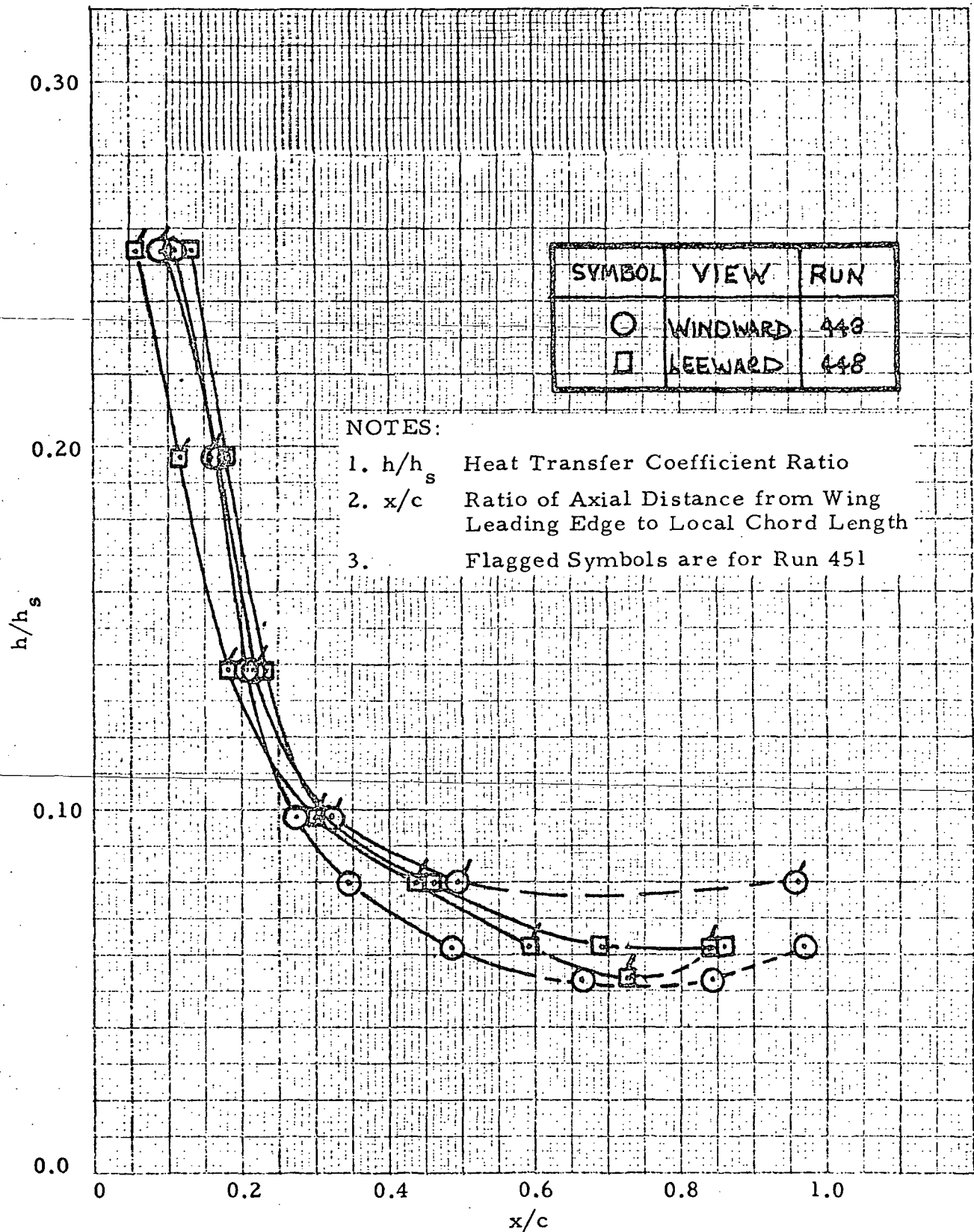


Fig. 66 - NASA-MSC Orbiter Configuration Wing Top Chordwise Heat Transfer Distribution at 50% Span, Alpha = 0°, yaw = 6°

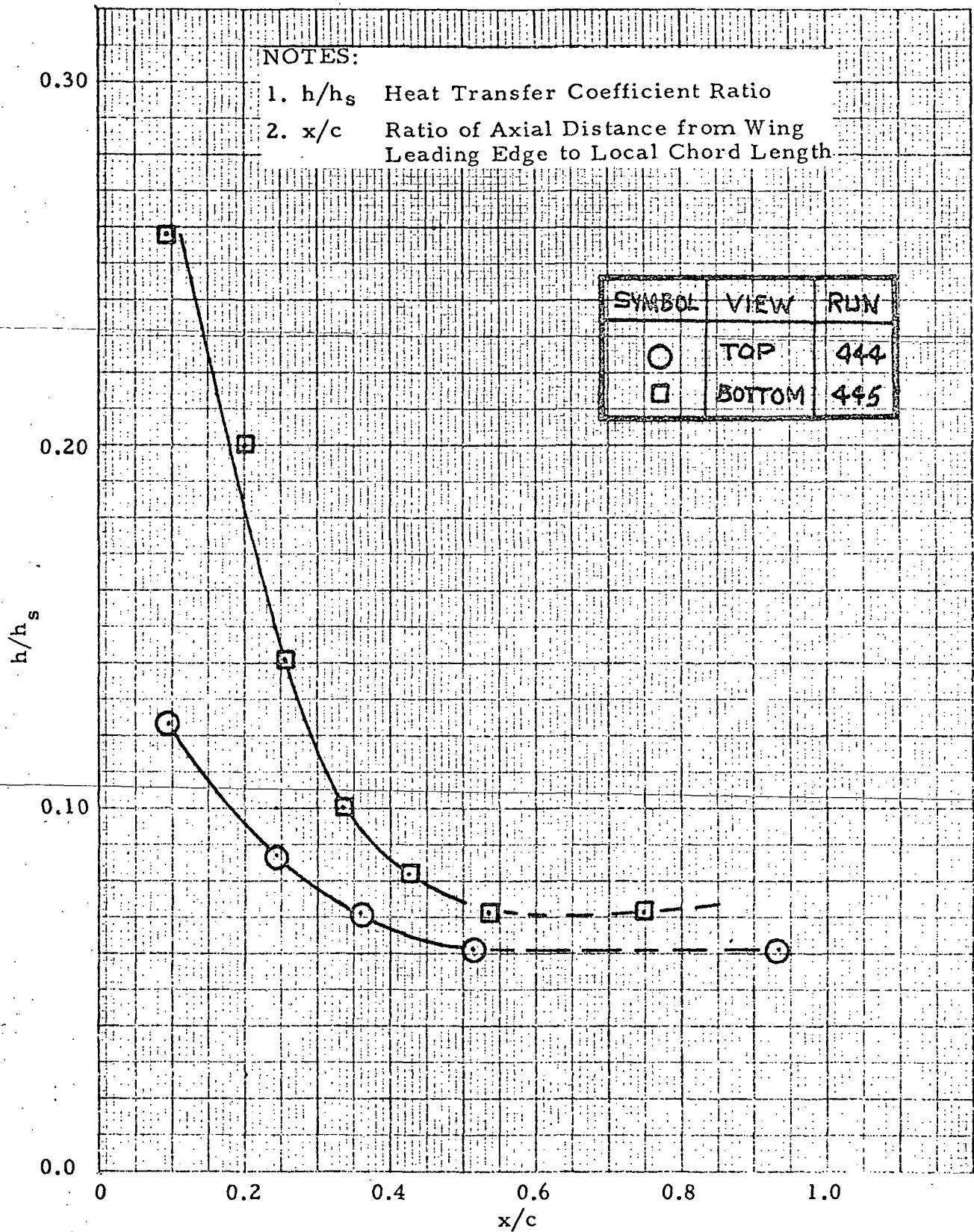


Fig. 67 - NASA-MSC Orbiter/Launch Configuration Wing Chordwise Heat Transfer Distribution at 50% Span, $\alpha = +10^\circ$, yaw = 0°

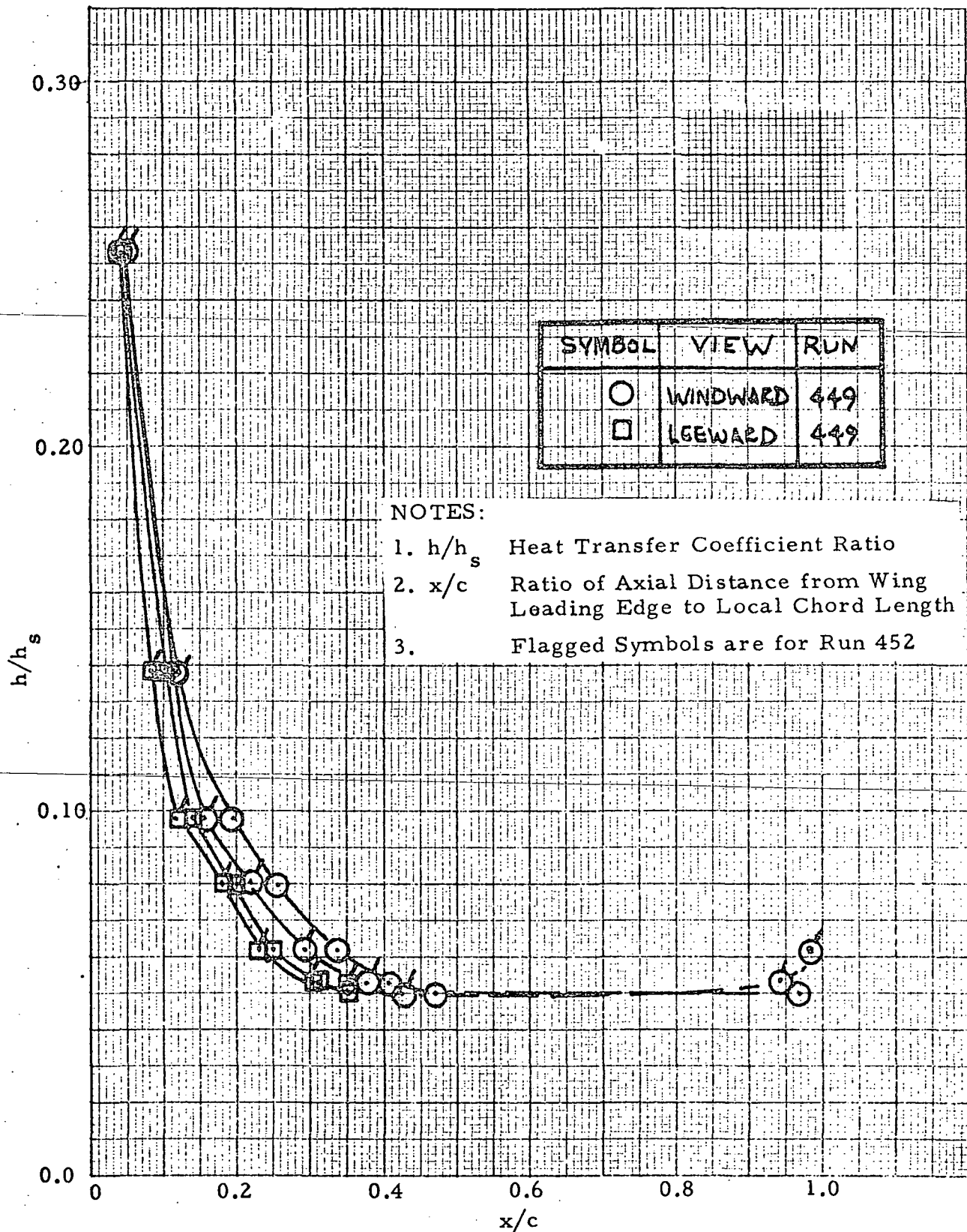


Fig. 68 - NASA-MSC Booster Configuration Wing Bottom Chordwise Heat Transfer Distribution at 50% Span, Alpha = 0°, yaw = 6°

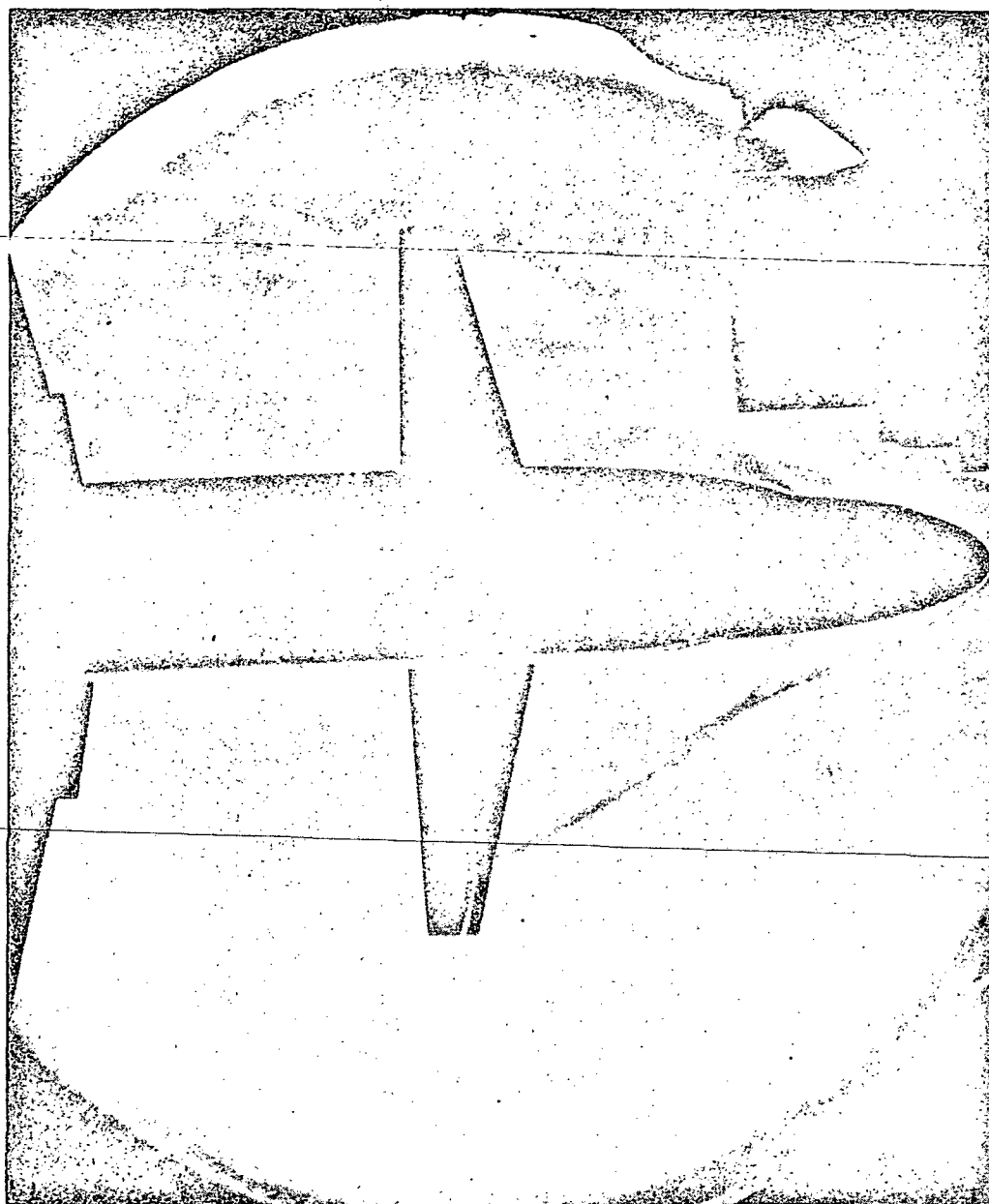


Fig. 69 - Schlieren Photographs of Run 430; Pitch = 0° , Yaw = 0° ,

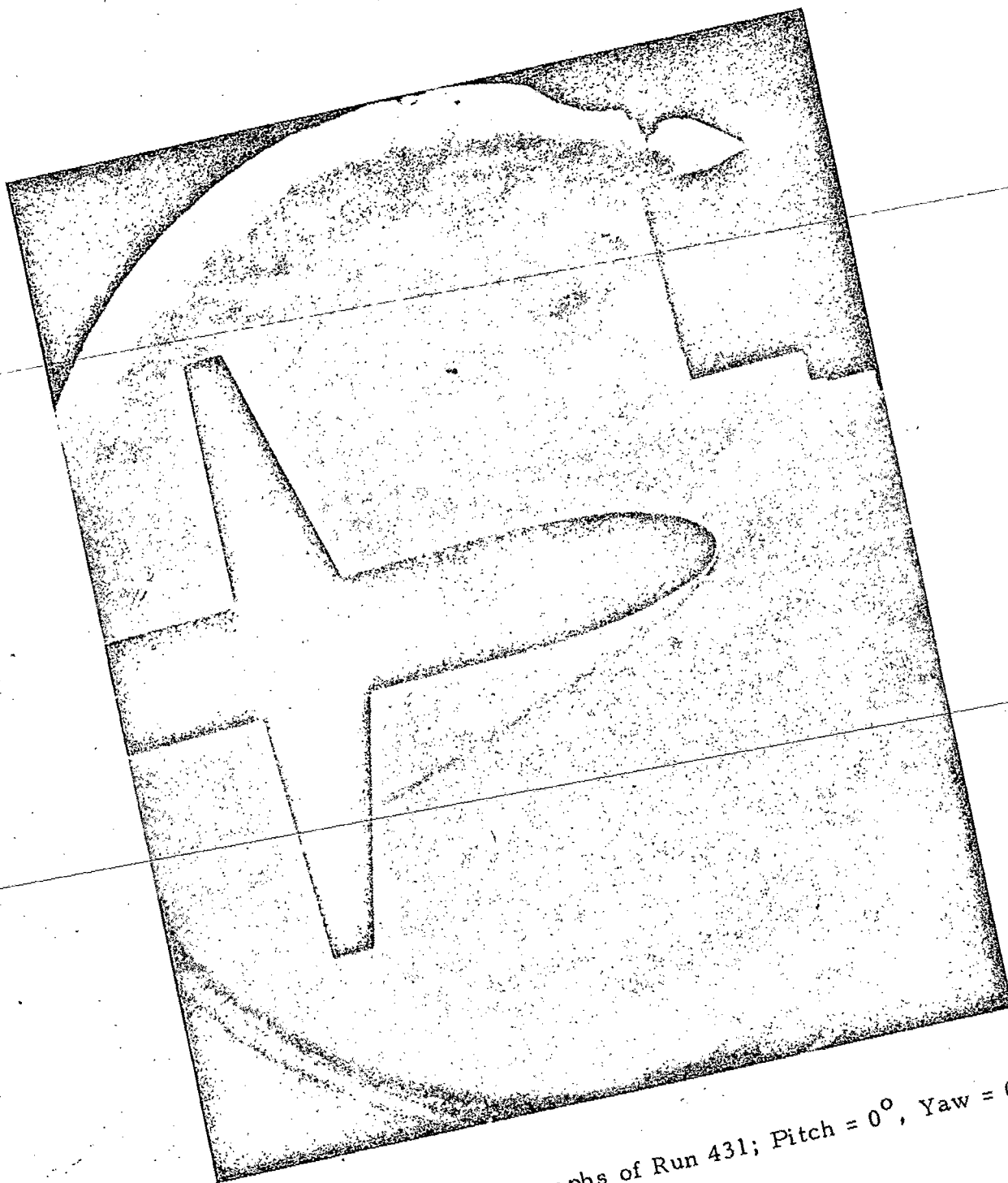


Fig. 70 - Schlieren Photographs of Run 431; Pitch = 0° , Yaw = 0° ,

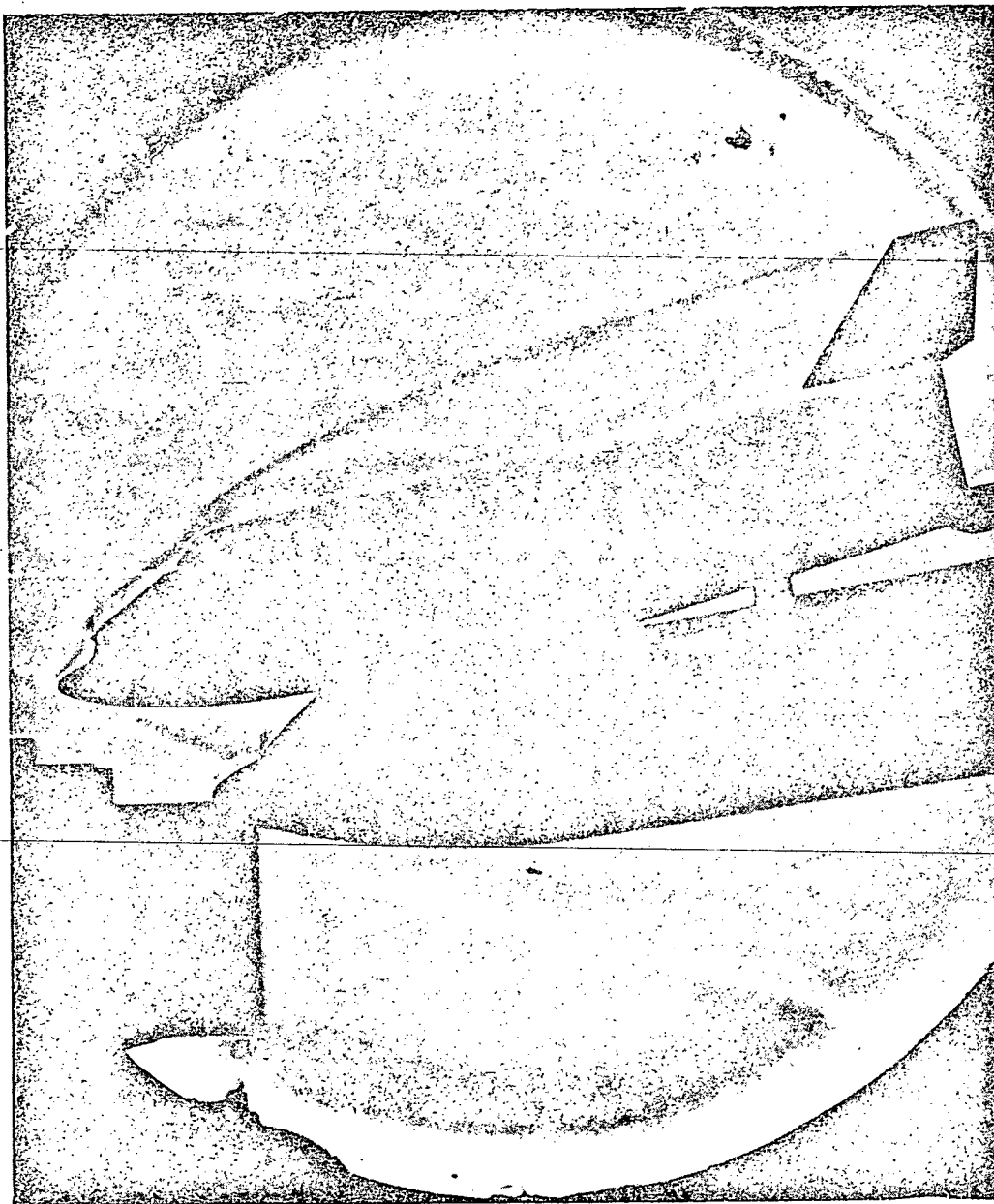


Fig. 71 - Schlieren Photographs of Run 434; Pitch = -10°
Yaw = 0°

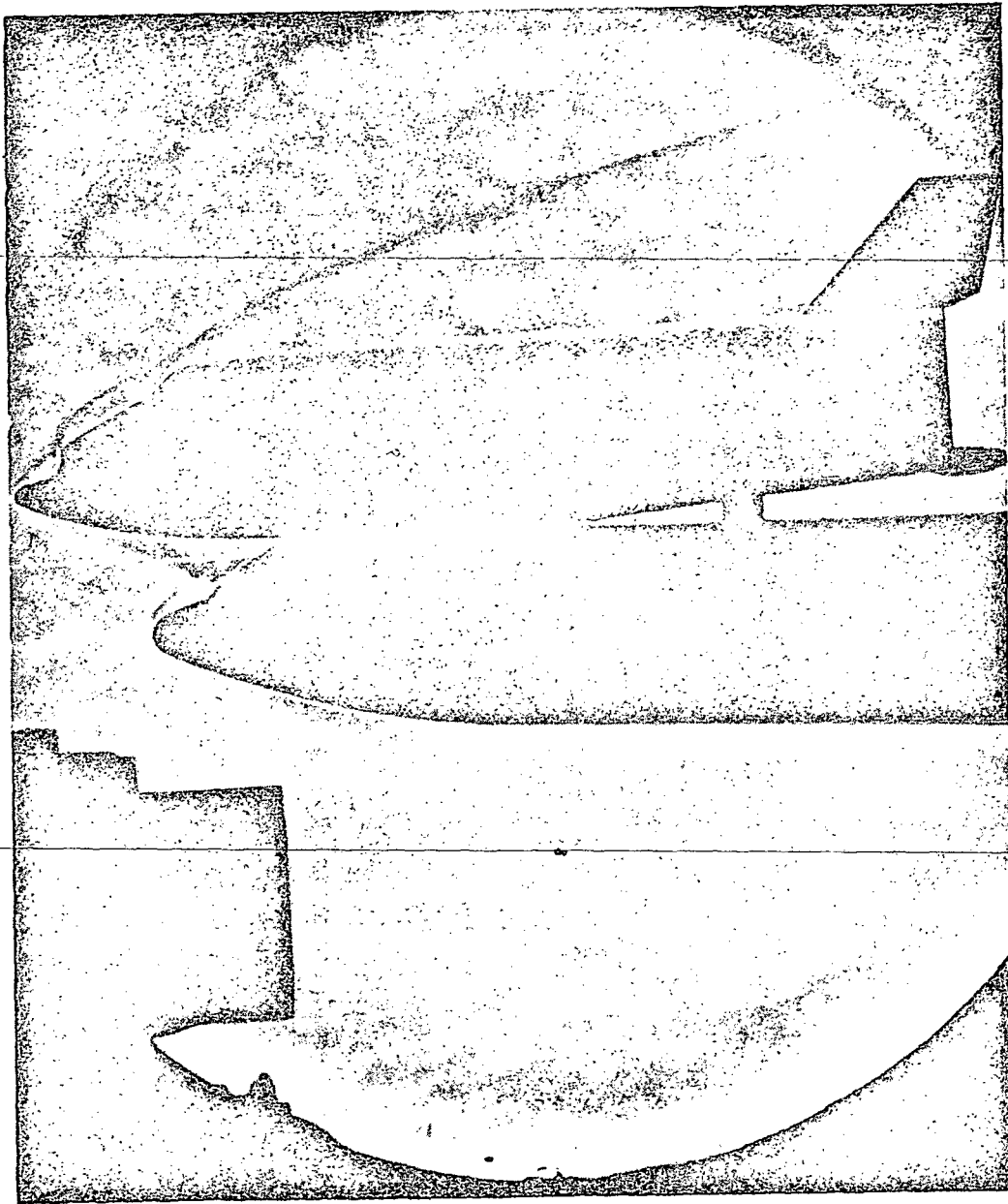


Fig. 72 - Schlieren Photographs of Run 441; Pitch = 0° , Yaw = 0° ,
 $R_N/FT = 0.026 \times 10^5$

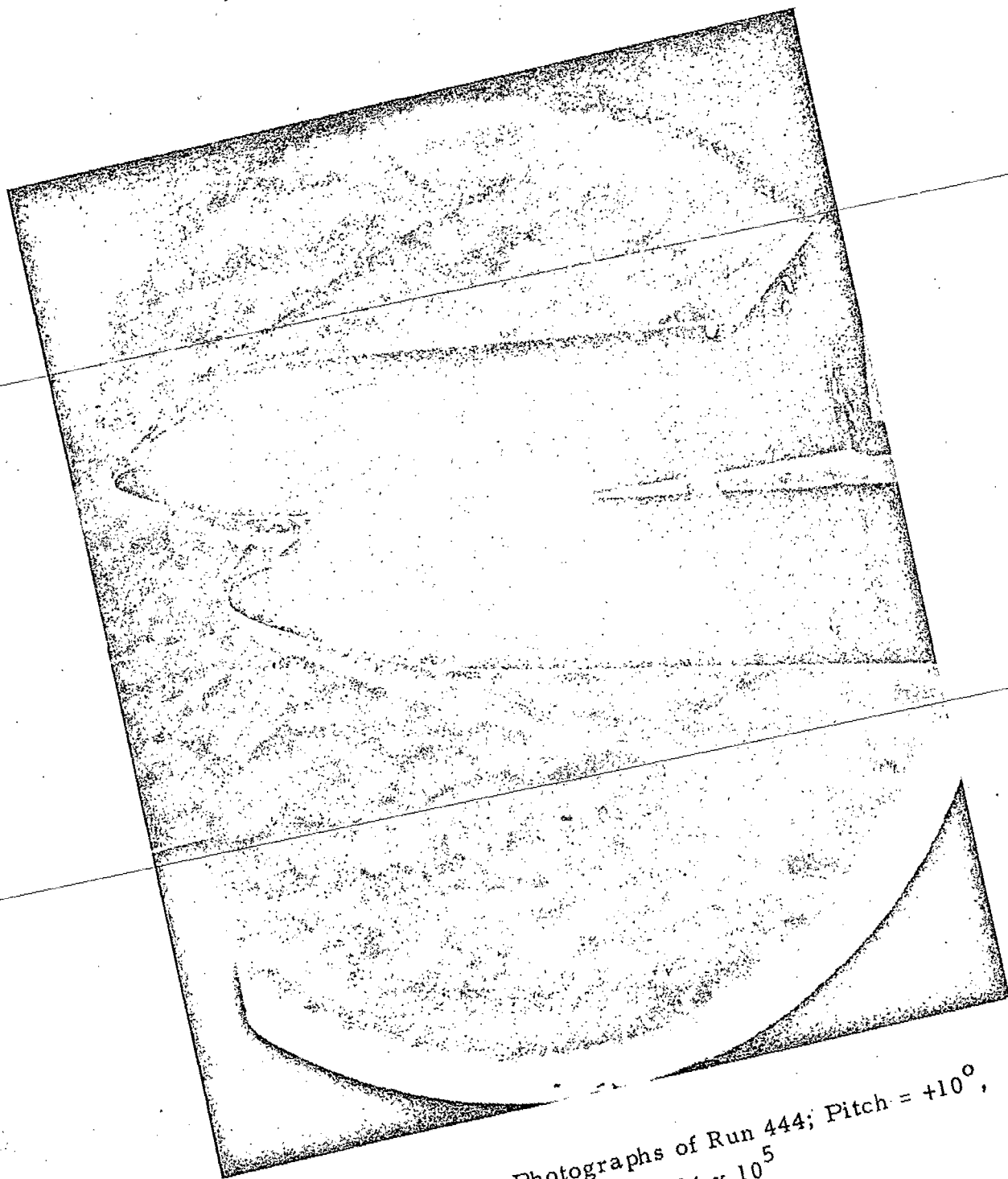


Fig. 73 - Schlieren Photographs of Run 444; Pitch = $+10^\circ$,
 Yaw = 0° , $R_N/FT = 5.84 \times 10^5$

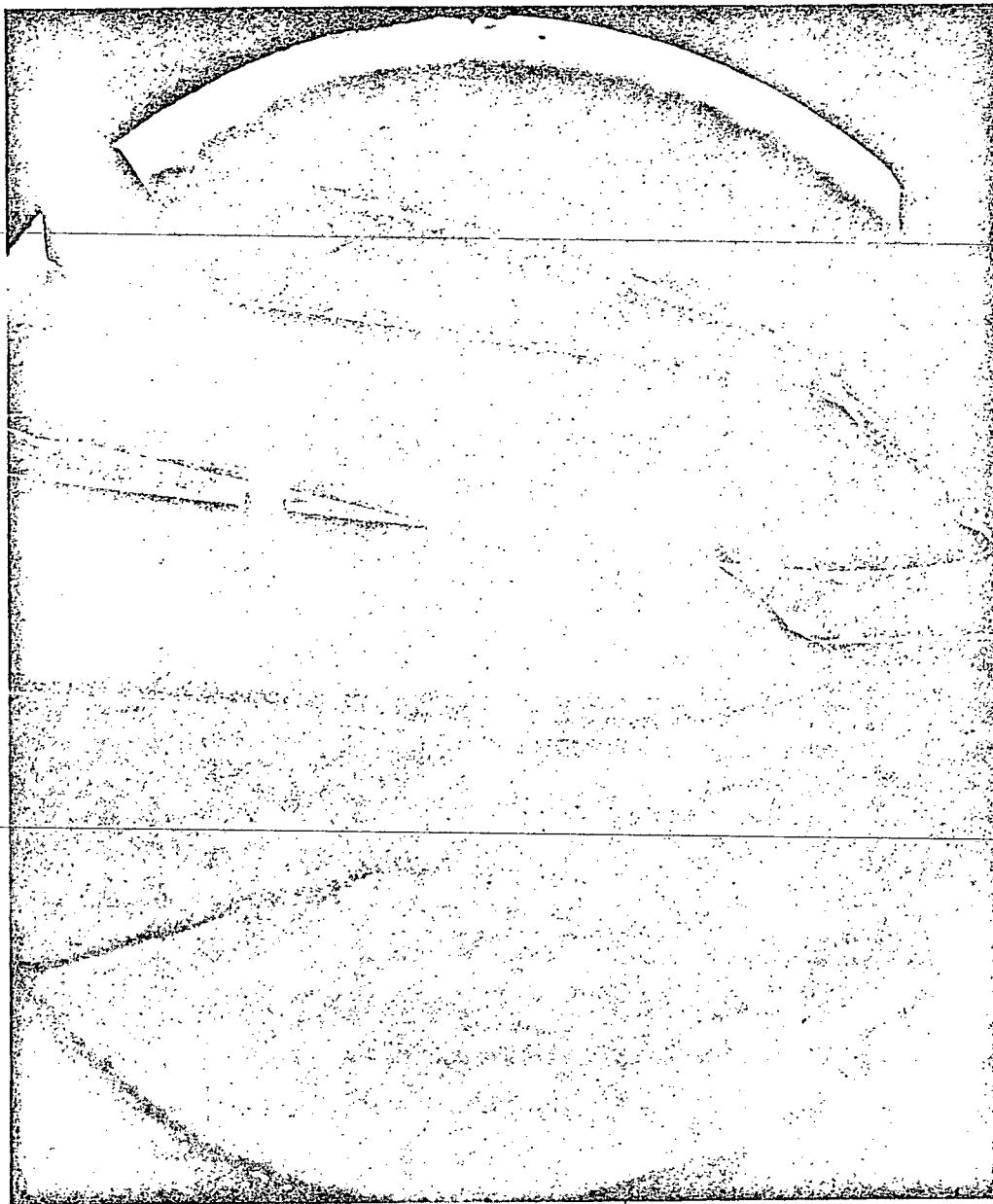


Fig. 74 - Schlieren Photographs of Run 445; Pitch = $+10^\circ$,
Yaw = 0° , $R_N/FT = 6.43 \times 10^5$

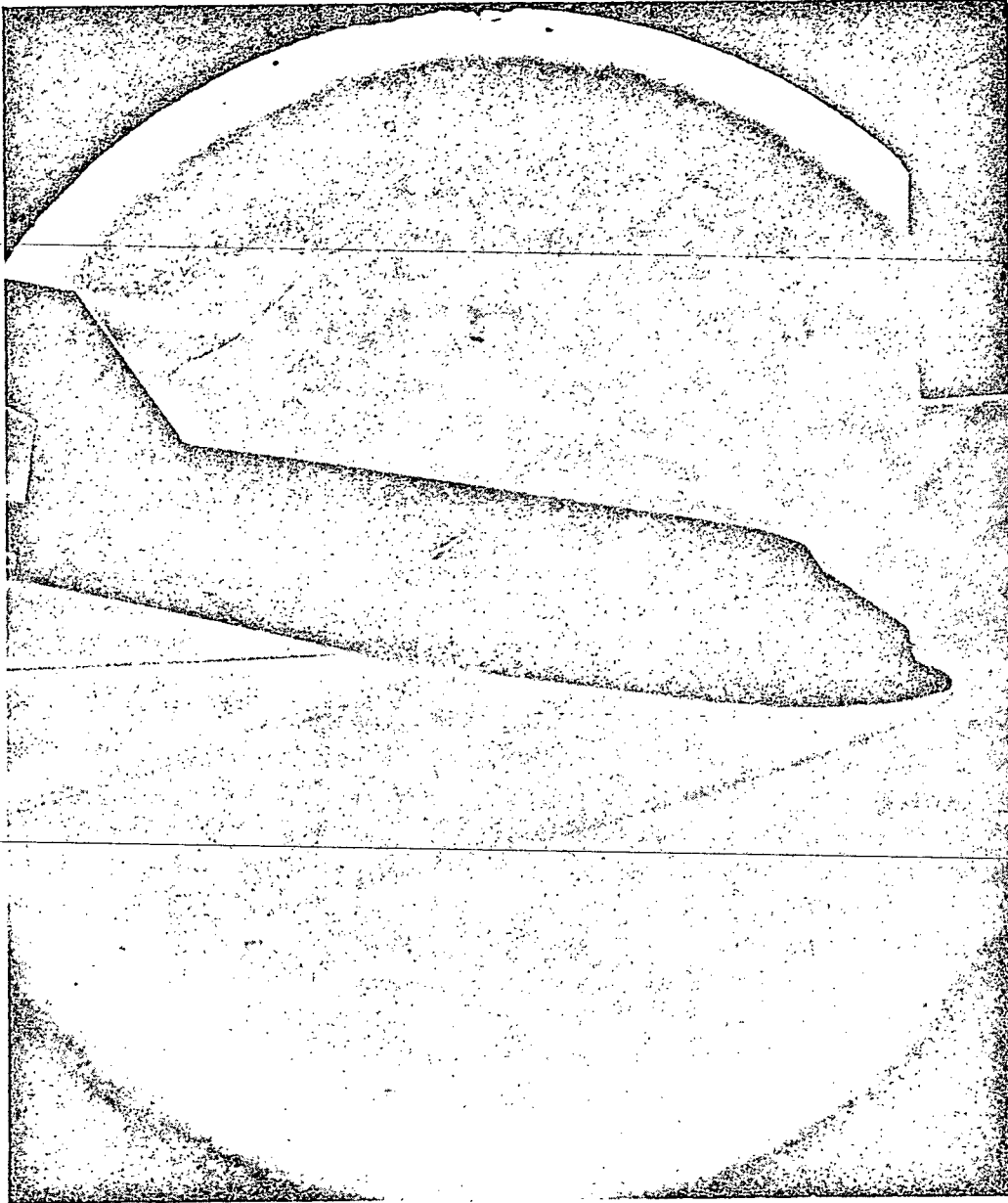


Fig. 75 - Schlieren Photographs of Run 446; Pitch = -10° ,
Yaw = 0° , $R_N/FT = 6.43 \times 10^5$

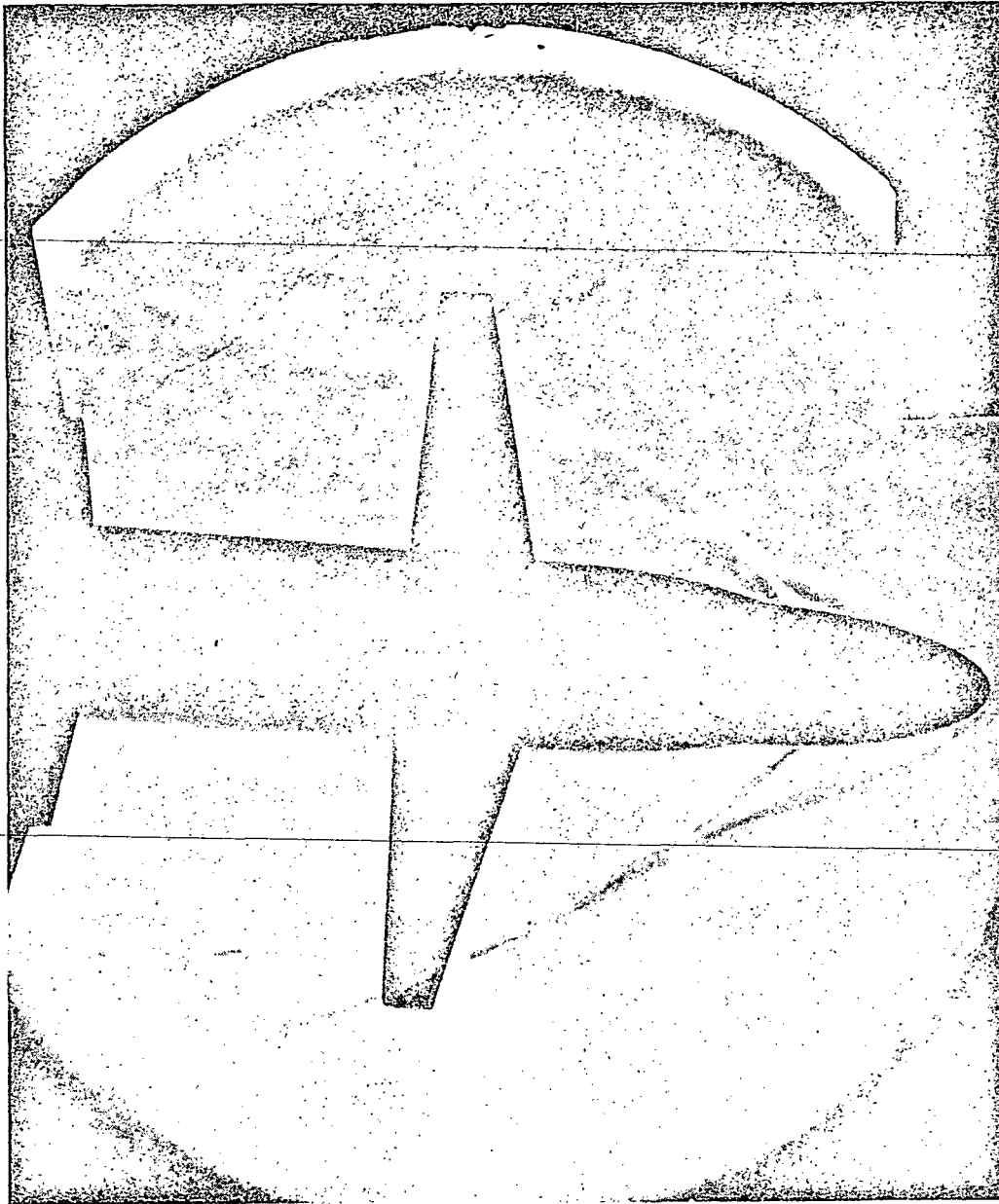


Fig. 76 - Schlieren Photographs of Run 447; Pitch = 0° ,
 Yaw = $+6^\circ$, $R_N/FT = 6.3 \times 10^5$

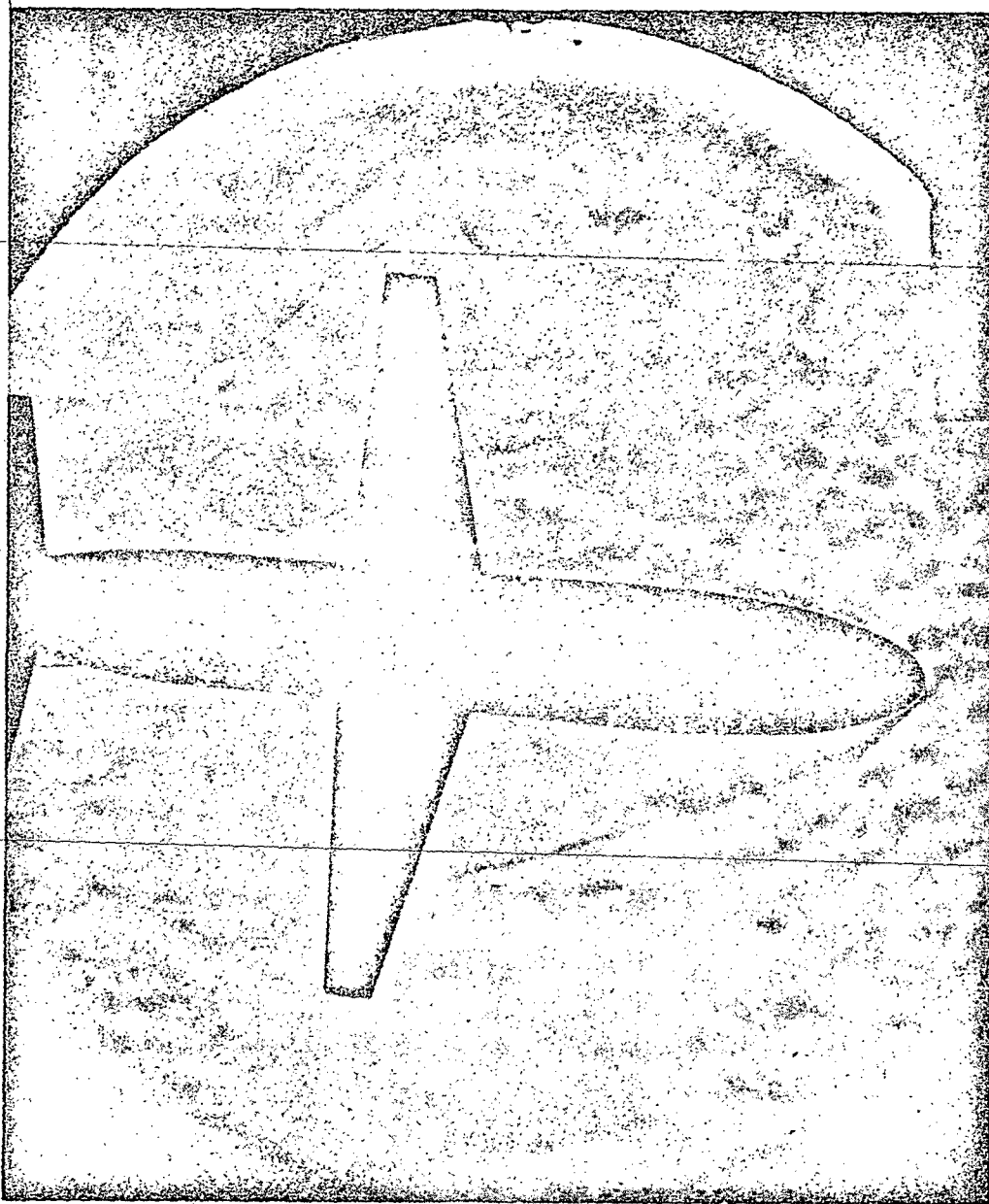


Fig. 77 - Schlieren Photographs of Run 448; Pitch = 0° ,
 Yaw = $+6^\circ$, $R_N/FT = 5.9 \times 10^5$

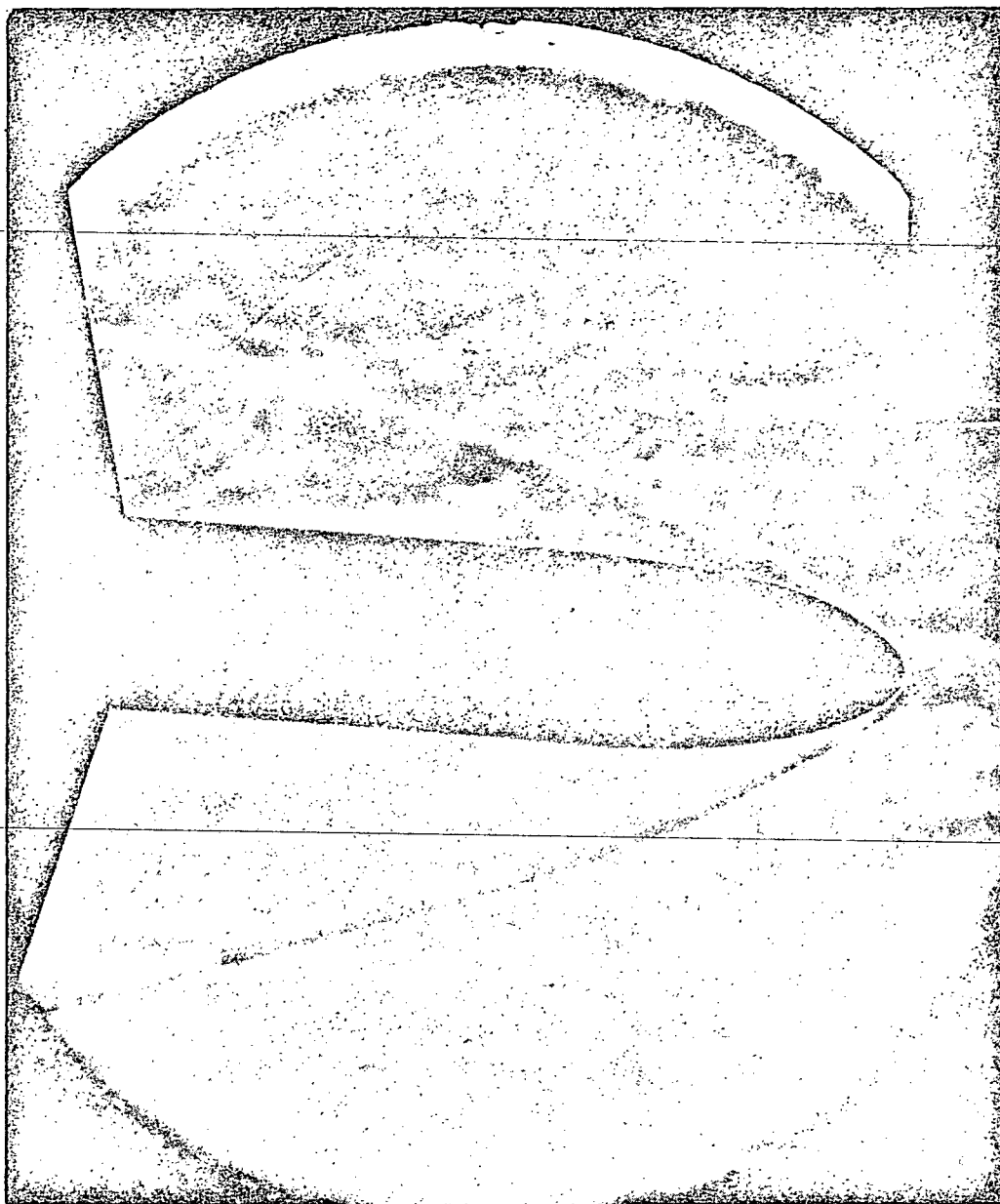


Fig. 78 - Schlieren Photographs of Run 449; Pitch = 0° ,
Yaw = $+6^\circ$, $R_N/FT = 5.99 \times 10^5$

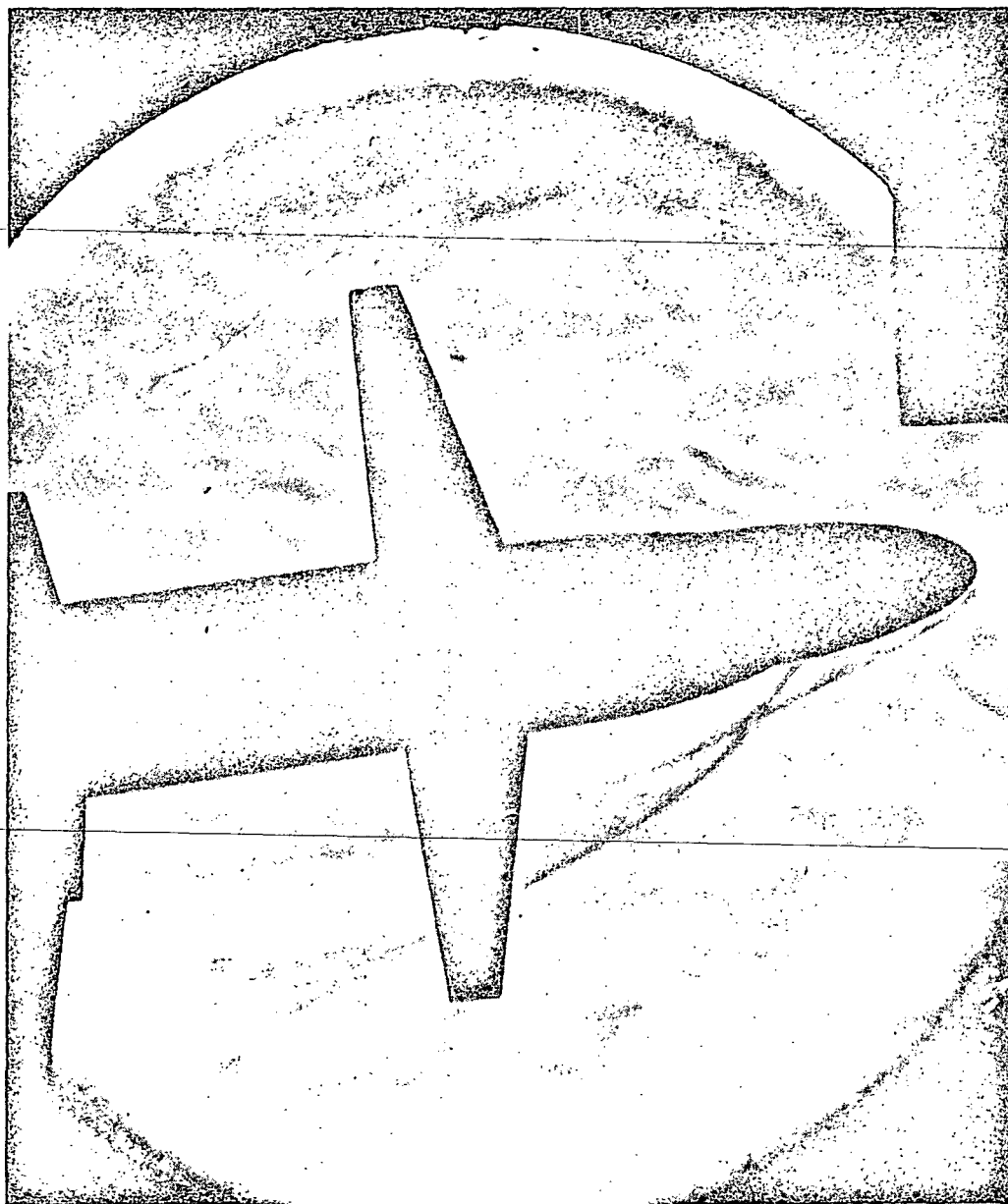


Fig. 79 - Schlieren Photographs of Run 450; Pitch = 0° ,
 Yaw = -6° , $R_N/FT = 6.26 \times 10^5$

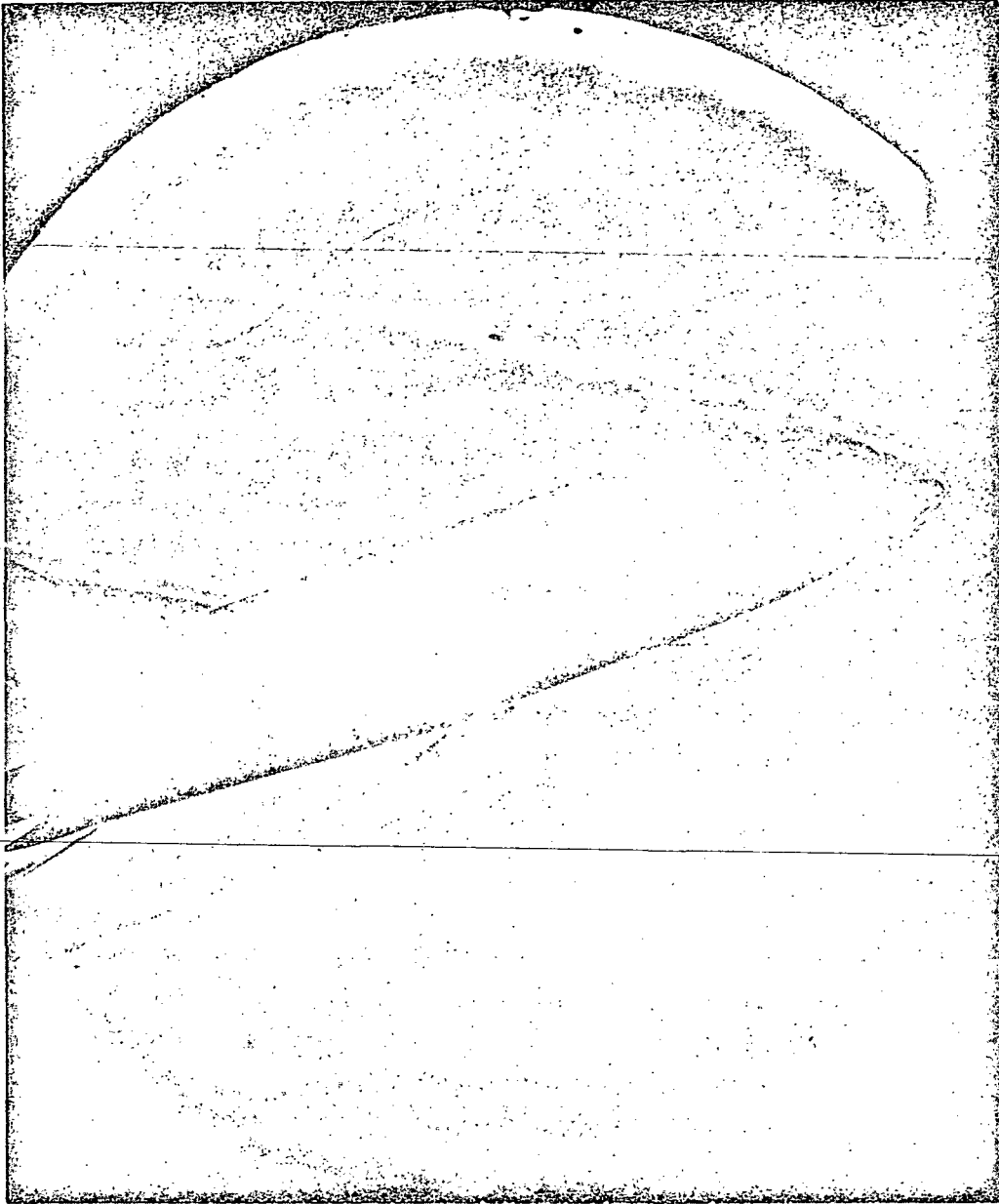


Fig. 80 - Schlieren Photographs of Run 454; Pitch = $+20^\circ$,
 Yaw = 0° , $R_N/FT = 2.04 \times 10^6$

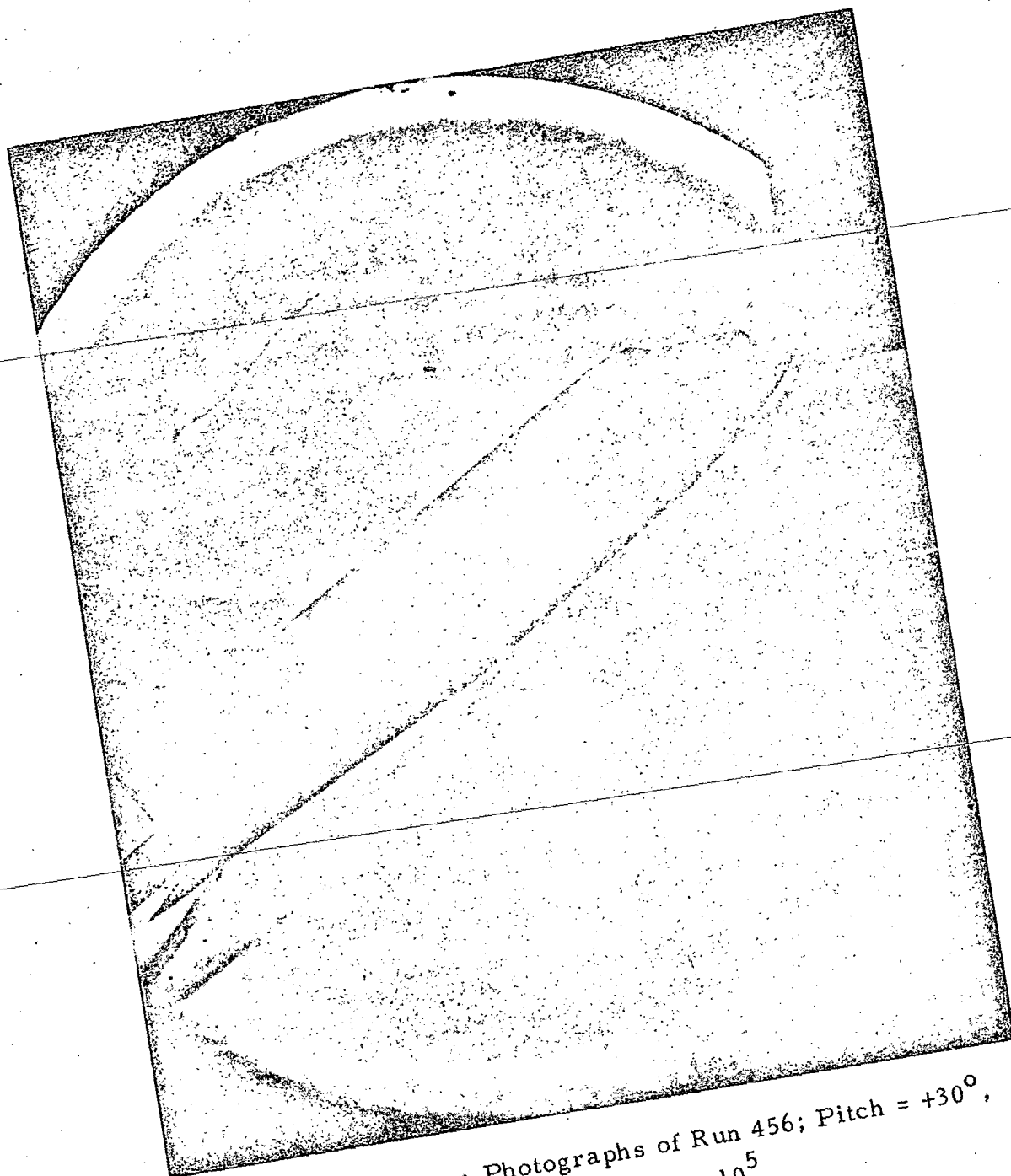


Fig. 81 - Schlieren Photographs of Run 456; Pitch = $+30^\circ$,
Yaw = 0° , $R_N/FT = 6.38 \times 10^5$

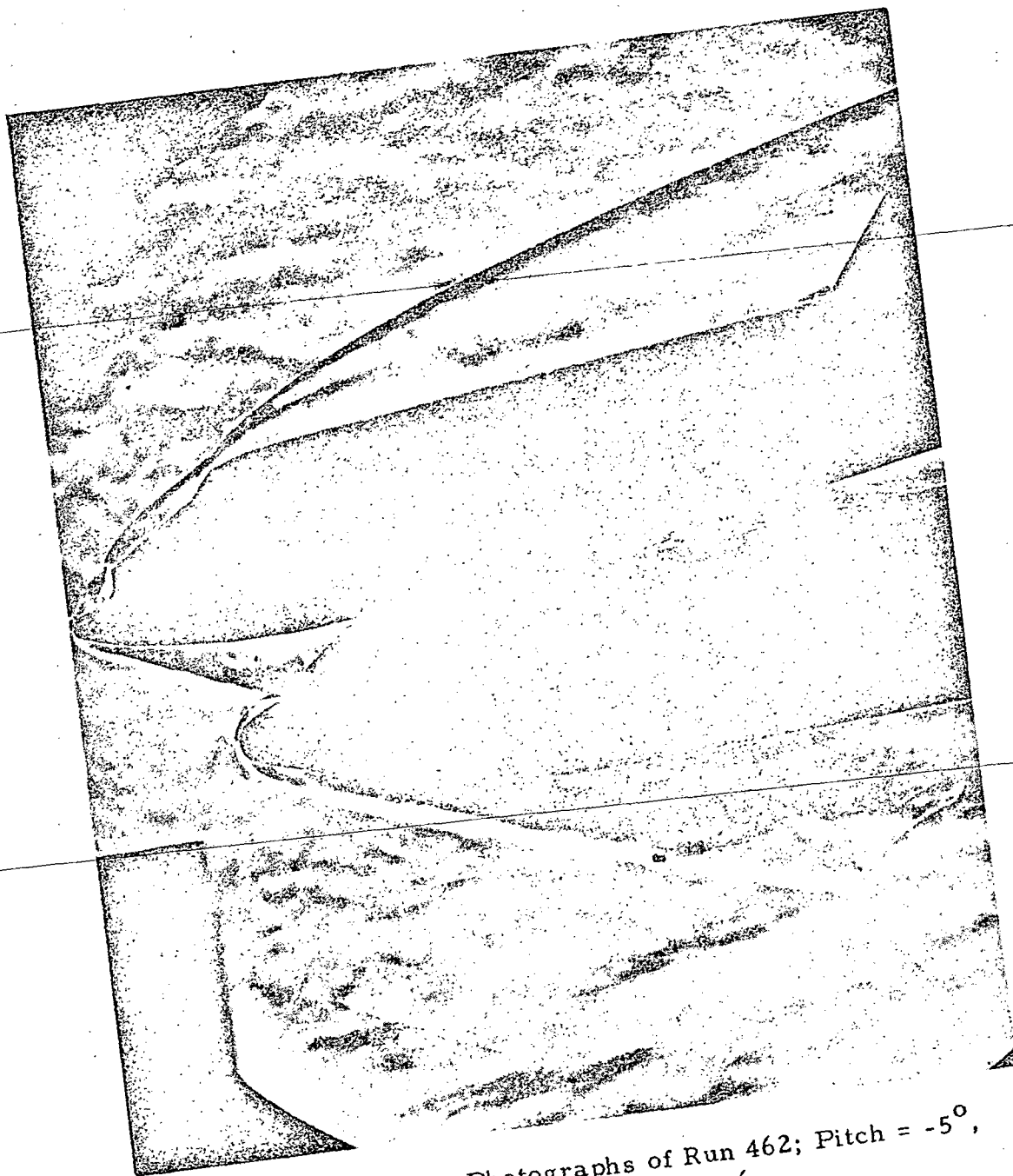


Fig. 82 - Schlieren Photographs of Run 462; Pitch = -5° ,
 Yaw = 0° , $R_N/FT = 3.72 \times 10^6$

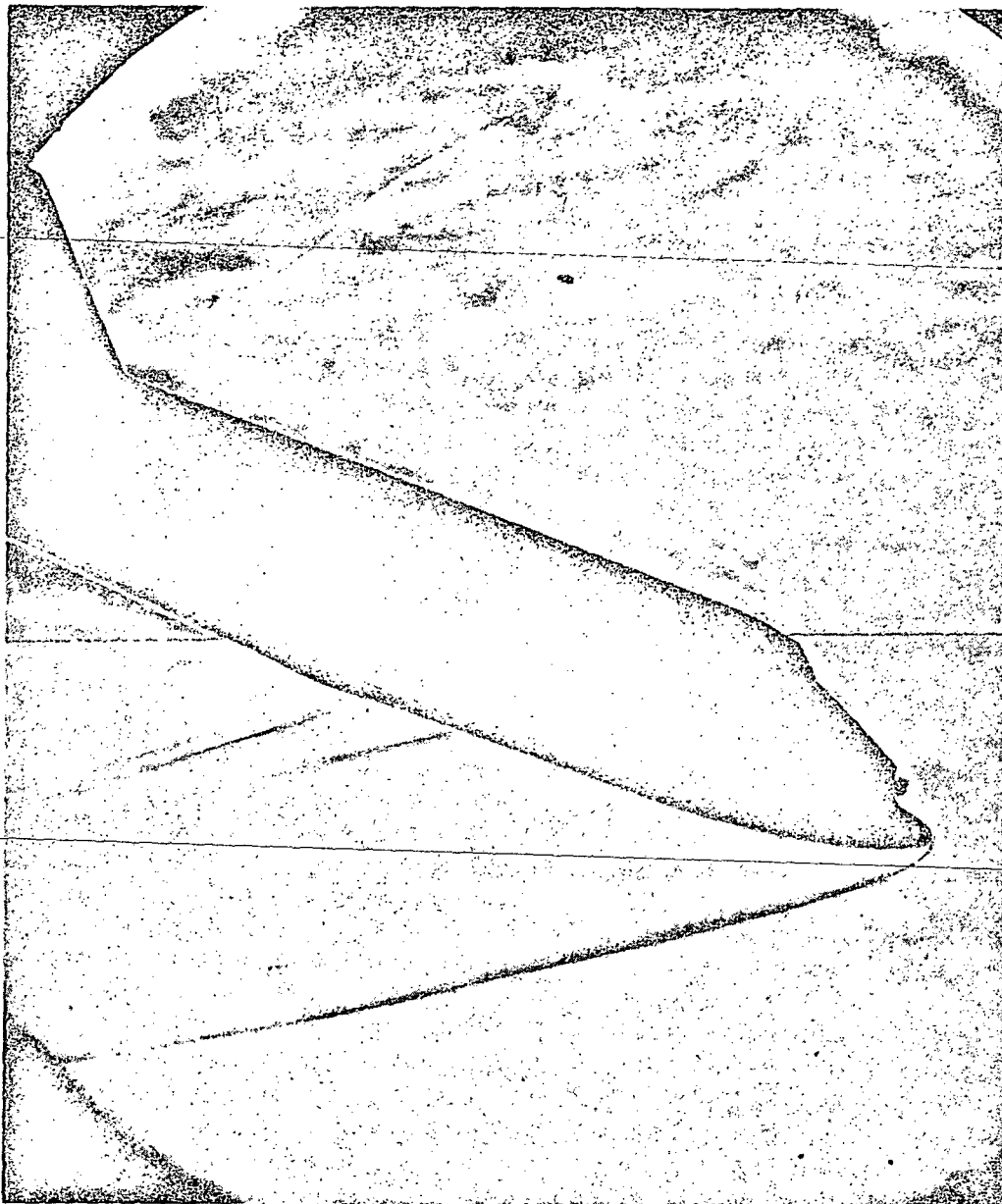


Fig. 83 - Schlieren Photographs of Run 464; Pitch = -20° ,
 Yaw = 0° , $R_N/FT = 1.97 \times 10^6$